Method of Lines Analysis of Gaussian Beam Coupling to Dielectric Slab Waveguide

by

Majid Jafar Al-Majid

A Thesis Presented to the

FACULTY OF THE COLLEGE OF GRADUATE STUDIES

KING FAHD UNIVERSITY OF PETROLEUM & MINERALS

DHAHRAN, SAUDI ARABIA

In Partial Fulfillment of the
Requirements for the Degree of

MASTER OF SCIENCE

In

ELECTRICAL ENGINEERING

February, 1994

Order Number 1360414

Method of lines analysis of Gaussian beam coupling to dielectric slab waveguide

Al-Majid, Majid Jafar, M.S.

King Fahd University of Petroleum and Minerals (Saudi Arabia), 1994

U·M·I
300 N. Zeeb Rd.
Ann Arbor, MI 48106

METHOD OF LINES ANALYSIS OF GAUSSIAN BEAM COUPLING TO DIELECTRIC SLAB WAVEGUIDE

BY

MAJID JAFAR AL-MAJID

A Thesis Presented to the

FACULTY OF THE COLLEGE OF GRADUATE STUDIES

KING FAHD UNIVERSITY OF PETROLEUM & MINERALS

DHAHRAN, SAUDI ARABIA

In Partial Fulfillment of the
Requirements for the Degree of

MASTER OF SCIENCE

In

ELECTRICAL ENGINEERING

FEBRUARY, 1994

KING FAHD UNIVERSITY OF PETROLEUM AND MINERALS
DHAHRAN 31261, SAUDI ARABIA

COLLEGE OF GRADUATE STUDIES

This thesis, written by ***Majid Jafar Al-Majid*** under the direction of his Thesis Committee, has been presented to and accepted by the Dean of the College of Graduate Studies, in partial fulfillment of the requirements for the degree of ***MASTER OF SCIENCE.***

Thesis Committee

DR. H. A. JAMID 24/2/1994
Thesis Advisor

DR. S. J. AL-BADER 26/2/94
Member

DR. K. H. BIYARI 26/2/1994
Member

DR. S. A. AL-BAIYAT
Member

Department Chairman

Dean, College of Graduate Studies

26.2.94
Date

كلية الدراسات العليا
COLLEGE OF GRADUATE STUDIES

بسم الله الرحمن الرحيم

« وعلّمكَ ما لمْ تكنْ تعلمُ
وكانَ فضلُ اللهِ عليكَ عظيما »

صدق الله العظيم

"And (God) taught you what thou knewest not , and great is the grace of God unto you".

الإهداء

إلى روح والديّ، كما ربياني صغيراً، وأنعما عليّ بعطفهما كبيراً ....
إلى من شاركتني هذا الجهد، إلى زوجتي المخلصة عرفاناً بصبرها وتشجيعها ...
وإلى كل من شجعني من أقاربي وأصدقائي.

ماجدة

ACKNOWLEDGMENT

Acknowledgment is due to King Fahd University of Petroleum and Minerals for supporting this research.

I wish to express my sincere appreciation and gratitude to my advisor Dr. Husain A. Jamid for his great assistance and careful guidance throughout the thesis work. I am also indebted to him for the time spent, the effort exerted and for his continuous support and inspiration.

I would also like to express my deep appreciation to my thesis committee member Dr. Samir J. Al-Bader for his constant help and encouragement. I wish also to thank other committee members Dr. Khaled H. Biyari and Dr. Sameer A. Al-Baiyat for their helpful comments.

I offer my thanks to Saudi Aramco management, in particular to Mr. Ahmad M. Al-Zayyat, Manager of the Communications Engineering and Operations Support Department for making it possible for me to complete this post graduate course.

Thanks are due also to my family, friends and colleagues for their continuous support.

At last, I am overwhelmingly grateful to my wife for her support and forbearance during the preparation of this thesis.

خلاصة الرسالة

إسم الطالب: ماجد جعفر أحمد الماجد

عنوان الرسالة: استخدام طريقة الخطوط في تحليل التقارن بين شعاع غاوسي وقائد موجي عازل.

التخصص: هندسة كهربائية

تاريخ الرسالة: شعبان ١٤١٤ هـ - فبراير ١٩٩٤ م.

إن الغرض من هذه الرسالة هو دراسة فعالية التقارن بين مصدر ضوئي لليزر ممثلا بشعاع جرسي الشكل (غاوسي) وبين قائد موجي عازل، عن طريق استخدام "طريقة الخطوط". وطريقة الخطوط هذه هي تكنيك شبه تحليلي يؤدي الى دقة أكبر ويحتاج إلى زمن حسابي أقل ومتطلبات ذاكرة أصغر، مقارنة بالطرق الرقمية الأخرى.

هناك عدة طرق للتقارن بين الحزم الضوئية والقوائد الموجية العازلة. في هذا البحث سوف نركز على تحليل واحدة منها وهي " التقارن الطرفي"، حيث سيتم تغيير المعطيات الأولية للمسألة، مثل اتساع الشعاع الغاوسي، موقع وسط الشعاع وعرض جوف القائد الموجي، وذلك من أجل إيجاد المعاملات المثلى المؤدية لأكبر قدر من فعالية التقارن. كما سيتم في هذه الرسالة أيضا، بحث تأثير الإزاحة العمودية والإزاحة الأفقية للشعاع. با لإضافة لذلك سيتم دراسة تأثير وجود طبقة مضادة للإنعكاس بين مصدر الضوء والقائد الموجي العازل.

درجة الماجستير في العلوم
جامعة الملك فهد للبترول والمعادن
الظهران - المملكة العربية السعودية
شعبان ١٤١٤ هـ

ABSTRACT

MAJID JAFAR AL-MAJID

METHOD OF LINES ANALYSIS OF GAUSSIAN BEAM COUPLING TO DIELECTRIC SLAB WAVEGUIDE

Electrical Engineering
February, 1994

The purpose of this thesis is to study the coupling efficiency from an optical laser source approximated by a normally incident Gaussian beam into a dielectric slab waveguide using the Method of Lines (MoL). The MoL is a semianalytical technique that results in higher accuracy, less computational time and smaller storage requirements in comparison with other numerical methods.

Light can be coupled into a slab waveguide by several methods. In this work, we will be concerned with the analysis of endfire coupling. The launching conditions such as the incident Gaussian beam spot size, the location of the beam waist and the waveguide core width will be varied in order to investigate the optimum values that results in the highest efficiency. The effect of lateral offset as well as longitudinal offset will be considered. In addition, the effect of the presence of an antireflective layer between the light source and the slab waveguide will be studied.

MASTER OF SCIENCE DEGREE

KING FAHD UNIVERSITY OF PETROLEUM AND MINERALS
Dhahran, Saudi Arabia

February, 1994

TABLE OF CONTENTS

LIST OF FIGURES

LIST OF TABLES

CHAPTER I

INTRODUCTION

1.1 Overview

Optical power coupling is an important design problem in Optical Fiber Communications [1,2] and Integrated Optics [3]. There has been a considerable interest during the past two decades in the development of new means of increasing the efficiency of this process. A substantial portion of the emitted light power can be lost in the region between the light source and the waveguide, making the analysis of the factors that influence the coupling efficiency of great importance.

In conjunction with the rapid development of Integrated Optics and Optical Waveguides in general, several numerical methods have been developed for the analysis of

longitudinally-dependent effects in these waveguide structures. Among these methods are the Beam propagation Method (BPM) [4], the Finite Difference Time Domain (FDTD) Method [5] and the Method of Lines [6,7].

The BPM cannot be used for the analysis of the coupling problem because of its inability to account for the back-scattered field at a longitudinal discontinuity. The Fast Fourier Transform (FFT) form of this method is also known to be inefficient in problems involving large transverse discontinuities.

The FDTD method is applicable to the problem under consideration. However, it will not be used in this work because it requires knowledge of a Gaussian expression that satisfies Helmholtz equation. Such expression is not available in the literature , and the available approximation [8] is rather poor for the problem to be treated in this thesis.

In this work, we will use the MoL for the analysis of the problem under consideration because of its simplicity, high accuracy, and its ability to account for back-scattered waves. In contrast to the other numerical methods mentioned, this technique is very efficient with respect to

computational time due to its semianalytical nature. This method has been applied in the analysis of various problems in planar longitudinally uniform waveguide structures [9,10], and recently, it has been extended to the treatment of planar waveguides with longitudinal discontinuities [11].

As will be explained in a subsequent section, light beams can be coupled to dielectric planar waveguide structures using different techniques. These Coupling techniques include prism coupling, grating coupling, and endfire or butt coupling [12,13,14]. Of these different methods, end-fire or butt-coupling techniques, are of particular interest because of their several advantages such as ease of handling of in-line input and output beams [15,16]. It is therefore the purpose of this thesis to consider the analysis of ***endfire coupling*** of a normally-incident Gaussian beam into a dielectric slab waveguide using the MoL.

1.2 Statement of the Problem

Consider a Gaussian beam of **Half Beam Width (HBW)** w_0, incident normally on a dielectric slab waveguide positioned at z=0. The waveguide has a core of thickness $2w$, as shown in figure (1.1). The axial position of the beam waist is located at $z=-z_0$, a distance z_0 from the input end of the waveguide. The lateral position of the beam axis is located at a distance x_0 from the waveguide axis.

The MoL requires knowledge of the Gaussian beam distribution at $z=-z_0$ only. This is given by the simple expression:

$$\psi(x,y) = E_0 \exp\left[-\frac{(x-x_0)^2}{w_0^2}\right] \qquad (1.1)$$

where E_0 is the beam amplitude at $x=x_0$ and $z=-z_0$. It is required to calculate the percentage of the beam power that will be coupled into the waveguide, and the percentages of this power that will be guided and radiated. The launching conditions such as the HBW; w_0, and the position of the beam waist will be varied to realize the optimum conditions that will result in the highest coupling efficiency. The effect of an anti-reflection layer will also be considered with the

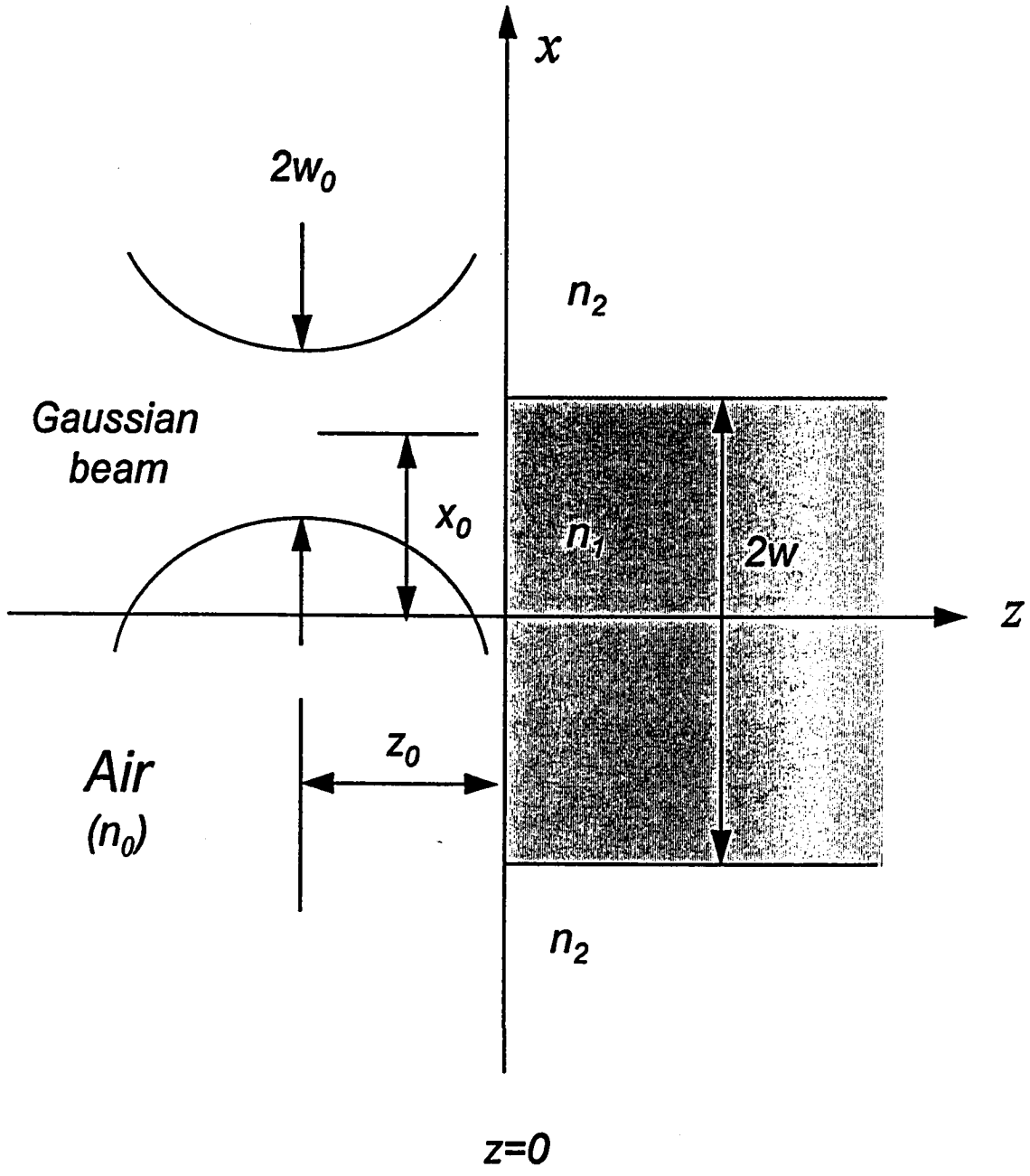

Figure (1.1) *Coupling of a Gaussian beam into a dielectric slab waveguide.*

view of increasing the coupling efficiency and to minimize the amount of power reflected.

1.3 Coupling to the Slab Waveguide

Consider the slab waveguide shown in figure (1.2), there exist two methods in which a TE or TM mode can be excited inside this thin film waveguide [3,17]. One method is to have a wave that matches the field pattern of the mode be incident on the end facet of the waveguide. This will result in the maximum possible portion of the incident wave power being coupled to the waveguide mode. Coupling techniques that follow this method are endfire and butt coupling.

The second method is known as evanescent coupling and it requires matching of the longitudinal propagation phase constant $e^{j\beta_m z}$ of the desired mth mode of the waveguide to that of the incident beam. This way of coupling involves distributed coupling over a prescribed interaction length [18]. Examples of this type of coupling are prism and grating coupling.

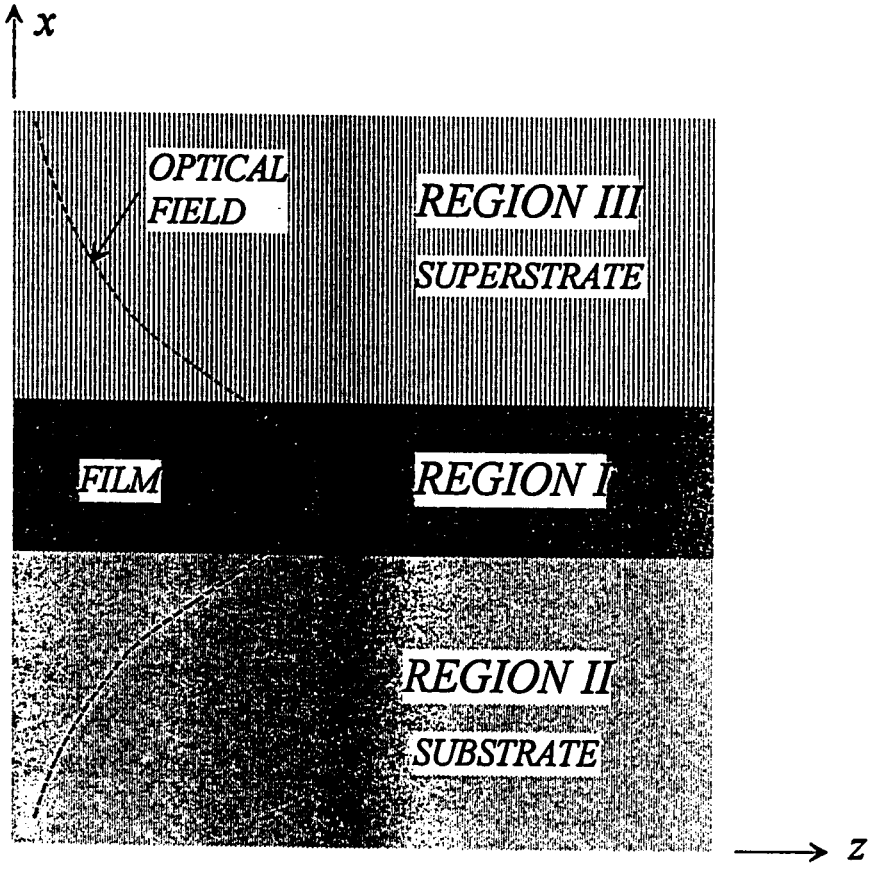

Figure (1.2) *Fundamental mode profile in a planar dielectric slab waveguide.*

The above coupling methods vary in their complexity, applicability and efficiency. In all cases, the main design parameter is to ensure that the maximum possible power coupling efficiency is obtained. This can be achieved by carefully tuning all the different parameters on both sides of the coupling interface which include the incident field parameters as well as the waveguide under investigation.

1.4 Thesis Organization

The main objective of this thesis is to study the coupling efficiency from an optical laser source into a dielectric slab waveguide. The thesis is composed of six chapters. In the first introductory chapter, we present an overview of the importance of efficient coupling in optical fiber communications and integrated optics. Various numerical methods used for the analysis of planar structures are briefly discussed and the advantages of using the Method of Lines are stated. A concise description of the problem under consideration is presented. An introductory notes on the subject of coupling to the slab waveguide is then provided.

In chapter II, the wave equation and the eigenvalue equation of the symmetric slab waveguide are derived from Maxwell's equations. The main light coupling techniques namely; prism, grating, endfire and butt coupling are discussed. More emphasis will be given to the endfire coupling technique as it is the technique used in our research work. Some sections will be devoted in this chapter to discuss the topics of microlenses, laser sources and integrated optics in general.

We review in chapter III the main principles of the *Method of Lines* and its application to the coupling problem is then presented. We will also review the convergence of the method. The objective of this chapter is to give the reader an idea about the accuracy of the technique and the simplicity of its implementation in different problems.

Chapters IV and V represent the main contribution of this thesis. In chapter IV, an expression for the power coupling efficiency is derived. This expression is then utilized by the MoL to calculate the coupling efficiency of a Gaussian beam into the fundamental mode of a dielectric slab waveguide. As a laser source radiation profile is required for the calculations of coupling efficiency, a Gaussian beam approximation of this profile will be

discussed. The application of the MoL is considered for perfect alignment and then both the lateral and the longitudinal offset effects are analyzed. At the end of this chapter we discuss the results of the above implementation and its computational constraints.

In chapter V we study the effect of the presence of an anti-reflection (AR) layer between the light source and the investigated slab waveguide. The effect is measured on both the efficiency and reflectivity. In order for the AR layer to give the maximum effect, its width and refractive index ought to have optimum values. These optimum values are derived for normally incident plane wave on a homogeneous half space and then used as an approximation for the Gaussian beam. As expected, the insertion of the AR layer increases the coupling efficiency and efficiency figures greater that 99% were obtained.

In the last chapter, we review the output results and present a brief conclusion and the recommended related future work. Two appendices are attached to this thesis which include the computer programs used in this work.

CHAPTER II

OPTICAL DIELECTRIC SLAB WAVEGUIDE

2.1 Introduction

The optical dielectric slab waveguide gained its importance from its vast applications in integrated optics and fiber optics communications. Dielectric waveguides are used in the integration of many optical and optoelectronic devices such as modulators, light sources, optical amplifiers, and switches.

The structure of the dielectric slab waveguide is simple. It consist of a thin layer of dielectric film (core) sandwiched between two semi-infinite layers having indices n_2 and n_3 as illustrated in figure (2.1). The refractive index of the core has to be larger than those of the other two layers to allow for the light to be trapped and guided inside the film by total internal reflection. If the

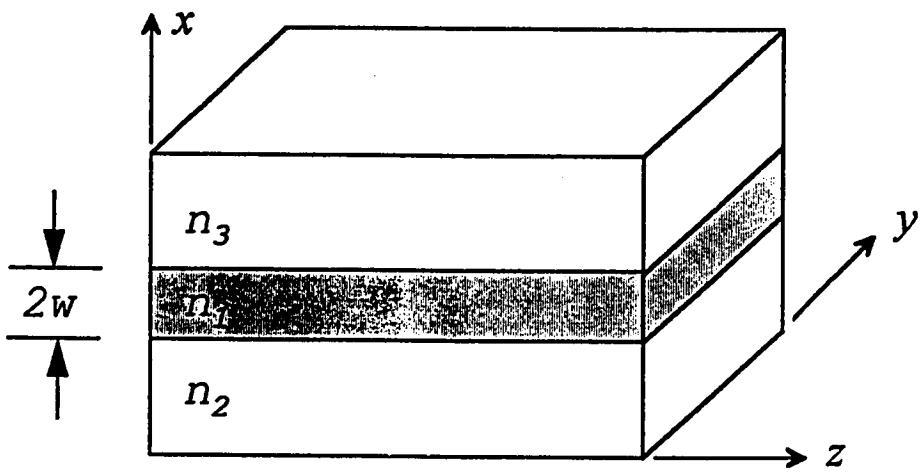

Figure (2.1) *Geometrical Structure of the dielectric Slab Waveguide.*

superstrate and the substrate have the same refractive index then the waveguide is called a *symmetric waveguide*. If they possesses different indices, the structure is called *asymmetric waveguide*. In the following analysis, we will be concerned with the treatment of the symmetric type of optical dielectric slab waveguides.

2.2 Mode Equations of the Symmetric Slab Waveguide

In what follows we will be concerned with deriving the mode equations of the symmetric slab waveguide directly from Maxwell's equations. Since we are dealing with Planar structures our discussion will be limited to the wave propagation in rectangular coordinates. To simplify the problem, we will assume that the waveguide of interest is infinitely extended in the y direction with no field or geometric variations along that direction. This implies that

$$\frac{\partial}{\partial y} = 0 \qquad (2.1)$$

We will assume also that all field quantities have $(e^{-j\omega t})$ time dependence, where ω is the angular frequency of the field. The media to be treated are nonmagnetic with free space permeability $\mu_0 = 4\pi 10^{-7} H/m$.

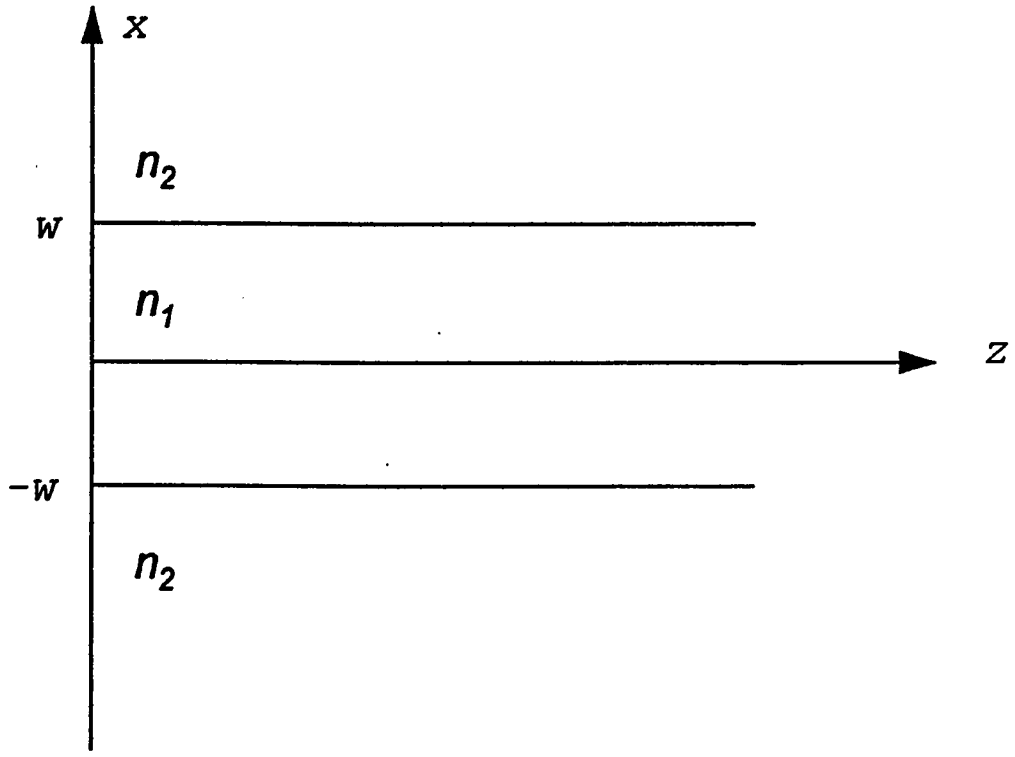

Figure (2.2) *A Schemetic of the Treated dielectric Slab Waveguide.*

2.2.1 Derivation of the Wave Equation

In source-free homogeneous media, Maxwell's equations for dielectric locally homogeneous media are expressed as [19]:

$$\nabla \times \overline{E} = -\mu \frac{\partial}{\partial t} \overline{H} \tag{2.2}$$

$$\nabla \times \overline{H} = \varepsilon \frac{\partial}{\partial t} \overline{E} \tag{2.3}$$

$$\nabla . \overline{H} = 0 \tag{2.4}$$

$$\nabla . \overline{E} = 0 \tag{2.5}$$

Where $\overline{E}$ = *electric field strength* *(volts/m)*

$\overline{H}$ = *magnetic field strength* *(amperes/m)*

μ = *permeability* *(henry/m)*

ε = *permittivity* *(farad/m)*

The bar over the variables is used to indicate that these variables are vectors. These vectors are functions of both space and time. The time-harmonic fields are expressed as:

$$\overline{E}(x,z,t) = \overline{E}(x,z)e^{-j\omega t} \tag{2.6}$$

and

$$\overline{H}(x,z,t) = \overline{H}(x,z)e^{-j\omega t} \tag{2.7}$$

and equations (2.2) and (2.3) become:

$$\nabla \times \overline{E} = j\omega\mu\overline{H} \tag{2.8}$$

$$\nabla \times \overline{H} = -j\omega\varepsilon\overline{E} \tag{2.9}$$

By taking the curl of equation (2.8)

$$\nabla \times \nabla \times \overline{E} = j\omega\mu(\nabla \times \overline{H}) \tag{2.10}$$

Substituting equation(2.9) in (2.10)

$$\nabla X \nabla X \overline{E} = j\omega\mu(-j\omega\varepsilon\overline{E})$$

$$= \omega^2\mu\varepsilon\overline{E} \tag{2.11}$$

By substituting equations (2.5) and (2.11) in the following vector identity

$$\nabla X(\nabla X\overline{E}) = \nabla(\nabla.\overline{E}) - \nabla^2\overline{E} \tag{2.12}$$

we obtain the ***wave equation*** of the electric field:

$$\nabla^2\overline{E} + \omega^2\mu\varepsilon\overline{E} = 0 \tag{2.13}$$

where ∇^2 is the *Laplacian operator* defined as:

$$\nabla^2 = \frac{\partial^2}{\partial x^2} + \frac{\partial^2}{\partial y^2} + \frac{\partial^2}{\partial z^2} \tag{2.14}$$

The form of the wave equation represented by (2.13) is called the ***Helmholtz equation.*** By definition, the wave number k is expressed as:

$$k = \omega\sqrt{\mu\varepsilon} \tag{2.15}$$

Using the above expansion of the Laplacian operator and the definition of the wave number together with the assumption that $\frac{\partial}{\partial y} = 0$, the wave equation (2.13) can be expressed as:

$$\frac{\partial^2 \overline{E}}{\partial x^2} + \frac{\partial^2 \overline{E}}{\partial z^2} + k^2 \overline{E} = 0 \tag{2.16}$$

where $\overline{E} = \overline{E}(x,z)$.

Assuming that the field components vary according to the following time and z-dependence

$$e^{-j\omega t + j\beta z} \tag{2.17}$$

where β is the propagation constant in the z-direction, then $\overline{E}(x,z)$ can be expressed as:

$$\overline{E}(x,z) = \overline{E}(x)e^{j\beta z} \tag{2.18}$$

and equation (2.16) reduces to

$$\frac{d^2 \overline{E}}{dx^2} + (k^2 - \beta^2)\overline{E} = 0 \tag{2.19}$$

where $\overline{E} = \overline{E}(x)$.

Following the same procedure, we can derive the wave equation for the magnetic field $\overline{H}$. In general, the wave equation can be expressed as:

$$\frac{\partial^2 \psi}{\partial x^2} + (k^2 - \beta^2)\psi = 0 \qquad (2.20)$$

where $\psi = \psi(x)$, represents any rectangular component of $\overline{E}$ or $\overline{H}$.

2.2.2 TE Modes Equation

The field propagating in a dielectric slab waveguide can be decomposed into Transverse Electric *(TE)* and Transverse Magnetic *(TM)* polarized fields. For the purpose of this thesis, our analysis will be limited to the TE polarized fields.

With the assumption that $\frac{\partial}{\partial y} = 0$, the only nonzero field components for TE modes are E_y, H_x and H_z. Substituting E_y in equation (2.20), we obtain the wave equation for TE polarized waves

$$\frac{\partial^2 E_y}{\partial x^2} + (k^2 - \beta^2)E_y = 0 \qquad (2.21)$$

using $$\beta = k_0 n_e \tag{2.22}$$

and $$k = \frac{2\pi}{\lambda} = k_0 n_i \tag{2.23}$$

leads to $$\frac{\partial^2 E_y}{\partial x^2} + k_0^2 (n_i^2 - n_e^2) E_y = 0 \tag{2.24}$$

where n_e = *the effective index*

n_i = *the ith layer refractive index*

Considering the symmetric slab waveguide structure depicted on figure (2.2), equation (2.24) leads to:

$$\frac{\partial^2 E_y}{\partial x^2} + k_0^2 (n_1^2 - n_e^2) E_y = 0 \qquad |x| < a \tag{2.25a}$$

$$\frac{\partial^2 E_y}{\partial x^2} + k_0^2 (n_2^2 - n_e^2) E_y = 0 \qquad |x| > a \tag{2.25b}$$

For guided modes, the effective index is constrained by

$$n_2 < n_e < n_1 \tag{2.26}$$

or

$$n_1 - n_e > 0$$

and $$n_2 - n_e < 0 \tag{2.27}$$

Equation (2.27) implies that the solutions of the differential equation (2.25) will have the form:

$$E_y = \begin{cases} Ee^{k_0\sqrt{n_e^2-n_2^2}x} + Fe^{-k_0\sqrt{n_e^2-n_2^2}x} & x > a \\ A\sin k_0\sqrt{n_1^2-n_e^2}x + B\cos k_0\sqrt{n_1^2-n_e^2}x & |x| < a \\ Ce^{k_0\sqrt{n_e^2-n_2^2}x} + De^{-k_0\sqrt{n_e^2-n_2^2}x} & x < -a \end{cases} \qquad (2.28)$$

The two constants D and E shall be set to zero, because they are coefficients of growing fields. In addition, we let

$$l = k_0\sqrt{n_1^2-n_e^2} \qquad (2.29)$$

$$\gamma = k_0\sqrt{n_e^2-n_2^2} \qquad (2.30)$$

Following the above consideration, equation (2.28) can be reduced to the following form:

$$E_y = \begin{cases} Fe^{-\gamma x} & x > a \\ A\sin lx + B\cos lx & |x| < a \\ Ce^{\gamma x} & x < -a \end{cases} \qquad (2.31)$$

Equation (2.31) represents the solutions for E_y in the three regions of the slab waveguide for a guided mode. Bear in mind that we have omitted the t-and-z-dependence for simplicity.

Since E_y is continuous at $x=a$ and $x=-a$; equation (2.31) takes the following form:

$$E_y = \begin{cases} (A\sin la + B\cos la)e^{-\gamma(x-a)} & x > a \\ A\sin lx + B\cos lx & |x| < a \\ (-A\sin la + B\cos la)e^{\gamma(x+a)} & x < -a \end{cases} \tag{2.32}$$

The magnetic field components H_x and H_z are related to the electric field component E_y through Maxwell's equation (2.8)

$$\nabla \times \overline{E} = j\omega\mu\overline{H}$$

results in

$$\overline{H} = -j\left(\frac{\nabla X\overline{E}}{\omega\mu}\right) = -\frac{j}{\omega\mu}\begin{vmatrix} \bar{a}_x & \bar{a}_y & \bar{a}_z \\ \dfrac{\partial}{\partial x} & \dfrac{\partial}{\partial y} & \dfrac{\partial}{\partial z} \\ 0 & E_y & 0 \end{vmatrix}$$

$$= -\frac{j}{\omega\mu}\left(-\frac{\partial E_y}{\partial z}\bar{a}_x + \frac{\partial E_y}{\partial x}\bar{a}_z\right) \tag{2.33}$$

from which

$$H_x = \frac{j}{\omega\mu}\frac{\partial E_y}{\partial z} \tag{2.34}$$

and

$$H_z = -\frac{j}{\omega\mu}\frac{\partial E_y}{\partial x} \tag{2.35}$$

Differentiating equation (2.32) with respect to x and substituting the result in (2.35), we get

$$H_z = -\frac{j}{\omega\mu}\begin{cases} -\gamma(A\sin la + B\cos la)e^{-\gamma(x-a)} & x > a \\ l(A\cos lx - B\sin lx) & |x| < a \\ \gamma(-A\sin la + B\cos la)e^{\gamma(x+a)} & x < -a \end{cases} \qquad (2.36)$$

Since H_z is also continuous at $x=a$ and $x=-a$, this leads to the following two equations:

at $x=a$: $$-\gamma(A\sin la + B\cos la) = l(A\cos la - B\sin la) \qquad (2.37a)$$

at $x=-a$: $$\gamma(-A\sin la + B\cos la) = l(A\cos la + B\sin la) \qquad (2.37b)$$

Dividing both sides of the above two equations by $(B\cos la)$ and taking the term $\frac{A}{B}$ as a common factor in both, yields the following result

$$\frac{A}{B} = \frac{\left(\frac{l}{\gamma}\tan la - 1\right)}{\left(\tan la + \frac{l}{\gamma}\right)}$$

and

$$\frac{A}{B} = \frac{-\left(\frac{l}{\gamma}\tan la - 1\right)}{\left(\tan la + \frac{l}{\gamma}\right)}$$

or

$$\frac{A}{B} = \frac{(\frac{l}{\gamma}\tan la - 1)}{(\tan la + \frac{l}{\gamma})} = -\frac{(\frac{l}{\gamma}\tan la - 1)}{(\tan la + \frac{l}{\gamma})} \qquad (2.38)$$

Equation (2.38) requires that either $\frac{A}{B}=0$ or $\frac{B}{A}=0$.

TE Even Modes:

If B is finite and $\left(\tan la+\frac{l}{\gamma}\right)\neq 0$, then A=0 and

$$\frac{l}{\gamma}\tan la-1=0 \tag{2.39}$$

The corresponding electric field is

$$E_y=\begin{cases}(B\cos la)e^{-\gamma(x-a)} & x>a\\ B\cos lx & |x|<a\\ (B\cos la)e^{\gamma(x+a)} & x<-a\end{cases} \tag{2.40}$$

which represents an even function of x. Equation (2.39) is therefore called the TE ***Even Mode*** equation or the eigenvalue equation for the TE even modes.

TE Odd Modes:

The second possibility to satisfy equation (2.38) is when A is finite and B=0 and $\left(\frac{l}{\gamma}\tan la-1\right)\neq 0$. This implies that

$$\frac{\gamma}{l}\tan la+1=0 \tag{2.41}$$

and the corresponding electric field is

$$E_y = \begin{cases} (A\sin la)e^{-\gamma(x-a)} & x > a \\ A\sin lx & |x| < a \\ (-A\sin la)e^{\gamma(x+a)} & x < -a \end{cases} \qquad (2.42)$$

which is an odd function of x. Equation (2.41), therefore represents the TE ***Odd Mode*** equation or the eigenvalue equation for the TE odd modes.

The eigenvalue equations for even and odd TE modes, equations (2.39) and (2.41) can be combined in a single eigenvalue equation by utilizing the trigonometric identity

$$\tan 2a = \frac{2\tan a}{1-\tan^2 a} \qquad (2.43)$$

This results in the following eigenvalue equation

$$\tan(2la) = \frac{2l\gamma}{l^2-\gamma^2} \qquad (2.44)$$

which is valid for both the even and the odd TE modes of the symmetric slab waveguide.

In addition to the finite number of guided modes, a dielectric slab waveguide supports also an infinite number of radiation modes [20] which are not included in the above relations.

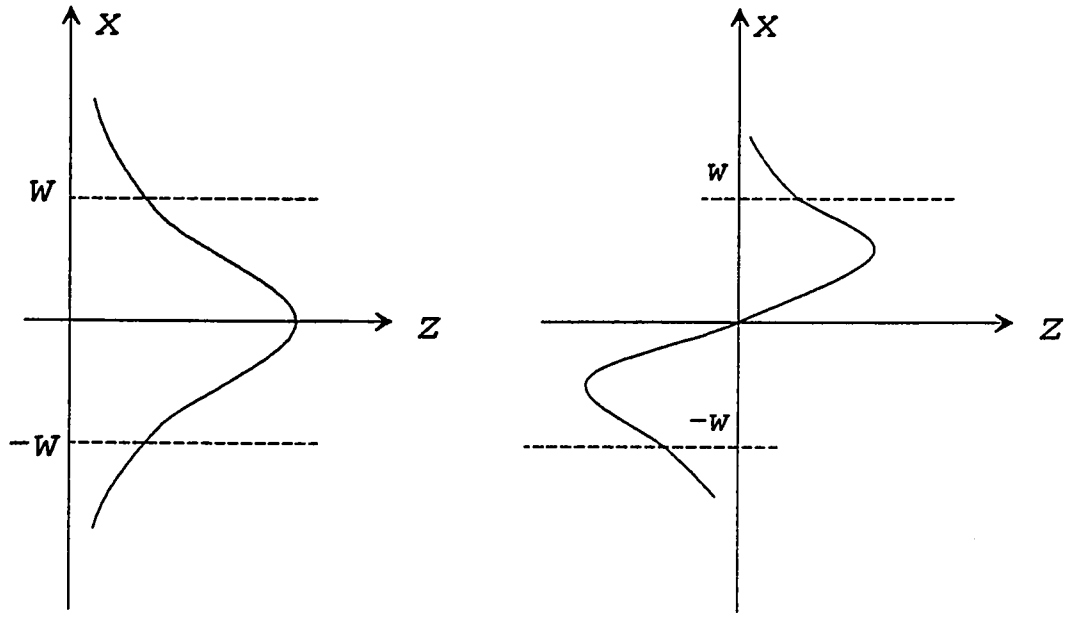

a) TE_0 (Even Mode)

b) TE_1 (Odd Mode)

Figure (2.3) *Examples of even and odd mode patterns in a symmetric dielectric slab waveguide.*

2.3 Coupling Techniques

As stated in the introductory Section (1.3), light can be coupled from a laser source into a slab dielectric waveguide by either evanescent [21] or endfire [22] coupling techniques. Evanescent coupling methods include prism and grating coupling and utilize the interaction between the evanescent field of the incident beam with the desired guided mode of the slab waveguide. Endfire or edge coupling involves shining the light beam directly or through a lens at the end facet of the slab waveguide. Examples of the edge coupling are the endfire and butt coupling. In the following subsections, we will provide a brief description of the above coupling techniques and investigate their most influencing parameters.

2.3.1 Prism Coupling

Figure (2.4) illustrates the prism coupling technique. In this method, the light is coupled into a dielectric slab waveguide through a triangular prism having a refractive index higher than that of the waveguide core. A small air

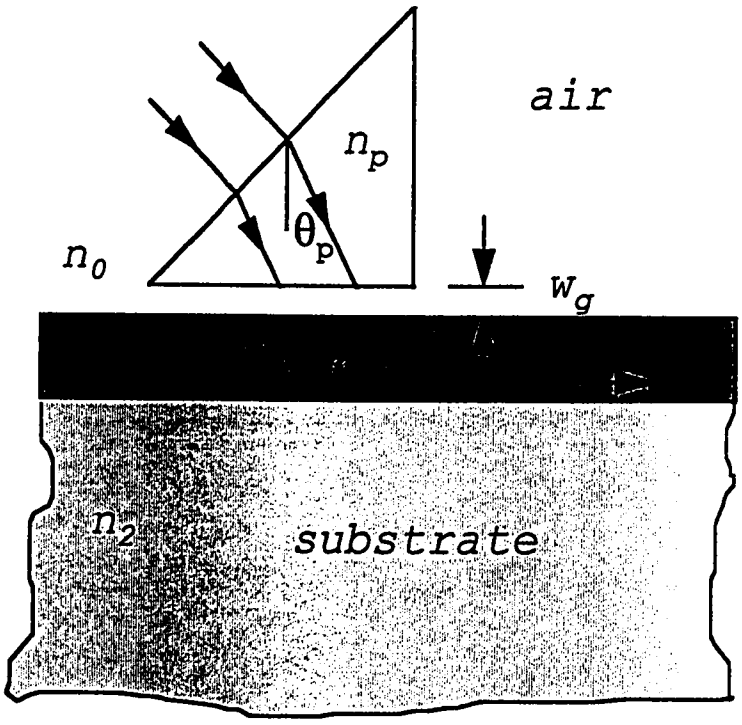

Figure (2.4) *Prism Coupling of light into a planar Waveguide.*

gap exists between the prism and the top surface of the waveguide.

If an incident beam strikes the prism at an angle greater than or equal to the critical angle, it will exhibit total reflection at the base of the prism. The interference between the incident and the reflected fields produces a standing wave in the prism in addition to a decaying field in the air gap between the prism and the waveguide.

For a sufficiently narrow air gap, interaction between the evanescent field in the prism and the propagating modes of the waveguide occurs which results in power coupling from the prism to the film. Efficient coupling requires matching of the longitudinal propagation constant β_m of the desired mth mode of the waveguide and that of the prism β_p. In other words,

$$k_0 n_p \sin\theta_p = k_0 n_1 \sin\theta_m$$

or

$$n_p \sin\theta_p = n_1 \sin\theta_m \qquad (2.45)$$

where n_p = *prism refractive index*

n_1 = *film refractive index*

θ_p = *incident angle*

θ_m = *mode-related angle*

The condition stated in equation (2.45) is often called *Synchronous or phase matching condition* [18,23]. It is clear from the above that in order to excite a particular waveguide mode, the incident angle (θ_p) must be adjusted so that the condition of synchronism is fulfilled. In addition to this condition, the air gap must be sufficiently small for efficient coupling and that the coupling length be optimum because, if allowed, the excited waveguide mode will couple back into the prism [15]. For a normal gap shape and a Gaussian beam, theoretical values of coupling efficiency of about 80% can be obtained [24]. Higher values can be achieved by using an air-gap with a tapered shape [12].

Prism coupling is practical for coupling light into a waveguide if the region above the film is air. It also does not require the critical alignment of edge coupling. Another advantage is that it is a mode selective coupling technique. Prism couplers however, require that the prism material refractive index be higher than that of the film [3,23]. That is

$$n_p > n_1 \tag{2.46}$$

This condition limits the application of the prism couplers for some waveguide materials and operational

wavelengths. Consequently, for waveguides having low and medium refractive indices, prism couplers might be easy to be fabricated. However, for guiding material with index higher than 2 such as Lithium Niobate *(LiNbO3);n=2.2* or Gallium Arsanide *(GaAs);n=3.6,* it is difficult to find a transparent material with a high refractive index that can be grounded into a prism [24].

2.3.2 Grating Coupling

The second example of evanescent field coupling is grating coupling. This type of coupling which was first introduced by Dakss et al., in 1970 [25], seems to be more compatible for use in integrated optics structures. Figure (2.5) depicts a schematic of a grating coupler. As can be seen from this figure, the structure of the grating coupler resembles that of the prism with the prism being replaced by a periodic dielectric grating layer. While in prism couplers, the incident plane wave is *refracted* into the thin film waveguide, in grating couplers, the incident beam is *diffracted* into the desired direction of propagation inside the thin film.

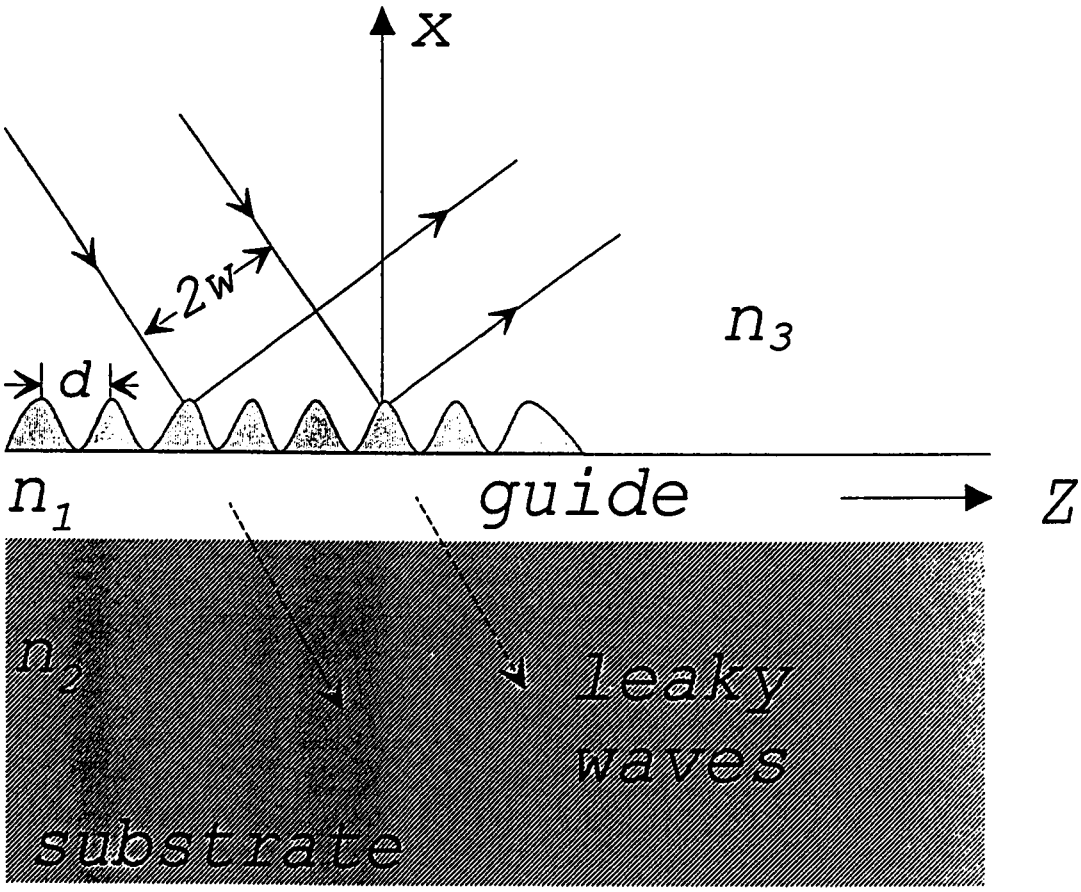

Figure (2.5) *A Schemetic of a grating coupler.*

Grating couplers can be classified according to the method of formation as etched, deposited, acoustic and holographic gratings [26]. These structures can be fabricated using photolithographic techniques by exposing a thick photoresist or dichromated gelatin layer to a periodic light pattern.

The way a grating coupler operates is similar to that of the prism. When an incident beam strikes the gratings, the beam is diffracted into transmitted waves. If the longitudinal propagation factor of any of these waves equals that of the desired propagating mode, it will excite it and power coupling takes place. A grating coupler can operate in the reverse direction as well by coupling a waveguide mode into a radiated field. In this scheme, the waveguide mode excites a radiation field at each periodic grating as shown in figure (2.6). If the scattering from these individual gratings adds up constructively, maximum coupling is achieved.

One feature of grating couplers is that they attain high efficiency only if the angle of the incident beam is maintained within a narrow range of coupling angles. This implies that grating coupling is sensitive to angle alignment. To avoid this sensitivity, the incident beam can

be focused which provides rays with an angular range that includes the optimum coupling angles [27].

Grating couplers are characterized by their convenient size and shape which allows them to be constructed directly on the integrated optics substrates since they can conform to the overall shape of the thin film. However, grating couplers have in general lower efficiency than prisms due to the fact that they produce more than one output beam.

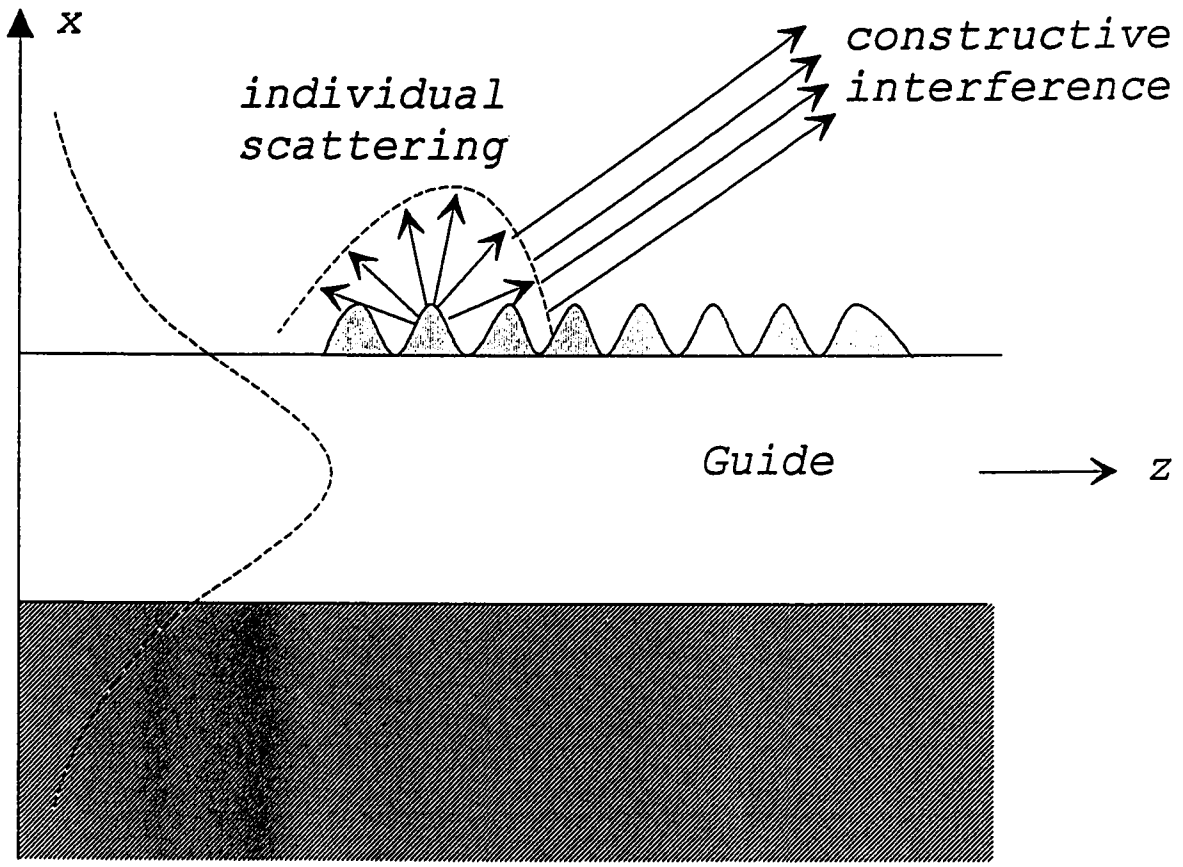

Figure (2.6) *Schemetic of a grating output coupler [18].*

2.3.3 Endfire/Butt Coupling

Excitation of a thin-film waveguide directly from a laser source known as edge coupling was first proposed by Marcuse and Marcatili [28] in 1971. Since then it has been investigated by several researchers [14,17,22,29,30,31,32].

Representatives of this coupling technique are *endfire* and *butt* coupling. In endfire coupling [33], light is focused using a lens into the facet of a wavequide. In butt coupling, light coupling is achieved by attaching the light source directly to the edge of the waveguide. This is illustrated in figure (2.7). In both ways, efficient coupling requires that the incident wave pattern matches that of the waveguide mode to be excited.

There are two main coupling losses associated with edge coupling. One is the power lost due to the miss-match between the incident field pattern and that of the guided modes. This is called *radiation loss*. The other is associated with the reflections from the coupled waveguide or *Fresnel loss*. The later can be reduced very dramatically by using antireflection coatings or an index-matching fluid.

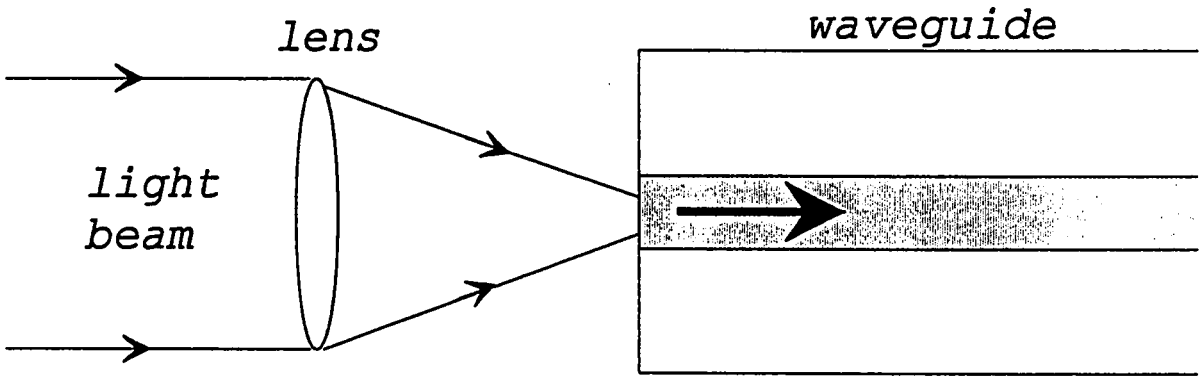

a) End-fire coupling

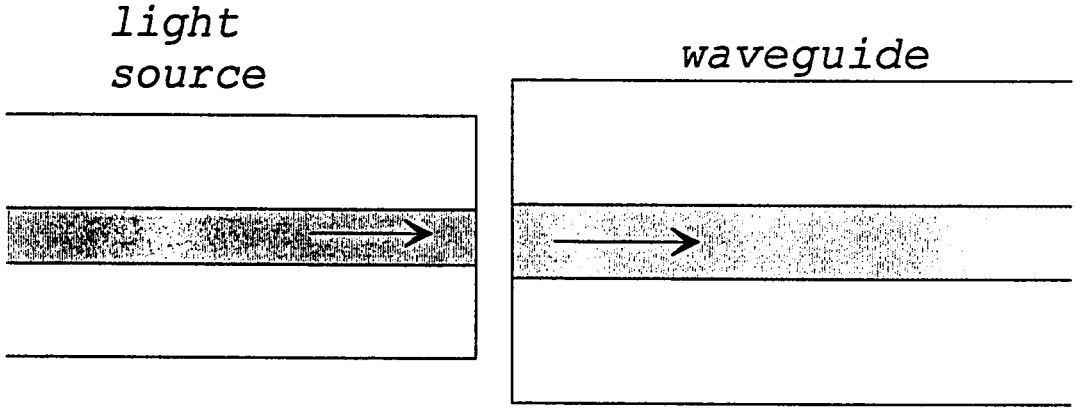

b) Butt-coupling

Figure (2.7) *Pictorial representation of edge coupling .*

Other losses might arise if the film face is not perfectly flat.

Butt coupling has the advantage of design simplicity and structural compactness. The spacing between the light source and the waveguide must be reduced to the smallest possible value. Lateral, axial, and angular alignment must also be observed.

2.3.3.1 Calculation of Power Coupling Efficiency in Edge Coupling

We start our derivation by using the fact that the field ψ at any point (x,z) can be expressed as a superposition of a complete set of normal modes $f_m(x)e^{j\beta_m z}$.

$$\psi(x,z) = \alpha_0 f_0(x)e^{j\beta_0 z} + \alpha_1 f_1(x)e^{j\beta_1 z} + \alpha_2 f_2(x)e^{j\beta_2 z} + \alpha_3 f_3(x)e^{j\beta_3 z} + \ldots\ldots$$

$$\ldots\ldots\ldots + \alpha_M f_M(x)e^{j\beta_M z} + \int_v \alpha_v f_v(x)e^{j\beta_v z}dv \qquad (2.47)$$

Here, α_m = *mth mode excitation coefficient.*

β_m = *mth mode propagation constant.*

$\int_{\nu}\alpha_{\nu}f_{\nu}(x)e^{j\beta_{\nu}z}d\nu$ represents an integration over the continuum of all radiation fields. The integer M represents the highest possible order of the guided modes. The modes $f_m(x)$, m=0,1,...,M describe a set of orthogonal functions that satisfy the complementary property

$$\int_{-\infty}^{\infty} f_n(x)f_m(x)dx = \begin{cases} 0 & n \neq m \\ c_n & n = m \end{cases} \qquad (2.48)$$

To calculate the coupling efficiency to the fundamental mode, we first evaluate the integral of $\psi(x,z)f_0(x)$ at z=0, and use the orthogonality principle. This leads to

$$\int_{-\infty}^{\infty}\psi(x,0)f_0(x)dx = \int_{-\infty}^{\infty}\alpha_0 f_0^2(x)dx + \int_{-\infty}^{\infty}\alpha_1 f_1(x)f_0(x)dx$$

$$+\int_{-\infty}^{\infty}\alpha_2 f_2(x)f_0(x)dx + \ldots\ldots\ldots + \int_{-\infty}^{\infty}\int_{-\infty}^{\infty}\alpha_{\nu}f_{\nu}(x)f_0(x)d\nu dx$$

$$= \alpha_0\int_{-\infty}^{\infty}f_0^2(x)dx = \alpha_0 c_0. \qquad (2.49)$$

resulting in

$$\alpha_0 = \frac{\int_{-\infty}^{\infty}\psi(x,0)f_0(x)dx}{\int_{-\infty}^{\infty}f_0^2(x)dx} \qquad (2.50)$$

where $\psi(x,0)$ represents the transmitted field distribution at $z=0$. In general, the *mth* mode excitation coefficient is given by

$$\alpha_m = \frac{\int_{-\infty}^{\infty} \psi_t(x) f_m(x) dx}{\int_{-\infty}^{\infty} f_m(x) f_m^*(x) dx} \tag{2.51}$$

For TE modes, the power flowing in the z direction per unit length of the y direction is given by [34]

$$P = \frac{1}{2}\int_{-\infty}^{\infty} \mathrm{Re}(E \times H^*)_z dx = -\frac{1}{2}\int_{-\infty}^{\infty} E_y H_x^* dx$$

$$= \frac{1}{2}\sqrt{\frac{\varepsilon}{\mu_0}}\int_{-\infty}^{\infty} |E_y|^2 dx = \frac{1}{2}\frac{n}{\eta_0}\int_{-\infty}^{\infty} |E_y|^2 dx \tag{2.52}$$

where n is the medium refractive index and η_0 is the intrinsic impedance of free space. Note that our earlier assumption that $\frac{\partial}{\partial y}=0$, implies that there is no field or geometrical variations in the y-direction.

Our main objective here is to calculate the efficiency of power coupling from a laser source into a slab waveguide. Coupling efficiency (η) is defined as the ratio of the guided power to the incident power, or

$$\eta = \frac{P_g}{P_i} \tag{2.53}$$

Consider a focused beam (region 1) having a field distribution ψ_i normally incident on the end face of a dielectric slab waveguide (region 2) as shown in figure (2.8). Assume that the difference between the refractive indices of the waveguide core and the cladding is small such that the medium in region 2 can be considered to be homogeneous with an effective index n_e. In such a case, the incident field time-averaged power flow P_i can be described by

$$P_i = \frac{1}{2}\frac{n_1}{\eta_0}\int_{-\infty}^{\infty} \psi_i(x).\psi_i^*(x)dx \qquad (2.54)$$

and the power coupled to the *mth* guided mode

$$P_g = \frac{1}{2}\frac{n_e}{\eta_0}|\alpha_m|^2 \int_{-\infty}^{\infty} f_m(x).f_m^*(x)dx \qquad (2.55)$$

where n_1 and n_e are the refractive indices in regions 1 and 2 respectively. Coupling efficiency is then given by

$$\eta = \frac{n_e|\alpha_m|^2}{n_1}\frac{\int_{-\infty}^{\infty} f_m(x).f_m^*(x)dx}{\int_{-\infty}^{\infty} \psi_i(x).\psi_i^*(x)dx} \qquad (2.56)$$

Substituting the value of the excitation coefficient of equation (2.51), equation (2.56) can be expressed as

$$\eta = \frac{n_e}{n_1}\frac{\left|\int_{-\infty}^{\infty} \psi_i(x).f_m^*(x)dx\right|^2}{(\int_{-\infty}^{\infty} f_m(x).f_m^*(x)dx)^2}\frac{(\int_{-\infty}^{\infty} f_m(x).f_m^*(x)dx)}{(\int_{-\infty}^{\infty} \psi_i(x).\psi_i^*(x)dx)} \qquad (2.57)$$

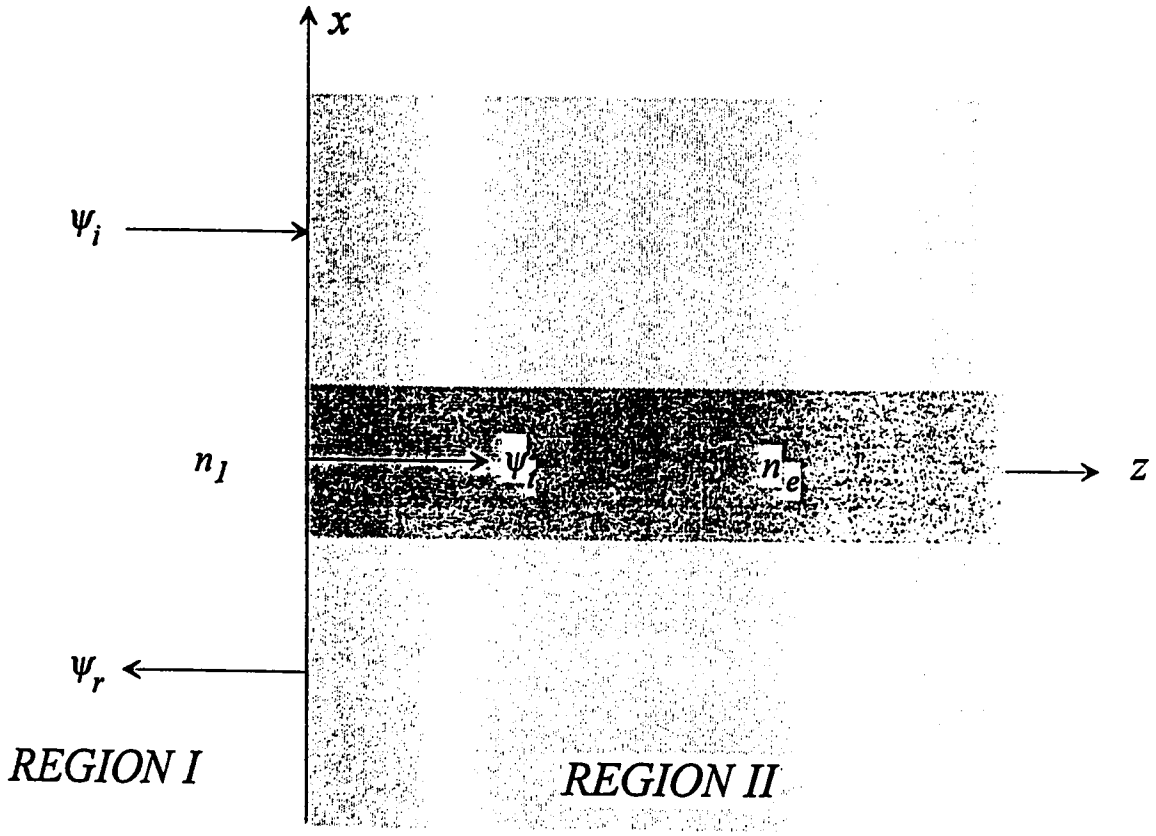

Figure (2.8) *The incident, reflected and transmitted fields of the coupling problem.*

which reduces to the following form

$$\eta = \frac{n_e}{n_1} \frac{\left| \int_{-\infty}^{\infty} \psi_t(x).f_m^*(x)dx \right|^2}{\int_{-\infty}^{\infty} \psi_i(x).\psi_i^*(x)dx \int_{-\infty}^{\infty} f_m(x).f_m^*(x)dx} \qquad (2.58)$$

Mueller et al.[29] stated that the coupling efficiency for the *mth* guided mode in endfire coupling can be described by the following overlap integral (see also [18] and [24])

$$\eta = \frac{\left| \int_{-\infty}^{\infty} \psi_i(x) f_m^*(x)dx \right|^2}{\int_{-\infty}^{\infty} \psi_i(x)\psi_i^*(x)dx \int_{-\infty}^{\infty} f_m(x) f_m^*(x)dx} \qquad (2.59)$$

It has been assumed in equation (2.59) that the end surface of the waveguide has an effective anti-reflection coating and the reflection losses are negligible such that the transmitted field can be replaced by the incident field. Comparing both of the above two expressions, we notice that in (2.59) the refractive indices for both media in regions 1 and 2 has been considered to be matched (no Fresnel loss) For the purpose of our treated waveguide, we cannot neglect the reflected power since the difference between the refractive indices of the waveguide and medium of incidence is considerable.

2.4 Laser Sources

Laser sources find many applications in optical fiber communications, manufacturing, medical fields, optical recordings, and space-based radar and tracking systems. There are many types of lasers examples of which are the semiconductor laser diode, the HeNe gas laser and the Nd:YAG solid-state ruby laser. Figure (2.9) shows schematically the structure of these three types. In what follows we will present a brief description of the main principle of the operation mechanism of laser sources in general.

According to quantum theory, the atoms of a gas (or isolated atoms) exist in discrete energy states. State transition from energy level E_2 to energy level E_1 occurs as a result of emitting or absorbing photons. The energy state difference is given by [35]

$$E = E_2 - E_1 = hf \qquad (2.60)$$

where $h = 6.626X10^{-34} J$ is Planck's constant and f is the radiation or absorption frequency. Atoms tend normally to be in the ground energy state. An atom in the upper energy level may drop to the ground level emitting a photon in the process. There are two types of emissions; spontaneous emission and stimulated emission.

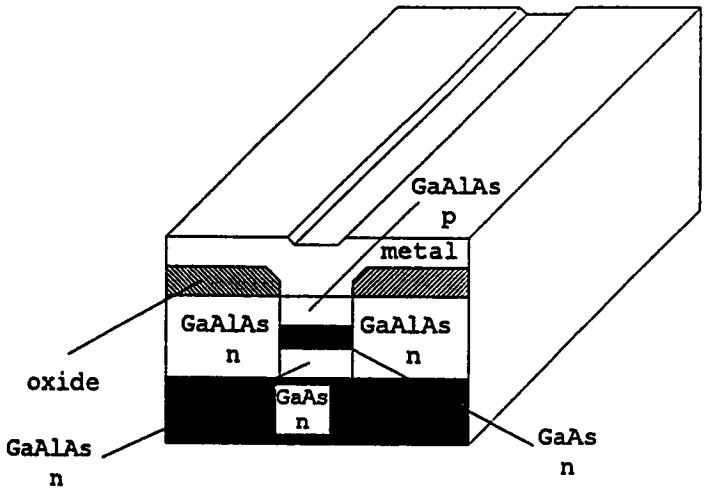

a) Semiconductor diode laser

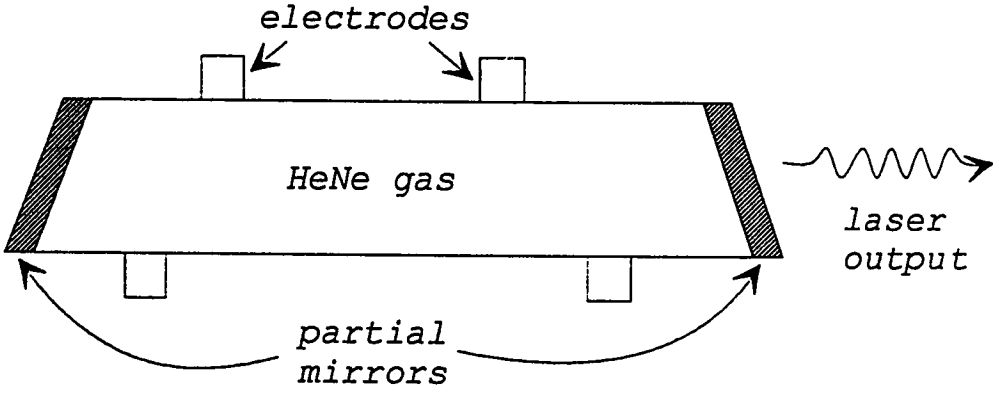

b) HeNe laser

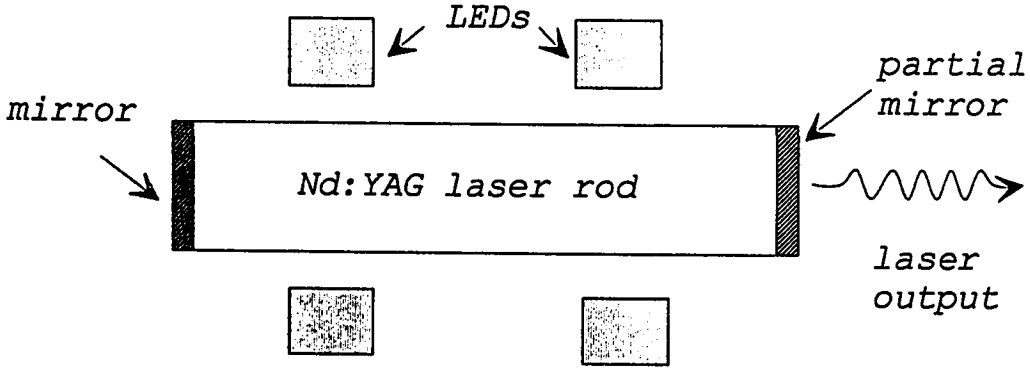

c) Nd:YAG laser

Figure (2.9) *Illustration of the laser sources types.*

In the *spontaneous emission*, the excited atoms decay back to the lower energy state by emitting a photon whose energy equals the difference between the two transition states $(E_2 - E_1)$. The phase, direction, and polarization of the emitted photon is random [36]. The light generated by an LED is an example of the spontaneous emission.

In contrast to the spontaneous emission, *stimulated emission* results in coherent amplification of the incident electromagnetic field. Stimulated emission takes place when a photon having energy $(E_2 - E_1)$; (i.e., frequency $f = \frac{E_2 - E_1}{h}$) interacts with an atom in its upper energy level stimulating it to drop to the lower level, thereby emitting a photon having the same frequency, phase, direction and polarization as that of the incident one. The light emitted by an LD is generated by stimulated emission. Figure (2.10) demonstrates both emission processes.

When the number of atoms in the upper energy level dominates; a condition known as *population inversion* exists. This means that more atoms can be stimulated to emit photons. The emitted photons will stimulate further emissions and thus resulting in coherent amplification. Laser oscillation requires optical feedback which is assured

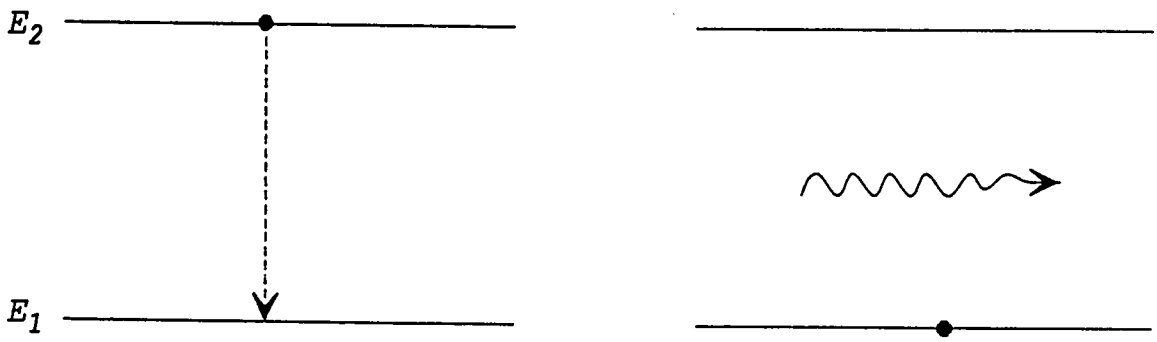

a) Spontaneous emission

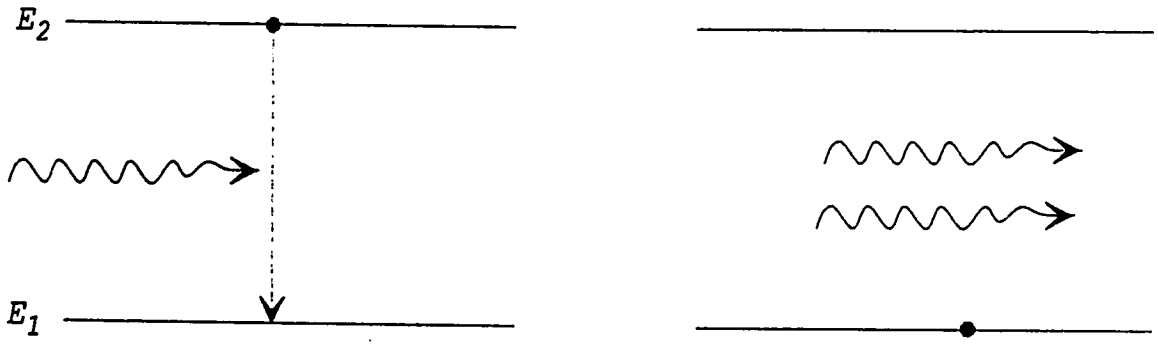

b) Stimulated emission

***Figure (2.10)** Spontaneous and stimulated emission.*

by placing partially reflecting walls at either side of the amplifying medium. In semiconductor lasers, this is achieved by cleaving both ends of the semiconductor crystal. In a gas laser, partially reflecting mirrors are placed at the two ends of the cavity.

Laser sources can produce multi-longitudinal modes or a single longitudinal mode. Single mode operation provides a narrower linewidth and more efficient coupling. Light emitted by a laser diode is normally polarized in the plane of the diode junction [18] and is elliptical in cross section with an angle of divergence of about 30 degrees. Recently, a team of researchers developed a semiconductor laser characterized by a nearly cylindrical beam that diverges by less than half a degree [37].

2.5 Microlens Systems

The purpose of lenses in lightwave systems is to focus the light source output into a spot that makes it more efficient for coupling to optical waveguides. The radiation surface of a laser source can have dimensions that vary from .5 to 4 μm in one direction and 4 to 15 μm in the other [38]. It is therefore required that a lens be inserted to focus the beam into a convenient spot size before coupling it into optical fibers or dielectric slab waveguides.

Figure (2.11) demonstrates the concept of focusing a light beam prior to coupling it into an optical waveguide using a thin lens. A collimated beam is focused into a spot that lies in a plane perpendicular to the axis of the lens known as *focal plane*. The center of the spot is called the *focal point*. The distance between the focal point and the lens is called the *focal length f*.

A thin lens acts as a phase transformer [20]. The incident plane wave in front of the lens is transformed into a spherical wave that converges behind the lens on the focal point as depicted in figure (2.12).

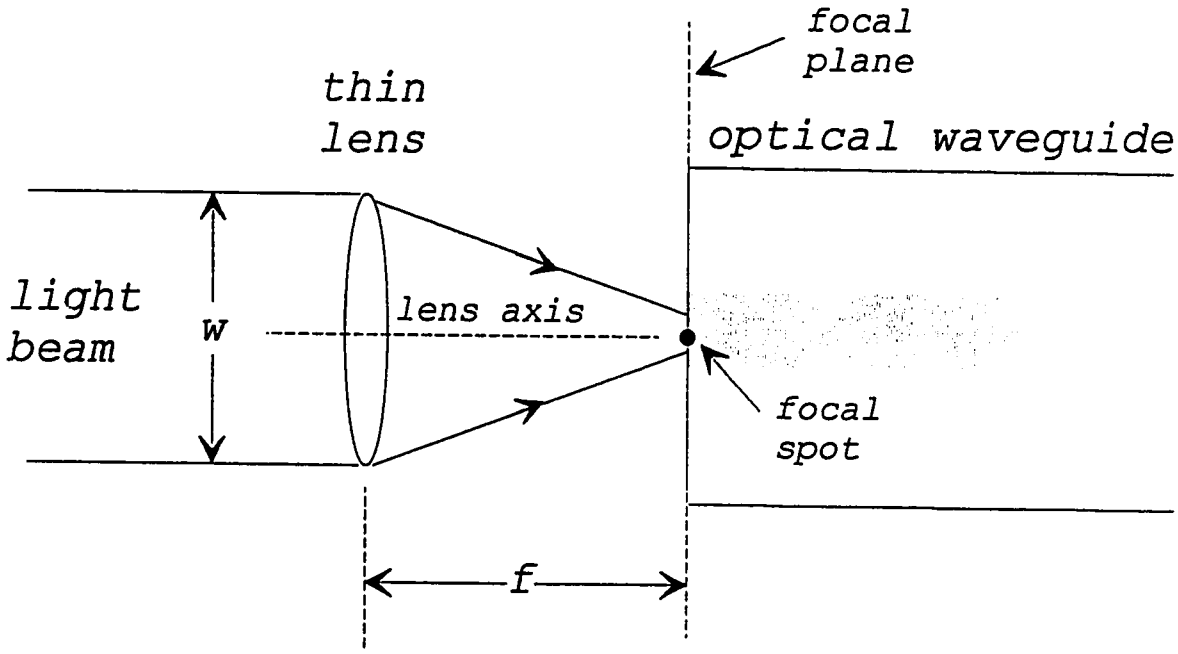

Figure (2.11) *Focusing of a light beam into an optical slab waveguide.*

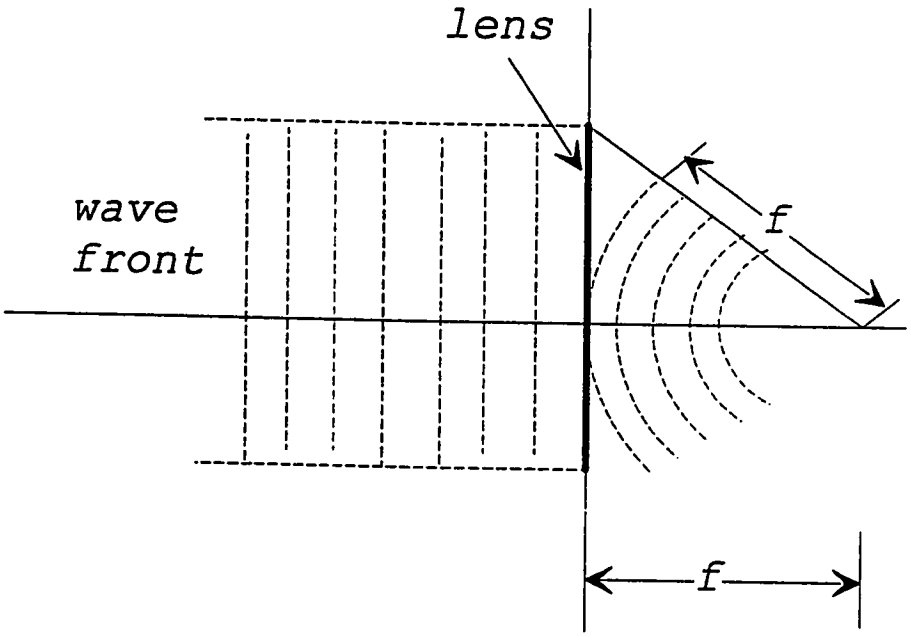

Figure (2.12) *Incident wave phase transformation [20].*

Cohen and Schneider [39] showed that improved coupling efficiencies can be obtained by using a sufficiently small lens fabricated on an optical fiber end surface. This lens is called a *microlens*. Since then, a variety of microlenses schemes were reported. This included microlens arrays and integrated microlenses.

Fabrication methods of microlenses can be listed as [38]: photolithography, chemical etching, thermal melting, and mechanical polishing methods. In the first technique, the microlenses are made directly from light-sensitive polymers called photoresist that is deposited on the end face of the optical fiber. Lenses fabricated by the chemical etching technique are formed by immersing the fiber into an etchant solution [38]. Because etching has different rates in the core and cladding, the endface becomes conical and a microlens is formed. In thermal melting technique, the fiber end is heated until it melts into a hemispherical shape. In the fourth technique, the fiber ends is mechanically polished into a particular shape and then melted to form the desired microlens.

In *integrated microlenses*, the first semiconductor lasers with converging output beams was reported by Mukai et al. in 1985 [40]. In this work, photoresist film was deposited on

the top of laser electrode. The film blocks electron injection and causes variation in the lateral distribution of the gain and refractive index. It was found that the resultant laser beam width decreases with distance from 30 μm at the facet down to 7 μm at 111 μm off the facet. Another work by Mukai et al. in 1985, reported the integration of a lens inside a diode-laser cavity for beam convergence [41]. The lens was formed on one end of the waveguide by making the refractive index decreases towards the edges. The lens resulted in a laterally converging laser beam. The resultant output beam width had a minimum of 4 μm at 18 μm off the diode facet. In 1989, Mukai and his colleagues integrated an electronic lens inside the laser diode cavity [42]. The lens controls the focus position of its laterally converging output beam by varying the current applied to the lens electrodes.

2.6 Integrated Optics

Integrated Optics is a field of technology that deals with the construction of optical devices and networks on planar thin films or strips. The objective here is to provide more convenient and compact interfaces between electronic and optical systems, thereby improving efficiency, increasing reliability, and decreasing power consumption. This potential gave integrated optics an increasing interest from researchers in the past years which resulted in the variety of optical devices and circuits that have been integrated. This includes optical switches, high speed modulators, filters, microlenses, light source couplers, photonic repeaters, and wavelength multiplexing circuits.

Two techniques are followed for the construction of integrated optics [21]. The first is known as *hybrid integration*, in which each optical component is realized individually with its optimum material. Different parts are then integrated together and interconnected using optical or electronic buses. This technique results in heavy and bulky structures. In addition, the internal interconnections have

associated losses and reflections which degrades the overall performance of the integrated system.

The second technique is called *monolithic integration* and it resembles the methods used in integrated circuits. Here, all the different components and functions are fabricated in a single semiconductor wafer. Representatives of this technique are the monolithic integration of a laser source or a photodiode and optical waveguide and the integration of a lens inside a diode-laser cavity (see for example [21], [41] and [43]).

CHAPTER III

THE METHOD OF LINES

3.1 Introduction

Various numerical algorithms have been adopted for the analysis of the different waveguide structures. Among these techniques is ***the Method of Lines (MoL)***. This method is a semi-analytical technique which results in higher accuracy, less computational time and smaller storage requirements [11,44].

The MoL was originally devised to solve partial differential equations. Therefore, its technique resembles that of the Finite Difference Method except for the fact that for an n-independent variable partial differential equations system, only (n-1) of these variables are discritized to obtain a system of ordinary differential equations [6].

In contrast to many numerical methods, the MoL can account for the back-reflected field due to longitudinal inhomogenities. The well-known Beam Propagation Method (BPM) [4] is an example of numerical methods which cannot account for the backward reflected field. The Finite Difference Time Domain (FDTD) method [5] can account for longitudinal discontinuities. However, this method is completely numerical which can be very inefficient especially in the treatment of multiple discontinuities. The FDTD is also a time-domain method. This causes it to be less efficient in the treatment of steady-state problems, such as the one under consideration. In the MoL, the computation of the reflected field can be achieved to a high accuracy which permits the analysis of planar waveguides having longitudinal inhomogenities, step discontinuities, or periodic structures. The MoL is also characterized by its easy and straight forward implementation through the use of linear algebra properties on the resulting matrices.

The MoL has been applied to several types of planar longitudinally uniform waveguide problems. It also has been applied in the analysis of planar microwave structures [9], in the analysis of microstriplines [45], in the analysis of planar multi-conductor transmission line systems existing in planar microwave components such as directional couplers and

phase shifters [46] and in the calculation of the mode characteristics of planar strip-loaded optical waveguides [44].

The MoL has also been extended to waveguide problems with two-dimensional variations. Examples of that are resonators, and longitudinally periodic structures in which the metallization contours are two dimensional which imposes that discretization be done in two directions. This has been applied by Worm and Pregla to various problems [10].

In a recent paper [11], the MoL has been applied to study longitudinally varying structures. It was demonstrated that the MoL is capable of treating longitudinal discontinuities in optical slab waveguides with calculations of the resultant reflections and radiation. In this thesis work, we will apply the MoL in Chapter IV for the treatment of one longitudinal discontinuity resulting from coupling of a Gaussian beam into a slab waveguide. The method is then extended in Chapter V for the analysis of problem containing two longitudinal discontinuities by inserting an anti-reflection layer at the end face of the waveguide.

3.2 Principle of the Algorithm

In the (MoL), equations are discretized in one coordinate and calculated analytically in the other coordinate [6]. For the waveguide structure under investigation, the waveguide geometry will be discretized in the transverse direction (the direction normal to the direction of propagation) and treated analytically in the longitudinal direction (the direction of propagation).

Figure (3.1) shows a planar waveguide structure in which the interfaces of layers are parallel to the x-axis. Consequently, discretization will be applied along the x-axis. This implies that the fields will be calculated on lines that are equidistant from each other and parallel to the *z*-axis. The investigated structure will be bounded by electrical walls. The resulting difference equations are then decoupled and manipulated through algebraic transformation.

In some instances, it might be more advantageous to have nonequidistant discretization. An Example of that is the case when the widths of the different structure layers exhibit extreme differences which results in increasing the

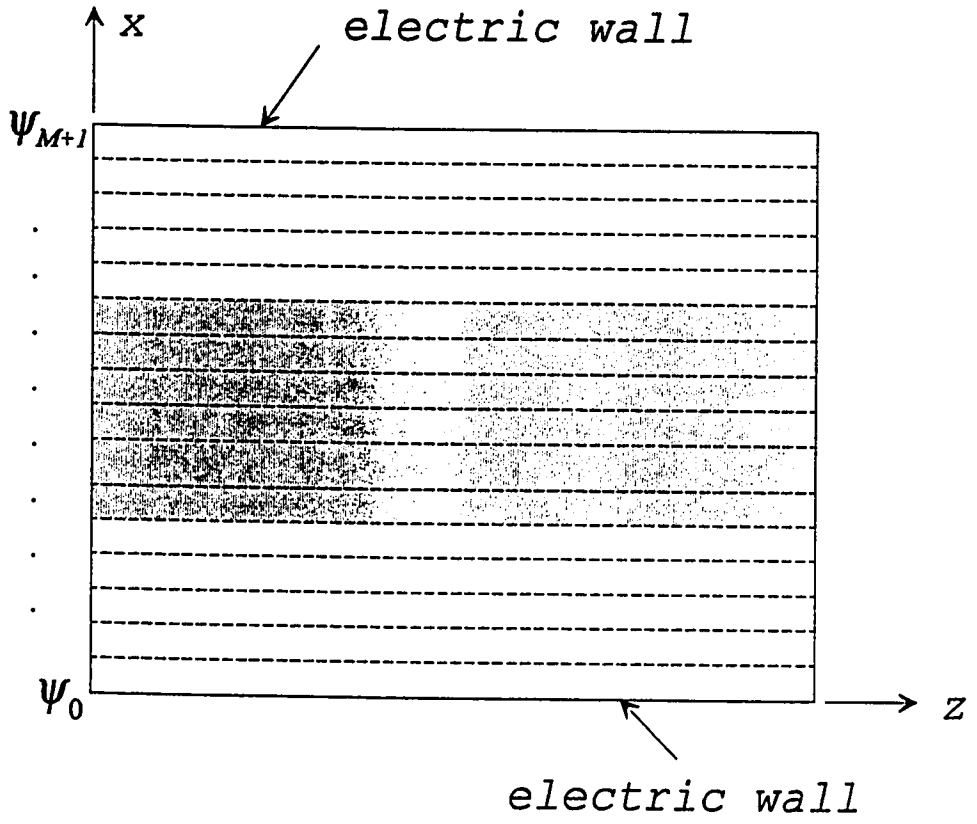

Figure (3.1) *Discretization lines on a planar waveguide.*

number of lines and, consequently the associated computational time can vary dramatically. In such cases, the distance between lines is increased in regions where the field exhibits smaller variations [46,47].

3.3 Mathematical Formulation

Starting with Maxwell's equations for TE polarized waves in two dimensions (assuming that $\frac{\partial}{\partial y}=0$) and following the analysis of section (2.2) we obtain the two-dimensional ***wave equation***:

$$\frac{\partial^2 \psi}{\partial x^2}+\frac{\partial^2 \psi}{\partial z^2}+k_0^2 n^2 \psi=0 \qquad (3.1)$$

where: $\psi = E_y$

$k_0 = \frac{2\pi}{\lambda_0}$

λ_0 = *free space wavelength*

n = *the refractive index of the medium*

In the MoL, both ψ and n in the above equation are discretized with respect to x and calculated on lines in the z-direction (direction of propagation). To put the field ψ

in a discretized form, we need to approximate its second derivative. This can be accomplished using the three-point central difference approximation as will be described in the following section.

3.3.1 The Three-Point Central Difference Approximation

In order to obtain an expression for the discretized second derivative of a certain function, we start by expressing this function in terms of a power series. By neglecting all but the first few terms of the resulting series, we can have a good approximation of the given function in terms of a polynomial. One of the most convenient power series is ***the Taylor's Series*** which can be expressed as:

$$f(x)=\sum_{n=0}^{\infty}\frac{f^{(n)}(a)}{n!}(x-a)^n \qquad (3.2)$$

where $f^{(n)}$ is the nth derivative with respect to x.

If Taylor's series is expanded about $x=0$, the resulting series is often called a ***Maclaurin's Series*** expansion. Expanding $\psi(x)$ about $x=0$, and following the above expression:

$$\psi(x)=\psi(0)+\frac{\psi'(0)}{1!}x+\frac{\psi^{(2)}(0)}{2!}x^2+\frac{\psi^{(3)}(0)}{3!}x^3+\frac{\psi^{(4)}(0)}{4!}x^4+\frac{\psi^{(5)}(0)}{5!}x^5+.....$$

Evaluating this equation at $x=\pm\Delta x$ results in:

$$\psi_1=\psi(\Delta x)=\psi(0)+\frac{\psi'(0)}{1!}\Delta x+\frac{\psi^{(2)}(0)}{2!}(\Delta x)^2+\frac{\psi^{(3)}(0)}{3!}(\Delta x)^3+\frac{\psi^{(4)}(0)}{4!}(\Delta x)^4+\frac{\psi^{(5)}(0)}{5!}(\Delta x)^5+.....$$

$$\psi_{-1}=\psi(-\Delta x)=\psi(0)-\frac{\psi'(0)}{1!}\Delta x+\frac{\psi^{(2)}(0)}{2!}(\Delta x)^2-\frac{\psi^{(3)}(0)}{3!}(\Delta x)^3+\frac{\psi^{(4)}(0)}{4!}(\Delta x)^4-\frac{\psi^{(5)}(0)}{5!}(\Delta x)^5+.....$$

Adding ψ_1 and ψ_{-1} :

$$\psi_1+\psi_{-1}=2\psi(0)+\psi^{(2)}(0)(\Delta x)^2+\frac{\psi^{(4)}(0)}{12}(\Delta x)^4+.....$$

this leads to:

$$\psi^{(2)}(0)=\frac{\psi_1-2\psi(0)+\psi_{-1}}{(\Delta x)^2}-\frac{\psi^{(4)}(0)}{12}(\Delta x)^2-.....$$

which can be approximated as:

$$\psi'(0)\approx\frac{\psi_1-2\psi(0)+\psi_{-1}}{(\Delta x)^2} \qquad (3.3)$$

It is apparent from equation(3.3) that the leading error resulting from the approximation is proportional to $(\Delta x)^2$.

3.3.2 Discretization of the Wave Equation

By replacing the second derivative of ψ with respect to x by the three-point central difference approximation, equation (3.1) can be written as:

$$\frac{\psi_{i+1}(z)-2\psi_i(z)+\psi_{i-1}(z)}{(\Delta x)^2}+\frac{d^2\psi_i(z)}{dz^2}+k_0^2n_i^2\psi_i(z)=0 \qquad (3.4)$$

with $x=i\Delta x$

If the field in the x-direction is discretized into M points, then equation (3.4) yields the following M equations:

$i=1:$ $$\frac{1}{(\Delta x)^2}[\psi_2-2\psi_1+\psi_0]+\frac{d^2}{dz^2}[\psi_1]+k_0^2n_1^2[\psi_1]=0$$

$i=2:$ $$\frac{1}{(\Delta x)^2}[\psi_3-2\psi_2+\psi_1]+\frac{d^2}{dz^2}[\psi_2]+k_0^2n_2^2[\psi_2]=0$$

$i=3:$ $$\frac{1}{(\Delta x)^2}[\psi_4-2\psi_3+\psi_2]+\frac{d^2}{dz^2}[\psi_3]+k_0^2n_3^2[\psi_3]=0$$

.

.

.

$$i=M: \qquad \frac{1}{(\Delta x)^2}[\psi_{M+1}-2\psi_M+\psi_{M-1}]+\frac{d^2}{dz^2}[\psi_M]+k_0^2 n_M^2[\psi_M]=0 \tag{3.5}$$

In matrix form, the above equations become

$$\frac{1}{(\Delta x)^2}\begin{bmatrix} -2 & 1 & 0 & 0 & \dots & 0 \\ 1 & -2 & 1 & 0 & \dots & 0 \\ 0 & 1 & -2 & 1 & : & : \\ : & 0 & 1 & -2 & : & 0 \\ : & : & 0 & : & : & 1 \\ 0 & 0 & 0 & \dots & 1 & -2 \end{bmatrix}\begin{bmatrix} \psi_1 \\ \psi_2 \\ \psi_3 \\ : \\ : \\ \psi_M \end{bmatrix}+\frac{d^2}{dz^2}\begin{bmatrix} \psi_1 \\ \psi_2 \\ \psi_3 \\ : \\ : \\ \psi_M \end{bmatrix}$$

$$+k_0^2\begin{bmatrix} n_1^2 & 0 & 0 & \dots & \dots & 0 \\ 0 & n_2^2 & 0 & 0 & \dots & 0 \\ 0 & 0 & n_3^2 & 0 & : & : \\ : & 0 & 0 & . & : & 0 \\ : & : & : & : & . & 0 \\ 0 & 0 & 0 & \dots & 0 & n_M^2 \end{bmatrix}\begin{bmatrix} \psi_1 \\ \psi_2 \\ \psi_3 \\ : \\ : \\ \psi_M \end{bmatrix}=\begin{bmatrix} 0 \\ 0 \\ : \\ : \\ 0 \\ 0 \end{bmatrix} \tag{3.6}$$

In the above representation, we have assumed that the structure under study is bounded by electric walls in the x-direction as shown in figure (3.1),i.e.,

$$\psi_0=0$$

and

$$\psi_{M+1}=0$$

Equation (3.6) can be represented in the following simplified vector form:

$$\frac{1}{(\Delta x)^2}C\Psi+\frac{d^2}{dz^2}\Psi+k_0^2N\Psi=0 \qquad (3.7)$$

Where: $C=$ a tri-diagonal second order central difference matrix.

$\Psi=$ $[\psi_1\psi_2\psi_3.....\psi_M]^T$

$N=$ a diagonal matrix, whose elements are $n_1^2,n_2^2,n_3^2,.....,n_M^2$.

Note that capital letters are used to indicate matrices.

By rearranging the terms of equation (3.7) and introducing a new MxM matrix, Q, this equation acquires the following form:

$$\frac{d^2}{dz^2}\Psi+Q\Psi=0 \qquad (3.8)$$

Where the MxM matrix Q is defined as:

$$Q=\frac{1}{(\Delta x)^2}C+k_0^2N \qquad (3.9)$$

Equation (3.8) is a second order ordinary matrix differential equation whose formal solution is:

$$\Psi=e^{jQ^{1/2}z}A+e^{-jQ^{1/2}z}B \qquad (3.10)$$

Where $(e^{jQ^{1/2}z})$ represents the part of the field propagating in the positive z-direction, while $(e^{-jQ^{1/2}z})$ is associated with the propagation in the opposite direction.

Substituting $z=0$, in equation (3.10) results in:

$$\Psi = A + B \tag{3.11}$$

This means that the Mx1 column matrix A represents the incident field at $z=0$, while matrix B represents the reflected field at $z=0$.

The matrices $(e^{jQ^{1/2}z})$ and $(e^{-jQ^{1/2}z})$ are calculated by diagonalizing the matrix Q and finding its eigenvalues and eigenvectors. If U is the eigenvector matrix and V is the eigenvalue matrix of Q satisfying the relation

$$Q = UVU^{-1} \tag{3.12}$$

then, the matrix exponential can be found using this fact from linear algebra

$$e^{jQz} = U.e^{jVz}.U^{-1} \tag{3.13}$$

3.4 The Application of the MoL to the Coupling Problem:

The MoL main principles introduced and the mathematical relations derived in the previous section will be applied in this section to analyze the coupling of an incident field into a slab waveguide.

Figure (3.2) depicts a field incident from air; region (0), into a slab waveguide residing in region (1). The field in region (0) is described by two terms; $e^{j\Omega_0^{1/2}z}A_0$ which represents that part of the field propagating in the positive z-direction, and $e^{-j\Omega_0^{1/2}z}B_0$ which represents the reflected field propagating in the negative z-direction. In region (1) there is only a transmitted field given by the term $e^{j\Omega_1^{1/2}z}A_1$.

A percentage of the incident field power will be transmitted to the slab waveguide and the rest will be reflected. Part of the transmitted power will be coupled to the guided modes. The other part of the transmitted power will be coupled to radiation modes and thus will be radiated.

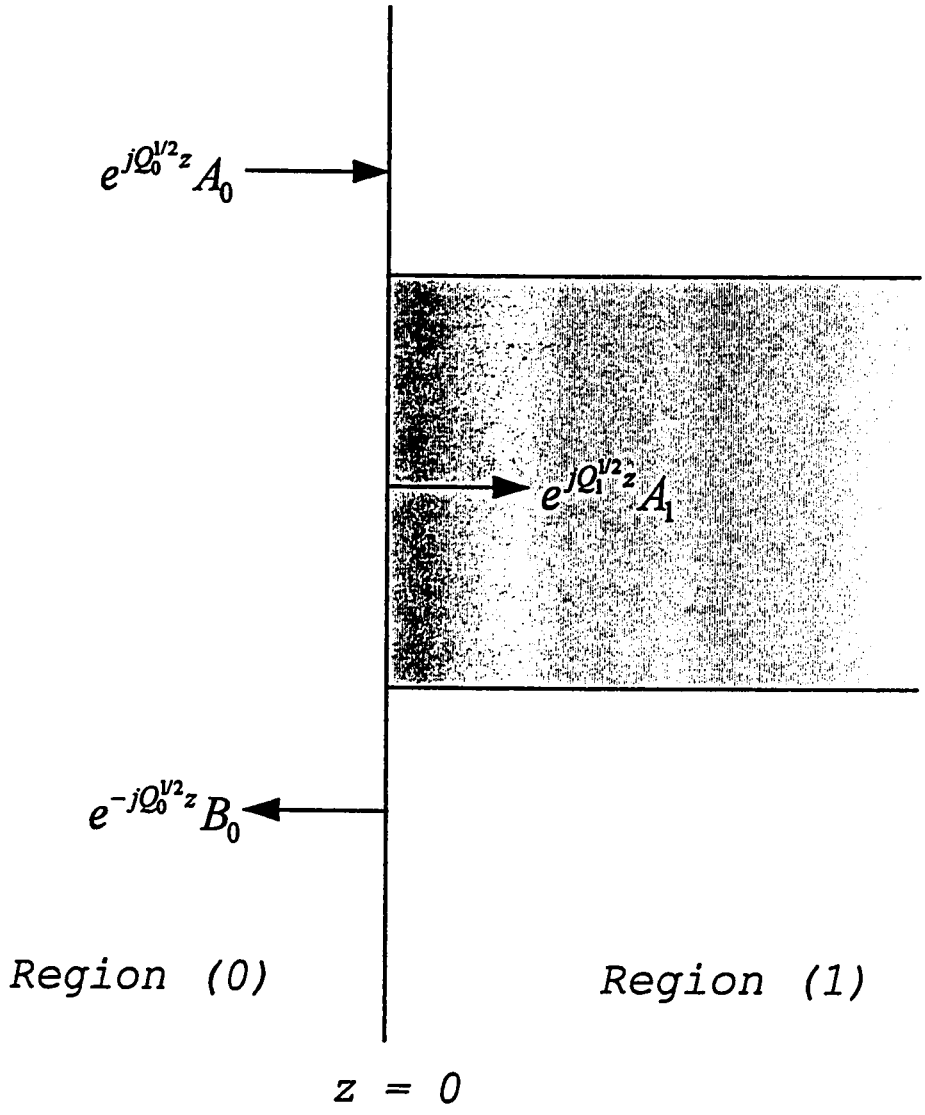

Figure(3.2) *The incident, reflected and transmitted fields using the Method of Lines.*

Based on the above and following equation (3.10), the existing fields in region (0); Ψ_0 and in region (1); Ψ_1 can be expressed as:

$$\Psi_0 = e^{jQ_0^{1/2}z}A_0 + e^{-jQ_0^{1/2}z}B_0 \tag{3.14}$$

$$\Psi_1 = e^{jQ_1^{1/2}z}A_1 \tag{3.15}$$

For TE polarized fields, both Ψ and its first derivative with respect to z are continuous at the boundary. Continuity of Ψ at $z=0$ yields:

$$\Psi_0 = \Psi_1 \tag{3.16}$$

which results in:

$$A_0 + B_0 = A_1 \tag{3.17}$$

or

$$B_0 = A_1 - A_0 \tag{3.18}$$

Continuity of $\frac{d}{dz}\Psi$ at $z=0$, yields:

$$\frac{d}{dz}\Psi_0 = \frac{d}{dz}\Psi_1 \tag{3.19}$$

Differentiating equations (3.14) and (3.15) with respect to z leads to:

$$\frac{d}{dz}\Psi_0 = jQ_0^{1/2}e^{jQ_0^{1/2}z}A_0 - jQ_0^{1/2}e^{-jQ_0^{1/2}z}B_0 \tag{3.20}$$

and

$$\frac{d}{dz}\Psi_1 = jQ_1^{1/2}e^{jQ_1^{1/2}z}A_1 \tag{3.21}$$

results in:

$$jQ_0^{1/2}e^{jQ_0^{1/2}z}A_0 - jQ_0^{1/2}e^{-jQ_0^{1/2}z}B_0 = jQ_1^{1/2}e^{jQ_1^{1/2}z}A_1 \tag{3.22}$$

Substituting $z=0$, in equation (3.22):

$$Q_0^{1/2}A_0 - Q_0^{1/2}B_0 = Q_1^{1/2}A_1 \tag{3.23}$$

or

$$A_0 - B_0 = Q_0^{-1/2}Q_1^{1/2}A_1 \tag{3.24}$$

B_0 can be eliminated by adding equations (3.17) and (3.24)

$$2A_0 = (I + Q_0^{-1/2}Q_1^{1/2})A_1 \tag{3.25}$$

where I is the identity matrix. Therefore,

$$A_1 = 2(I + Q_0^{-1/2}Q_1^{1/2})^{-1}A_0 \tag{3.26}$$

The incident field at $z=0$; A_0 is known. Therefore, the transmitted field at $z=0$; A_1 can be calculated from (3.26). The value of the transmitted field for $z>0$ can be easily calculated by multiplying A_1 by $e^{jQ_1^{1/2}z}$

$$A\big|_{z=z_1} = e^{jQ_1^{1/2}z_1}A_1 \tag{3.27}$$

3.5 Convergence of the MoL

The Convergence behavior of the results of a numerical method serves as a good indicator of the accuracy of the chosen parameters. One important parameter in the MoL is the number of discretization lines (M). The accuracy of the results should improve as the number M increases. However, as M increases, the computational time increases dramatically. Therefore, it is important to choose the proper number of M that results in convergence of solutions.

For planar waveguide structures, singularities might appear at the edges or borders of two different layers and the solutions at these particular points might not converge. The problem of improper solution convergence does not occur in the MoL. However, in the case of existence of singularities, larger discretization errors might be observed [6]. Reference [48] presents a detailed procedure for minimizing these errors. One possible solution to this problem is to ensure that the edges of the investigated structure are contained between two discretization lines. In our analysis, we ensured that the structure borders are contained between lines to minimize the discretization errors at these singular points.

The validity of the MoL results can be tested by monitoring the power conservation at the coupling boundary. The ratio of the reflected power to the incident power, R is defined as

$$R=\frac{P_r}{P_i} \tag{3.28}$$

Similarly, the ratio of the transmitted power to the incident power, T is defined as

$$T=\frac{P_t}{P_i} \tag{3.29}$$

In order to have conservation of power, R and T shall sum to unity, i.e.,

$$R+T=1 \tag{3.30}$$

In Chapter IV, we present numerical results that show the convergence behavior of the MoL. The effect of increasing the number of discretization lines M on the computational time will be also provided.

CHAPTER IV

ANALYSIS OF GAUSSIAN BEAM COUPLING TO DIELECTRIC SLAB WAVEGUIDE

4.1 Introduction

The problem of efficient light coupling from a laser source into a slab waveguide is a crucial design parameter in the implementation of high-speed optical communications as well as in the fabrication of integrated optics. The development of low-loss optical waveguides makes the lost power at the coupling interface of great importance since it will account for a considerable percentage of the overall power loss.

The main problem associated with the coupling of the laser source beam output is that this beam diverges from the emitting surface. Another problem is that the dimensions related to this coupling operation are very small, thus

making the allowable alignment tolerances very limited. Typically, the dimensions of laser diode radiating surface ranges between .5 and 4 μm in one side, and 4 to 15 μm in the other side [38]. As will be explained later, the laser source radiation output profile can be approximated by a two-dimensional Gaussian beam. A lens system will focus the laser source output beam into a symmetrical Gaussian beam which can be then coupled to the dielectric slab waveguide under consideration.

The MoL will be implemented in this chapter to investigate the optimum value of the parameters that mostly affect the coupling efficiency. These parameters include the incident Gaussian Half Beam Width (HBW), the location of the beam waist, the waveguide core width as well as the effect of the lateral and longitudinal offsets.

4.2 Gaussian Beam Approximation of the Laser Source Radiation Profile

For the purpose of calculating the power coupling efficiency between a laser source and a dielectric slab waveguide, an expression for the laser source output electric field pattern is required. Different forms of field profiles approximating the pattern of laser sources have been reported in the literature [8,20,29,38]. Whereas Zachos [49] showed experimentally that semiconductor laser beams have Gaussian intensity profiles, most researchers based their expressions on the concept that the radiation field ψ_{nm} of a laser source can be *approximated* by the following elliptical Hermite-Gaussian product [50]

$$\psi_{nm} = E_0 H_n\left(\sqrt{2}\frac{x}{w_x}\right) H_m\left(\sqrt{2}\frac{y}{w_y}\right) \exp\left[-\frac{x^2}{w_x^2} - \frac{y^2}{w_y^2}\right] \qquad (4.1)$$

where w_x and w_y are functions of z and define the Gaussian Half Beam Width (HBW) along the x and the y axes respectively (with $w_x \neq w_y$), and $H_k(x)$ are *Hermite polynomials* defined by

$$H_k(x) = (-1)^k e^{x^2} \frac{d^k}{dx^k} e^{-x^2} \qquad (4.2)$$

where the subscript k in the above expression stands for either n or m. The first three Hermite polynomials are therefore given by

$$\begin{aligned} H_0(x) &= 1 \\ H_1(x) &= 2x \\ H_2(x) &= 4x^2 - 2 \end{aligned} \tag{4.3}$$

Using the results of equation (4.3) in (4.1), we can plot ψ_n for n = 1, 2 and 3 as shown in figure (4.1).

Most laser diode outputs can be approximated by the lowest order Hermite-Gaussian mode which corresponds to a pure two dimensional Gaussian mode since the lowest order Hermite polynomial is unity. Applying this approximation, equation (4.1) reduces to

$$\psi_{nm} = E_0 \exp\left[-\frac{x^2}{w_x^2} - \frac{y^2}{w_y^2}\right] \tag{4.4}$$

If we consider the dimensions of a laser source radiating surface [38], we notice that the dimensions along the y-axis are multiples of those along the x-axis. This implies that the Gaussian beam along the y-axis has a larger HBW as compared to its HBW along the x-axis. The field can then be considered with very good approximation to have a uniform profile along the y-axis, and the expression of (4.4) reduces to

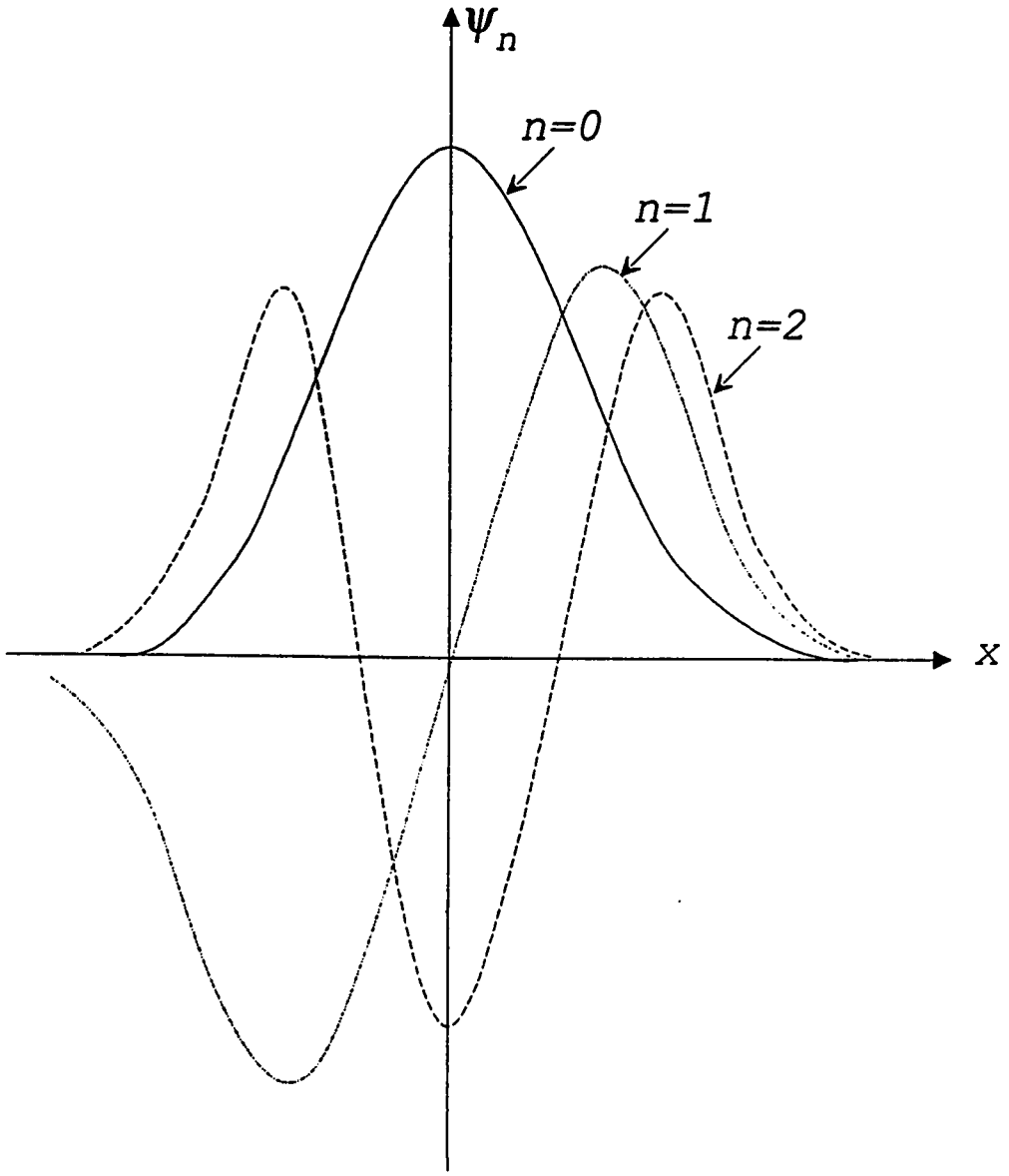

Figure(4.1) *Schemetic of the first three Hermite-Gaussian modes.*

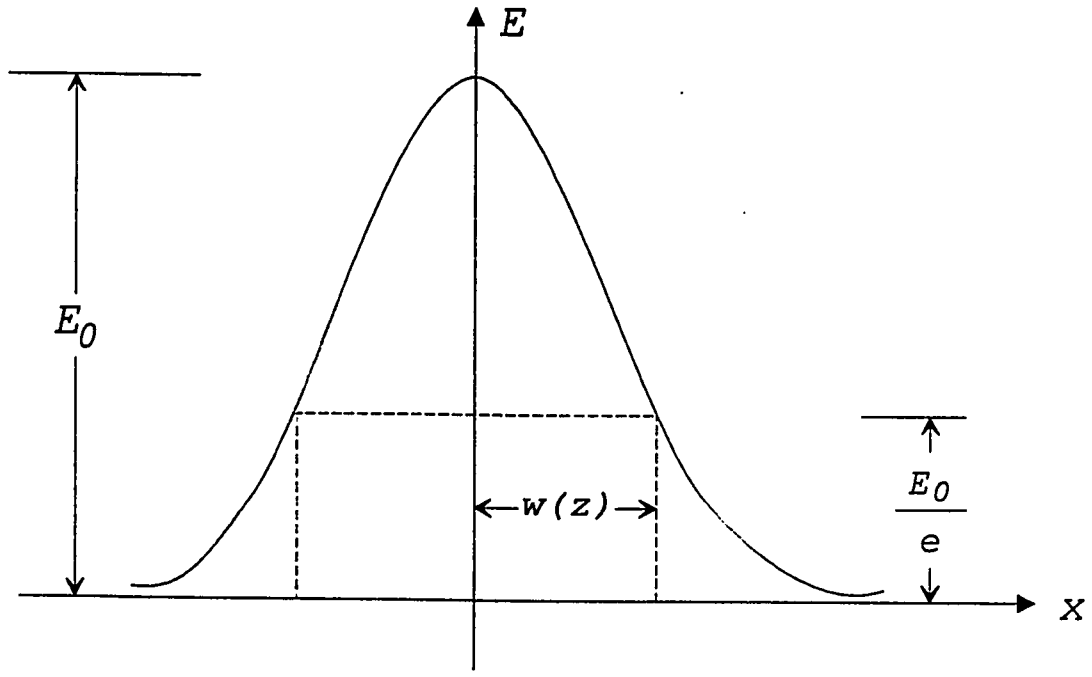

Figure (4.2) *Amplitude distribution of the Gaussian beam.*

$w(z)=w_0$ *at* $z=-z_0$

$$\psi_{nm} = E_0 \exp\left[-\frac{x^2}{w_x^2}\right]$$

$$= E_0 \exp\left[-\frac{x^2}{w_0^2}\right] \qquad (4.5)$$

where $w_0 = w_x$.

The previous expression is valid for a focused Gaussian beam (at $z = -z_0$). If the beam peak along the x-axix is positioned at $x = x_0$, this expression takes the following form

$$\psi_{nm} = E_0 \exp\left[-\frac{(x-x_0)^2}{w_0^2}\right] \qquad (4.6)$$

The distribution of the field at z=0 can be calculated by the MoL.

Marcuse [8] gives an approximate form for the electric field distribution of a laser source output. This approximation is very poor when the HBW becomes small as in the case treated in this thesis. To confirm this notion, we have tried this expression in the MoL routines and the results showed a poor power balance.

4.3 Application of the MoL to The Gaussian Beam Coupling Problem

Following the principles of the MoL presented in Chapter III, we will apply this method to the endfire coupling of a converging Gaussian beam incident from air into a dielectric slab waveguide. The incident Gaussian beam has a minimum HBW w_0. The beam is focused at the point $(x=x_0,\ z=-z_0)$ as shown in figure (4.3). The operational wavelength used is $\lambda=$ .86 μm.

The waveguide is symmetric and its input end is located at $z=0$. The core has a width of $2w$ and a refractive index n_1. The value of n_1 is chosen to be 3.6 which corresponds to a waveguide made of the semiconductor, GaAs. Both the cladding and the substrate have a refractive index n_2. The corresponding effective index of the waveguide is found from the eigenvalue equations by utilizing a zero-finding routine. Appendix-A contains a computer program called *STF-1* which has been used for this purpose.

The computation along the x-axis is limited to a length of lx as shown in figure (4.3). This length shall be large enough to ensure that the electromagnetic field will not

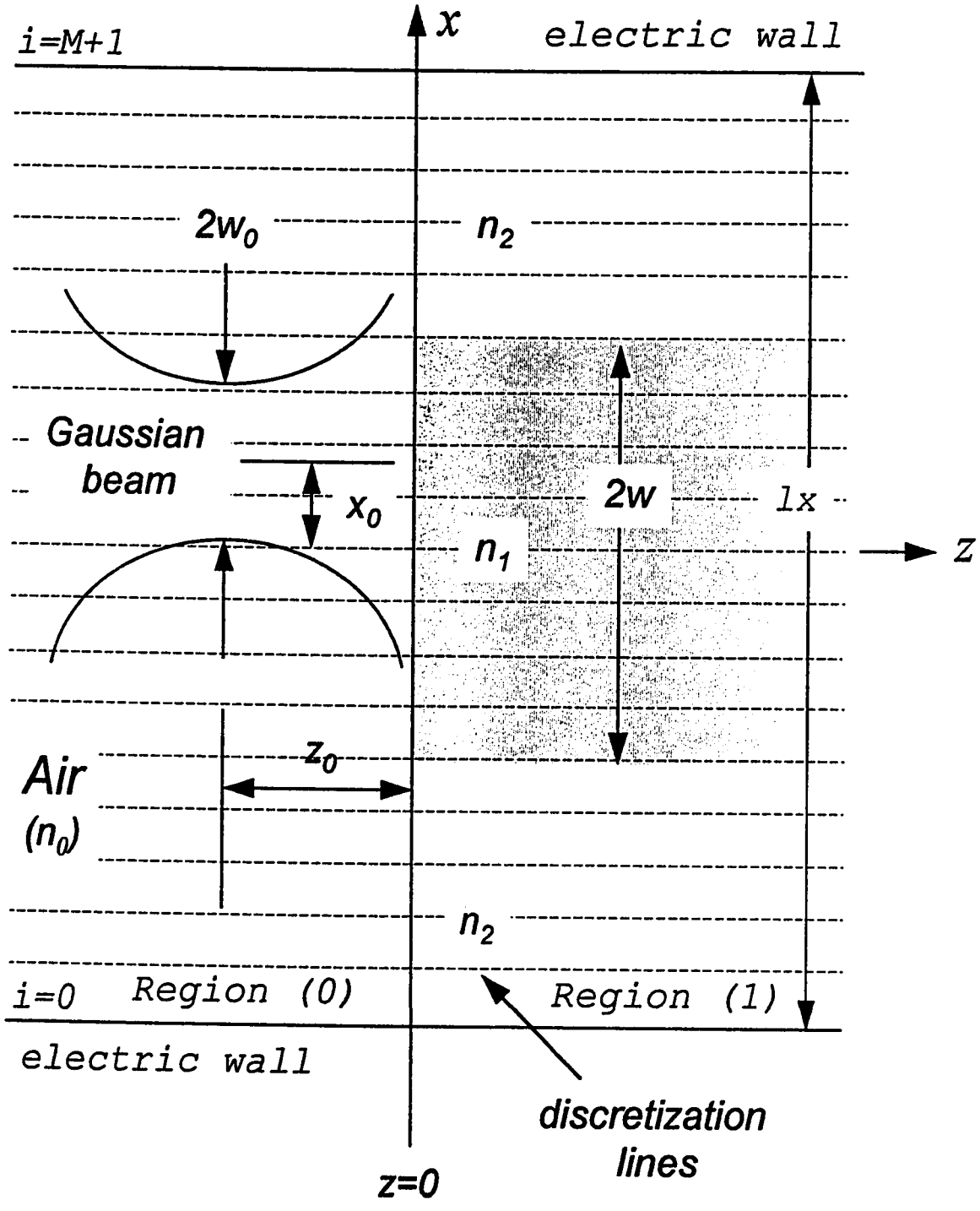

Figure (4.3) *Application of the MoL to the coupling problem.*

interact with the electric walls imposed by the MoL at both ends of the investigated structure. The field in the x-direction is discretized into M points equally spaced by Δx, with Δx given by:

$$\Delta x = \frac{lx}{M} \tag{4.7}$$

Whereas the number M shall be minimized to decrease the required computational time and computer memory requirement, M is chosen such that Δx will result in the most accurate results possible. Another important factor in choosing M is that all the structure borders shall be contained between discretized points to minimize the discretization errors at these singular points. The accuracy of the numerical scheme is tested by monitoring power conservation. As has been shown in Section (3.5), this is achieved by ensuring that the ratios of both the reflected and the transmitted powers to the incident power add to unity, i.e,

$$R+T=1 \tag{4.8}$$

Assuming that we have chosen the proper values of M and lx, we can apply the MoL to evaluate the effect of the launching conditions, but prior to that an expression for calculating the coupling efficiency is required.

4.3.1 Calculation of Power Coupling Efficiency Using the MoL

Consider the illustration of the coupling problem depicted in figure (4.3). The electric field continuity at z=0 implies that

$$\psi_i + \psi_r = \psi_t$$

where ψ_t is the transmitted field (region (1)), and ψ_i and ψ_r are the incident and reflected fields (region (0)) respectively. Our aim here is to find the percentage of power coupled to the fundamental mode of the waveguide. Endfire coupling efficiency to the fundamental mode depends on the spatial overlap between the incident beam and the mode. As in section (2.3.3.1), the power coupling efficiency is defined as:

$$\eta = \frac{p_g}{p_i} = \frac{\mathrm{Re}\int_{-\infty}^{\infty} E_{y_g}.H_{x_g}^{*}.dx}{\mathrm{Re}\int_{-\infty}^{\infty} E_{y_i}.H_{x_i}^{*}.dx} \qquad (4.9)$$

In the MoL, the incident electric field is given by

$$E_{y_i} = e^{jQ_0^{1/2}z}A_0 \qquad (4.10)$$

where the M×1 column matrix A_0 represents the incident field at $z=0$, and the M×M matrix Q_0 is defined in Section (3.3.2).

Using Maxwell's equations, the incident magnetic field is given by

$$H_{x_i} = \frac{j}{\omega\mu}\frac{\partial E_{y_i}}{\partial z} \tag{4.11}$$

therefore,

$$H_{x_i} = \frac{j}{\omega\mu}\frac{\partial}{\partial z}\left[e^{j\Omega_0^{1/2}z}A_0\right]$$

$$= -\frac{\Omega_0^{1/2}}{\omega\mu}e^{j\Omega_0^{1/2}z}A_0$$

and

$$H_{x_i}\Big|_{z=0} = -\frac{1}{\omega\mu}\Omega_0^{1/2}A_0 \tag{4.12}$$

The incident average power is given by

$$P_i = -\frac{1}{2}\mathrm{Re}\left(\int_{-\infty}^{\infty} E_{y_i}H_{x_i}^{*}dx\right) \tag{4.13}$$

For discrete quantities, the integration is replaced by a summation over the range of values. Consequently, the incident average power becomes

$$P_i = -\frac{1}{2}\mathrm{Re}\left\{\sum_{m=1}^{M} E_{y_i}(m)H_{x_i}^{*}(m)\Delta x\right\}$$

$$P_i\Big|_{z=0} = \frac{1}{2\omega\mu}\mathrm{Re}\left\{\left(\Omega_0^{1/2}A_0\right)^{*}A_0\right\}\Delta x \tag{4.14}$$

Similarly, the transmitted field is given by

$$E_{y_t} = e^{j\Omega_1^{1/2}z}A_1 \tag{4.15}$$

where the vector A_1 represents the transmitted field at $z=0$. Following equation (2.50), the fundamental mode excitation coefficient can be expressed as

$$\alpha_0 = \frac{A_1^{'} F_0}{F_0^{'} F_0} \tag{4.16}$$

where the MX1 F_0 vector describes the discretized fundamental mode distribution in region (I), and $A_1^{'}$ and $F_0^{'}$ are the transposed forms of the matrices A_1 and F_0. The guided electric field of the fundamental mode is therefore equal to

$$E_{y_g} = \alpha_0 F_0 \tag{4.17}$$

from which the corresponding magnetic field can be written as

$$H_{x_g} = -\frac{1}{2\omega\mu}\left[Q_1^{1/2}.(\alpha_0 F_0)\right] \tag{4.18}$$

Referring to equations (4.24) and (4.25) the average guided power is given by

$$P_g\Big|_{z=0} = \frac{1}{2\omega\mu}\mathrm{Re}\left\{\left(Q_1^{1/2}.\alpha_0 F_0\right)^{*}.\alpha_0 F_0\right\}\Delta x \tag{4.19}$$

As a result, the power coupling efficiency for TE polarized waves at $z=0$, can be written in the following discretized form

$$\eta = \frac{\mathrm{Re}\left\{\left(Q_1^{1/2}.\alpha_0 F_0\right)^{*}\alpha_0 F_0\right\}}{\mathrm{Re}\left\{\left(Q_0^{1/2} A_0\right)^{*} A_0\right\}} \tag{4.20}$$

All matrix manipulations including the calculations of eigenvectors and eigenvalues are achieved by using ***MATLAB*** programming software. Appendix-B contains all Matlab programs developed for the analysis of this thesis.

We are interested only in the power coupled to the fundamental mode. The incident field is assumed to be Gaussian which is symmetric about the waveguide axis. As a result, it will excite only the even modes of the waveguide. If this Gaussian field is laterally offset, it will not look even to the waveguide and thus it will excite even and odd modes in general. In the following three sections, we will take a look at the effect of such disturbances by utilizing the programs developed for this purpose.

4.3.2 Perfect Alignment

In order to study the case of perfect alignment of the incident beam, a Gaussian beam with a beam waist positioned at $x_0 = 0$ and $z_0 = 0$ as shown in figure (4.3) and a variable HBW w_0 has been applied to a symmetric slab waveguide having a core refractive index; $n_1 = 3.6$ and an operational wavelength; $\lambda = .86\ \mu m$. These values of n_1 and λ will be fixed throughout this thesis. In the majority of cases, the total length used by the MoL along the x-axis is $lx = 5\ \mu m$ discretized into mx mesh points to represent both; the field and the refractive index distributions.

The convergence behavior of the MoL has been first tested by calculating the coupling efficiency to a waveguide having a core halfwidth; $w = .6\ \mu m$ and a cladding refractive index; $n_2 = 3.4$. The results were obtained for different numbers of discretization points mx ranging from 10 mesh points upto 200 points, as illustrated in table (4.1). It can be noticed that the required computational time increases very dramatically by increasing mx. Efficiency versus w_0 curves are shown in figure (4.4) for mx=10, 30, 50 and 100. It is seen that convergence is achieved with mx=50. Thus, the

mx	lx (μm)	Δx (μm)	time* (sec)
10	5	.5	7
20	5	.25	14
30	5	.1667	40
40	5	.125	85
50	5	.1	154
80	5	.0625	696
100	5	.05	1333
200	5	.025	13958

Table (4.1) *The variations of the computational time for different numbers of discretization points (mx).*

* (Using a 66 MHz, 486-DX2 CPU).

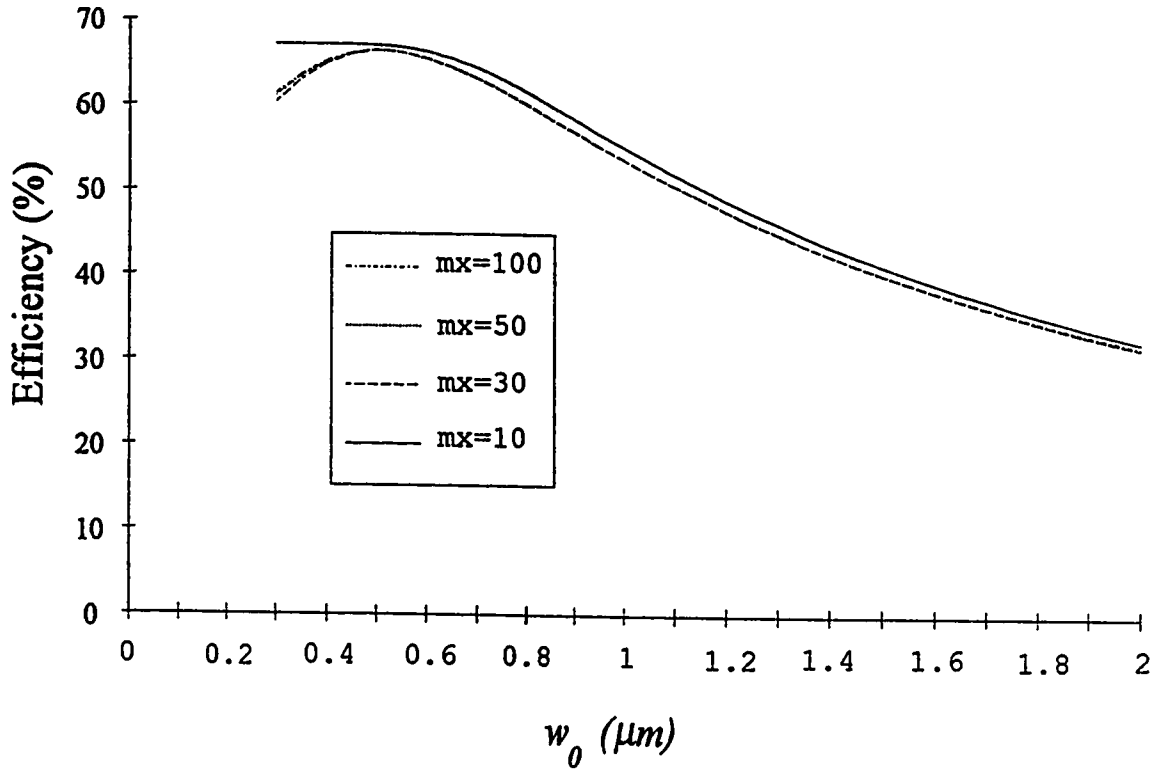

Figure(4.4) *Convergence behavior of coupling efficiency (n_2 =3.4, w=.6 μm).*

field in the x-direction will be discretized into 50 mesh points hereafter.

To continue with the analysis of the perfect alignment case, the cladding refractive index; n_2 was chosen to be equal to 3.4, and w_0 was varied from .05 to 1.2 μm. The results were obtained for three different core halfwidths; w corresponding to .2, .4 and .6 μm. The resulting curves are shown in figure (4.5). It can be seen from this figure, that the value $w=.6$ μm results in higher efficiency in general. The turnover point or the point of maximum, appears clearly for this value of core width whereas for the other two curves their maxima do not appear in the range of the graph.

To ensure the validity of the MoL results, power conservation is monitored. At any boundary, the sum of the transmitted power and the reflected power shall be equal to the incident power (i.e., $P_t+P_r=P_i$). It can be seen from figure (4.6) that the term $R+T$ where $R+T=\frac{1}{P_i}(P_t+P_r)$ has values that exceed unity for $w_0<.3$ μm. For this reason efficiency calculations for the interval $0<w_0<.3$ have been excluded from the range of interest as they could lead to inaccurate conclusions. The error in the $R+T$ term is

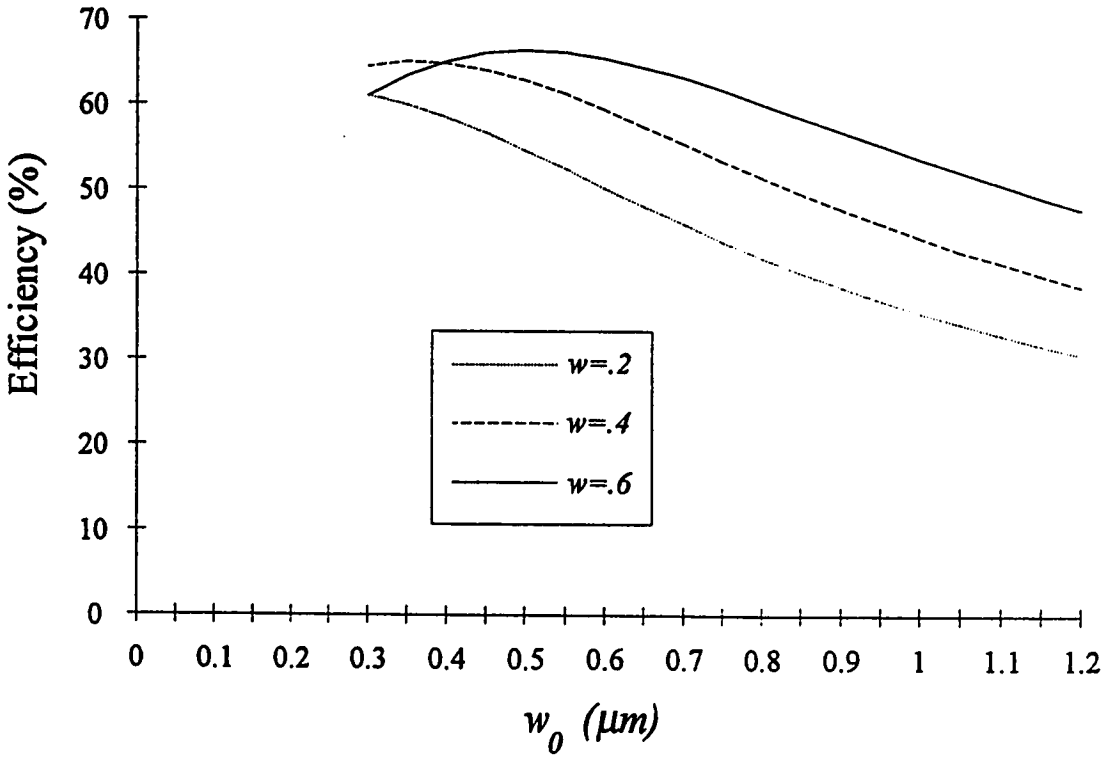

Figure(4.5) *Efficiency versus w_0 for different core widths.*

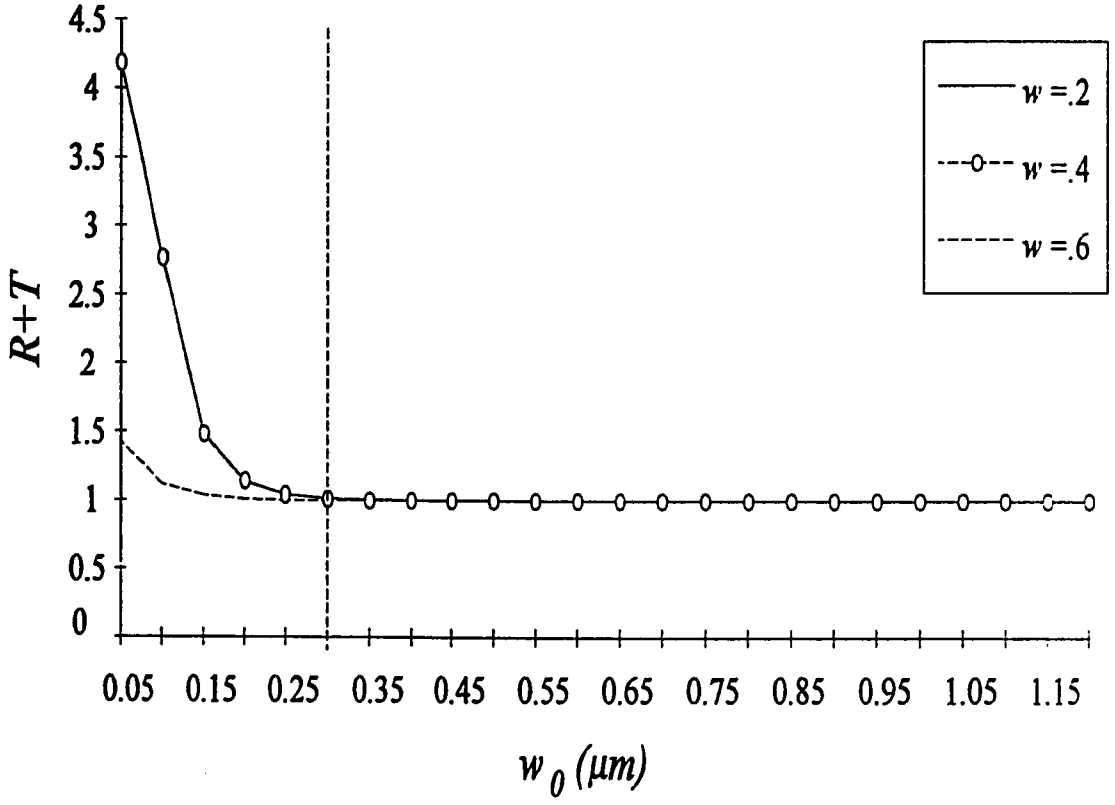

Figure (4.6) *Illustration of the (R+T) term behaviour Versus* w_0.

$$R+T=\frac{1}{P_i}(P_t + P_r)$$

attributed to the error that results from the three-point central difference approximation used in the MoL. This approximation has been discussed in details in Section (3.3.1).

The relation between this error and w_0 can be estimated by referring to equation (3.3), which indicates that the major term influencing the error is $\frac{\Delta x^2}{12}\psi^{(4)}$. For a Gaussian beam , the field ψ is described by $\psi = e^{-\left(\frac{x^2}{w_0^2}\right)}$. The first derivative is therefore given by

$$\psi' = -\frac{2x}{w_0^2} e^{-\left(\frac{x^2}{w_0^2}\right)}$$

and the following derivatives are

$$\psi^{(2)} = \frac{4x^2}{w_0^4} e^{-\left(\frac{x^2}{w_0^2}\right)} - \frac{2}{w_0^2} e^{-\left(\frac{x^2}{w_0^2}\right)}$$

$$\psi^{(3)} = -\frac{8x^3}{w_0^8} e^{-\left(\frac{x^2}{w_0^2}\right)} + \ldots\ldots$$

$$\psi^{(4)} = \frac{16x^4}{w_0^{16}} e^{-\left(\frac{x^2}{w_0^2}\right)} + \ldots\ldots \qquad (4.21)$$

In order to decrease the above error for smaller values of w_0, Δx has to be reduced far enough to equalize the effect of the denominator w_0^{16}. This requires Δx to be very

small, resulting in more mesh points in the x-direction and further to that leading to excessive computational memory and time. Based on the above, we will exclude any calculation corresponding to values of w_0<.3 μm in all the subsequent work.

To see further the effect of the HBW w_0 of the Gaussian beam on the power coupling efficiency, η is shown in figure (4.7) as a function of w_0 for the following different cladding refractive indices, n_2= 3.3, 3.4, 3.5 and 3.55. The core halfwidth is w=.2 μm. Figures (4.8) and (4.9) show similar graphs for w=.4 μm and w= .6 μm respectively. It can be noticed from these three figures that as the difference between the refractive indices of both the core and the cladding decreases, the efficiency increases. We note also that the difference between the efficiency curves for different n_2 decreases as the core width increases. It is observed also that the maximum efficiency occurs at a larger value of w_0 as w increases. The reason for this is due to the fact that the field of the fundamental mode has a larger spatial spread when the difference between n_1 and n_2 decreases. The spread of the fundamental mode field also increases as w increases.

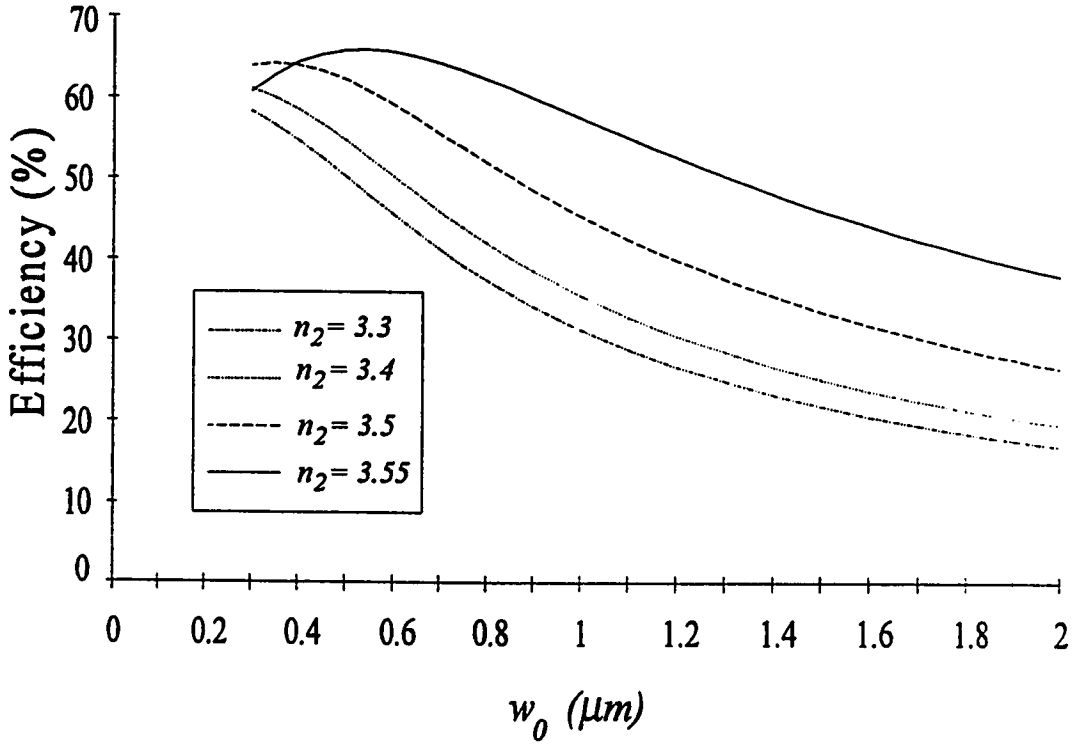

Figure(4.7) *Efficiency versus w_0 for different values of n_2 (w= .2 μm).*

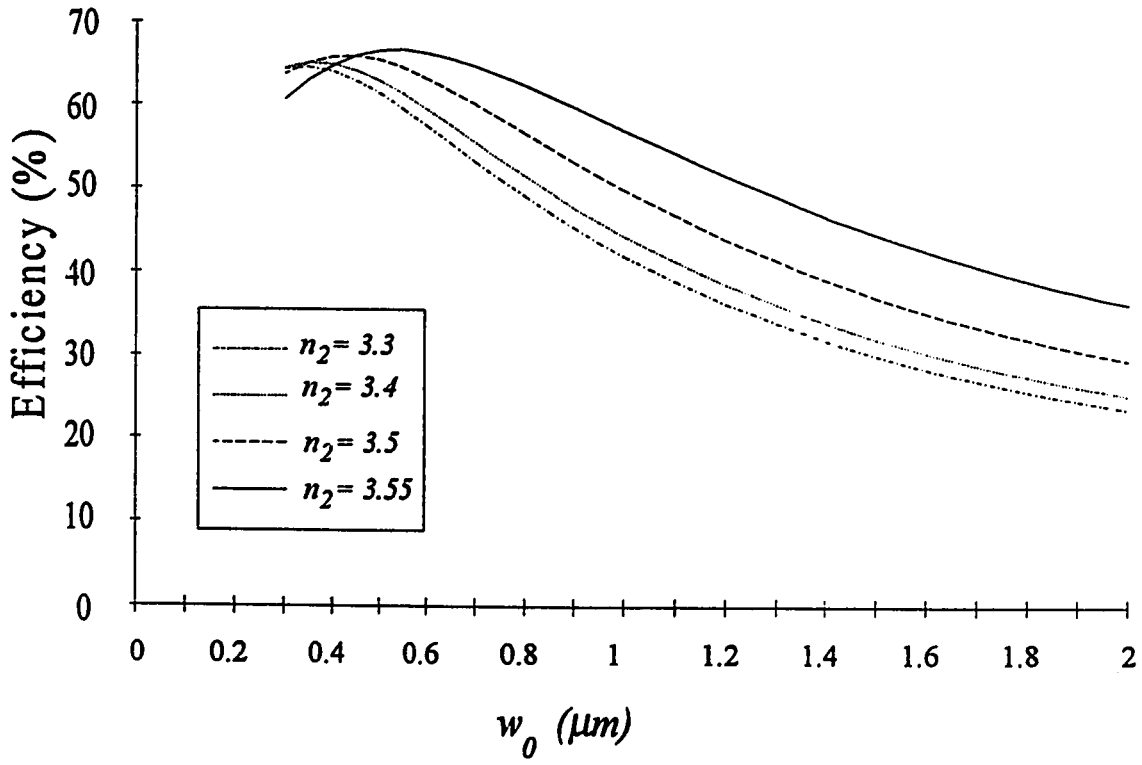

Figure(4.8) *Efficiency versus w_0 for different values of n_2 (w= .4 μm).*

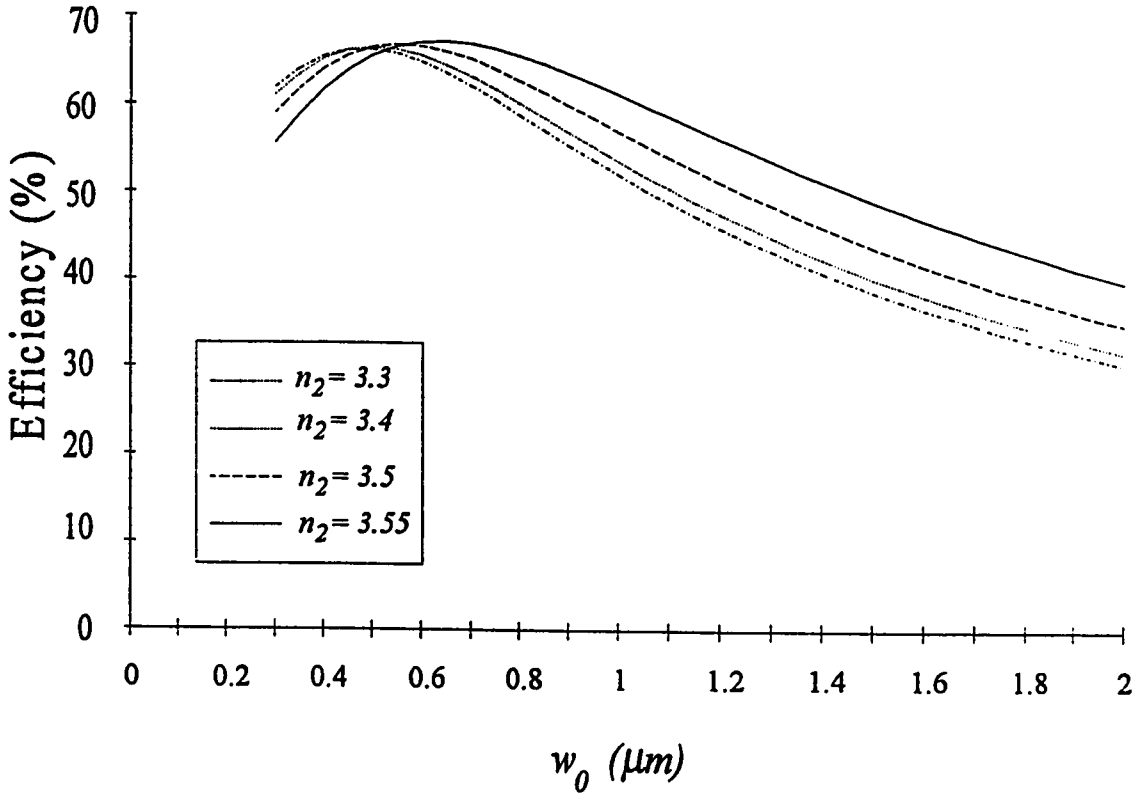

Figure(4.9) *Efficiency versus w_0 for different values of n_2 (w= .6 μm).*

Figure (4.10) illustrates pictorially the incident field distribution as it propagates in a homogeneous medium (air). As expected, the beam widens as it travels away from the focusing plane located at z=0. Figure (4.11) shows similar curves for the reflected beam as it propagates in the opposite direction, in the region z<0. The same behavior is noticed here. Moreover, the reflected field maintains a Gaussian profile. Note that the two parallel lines are shown in the above two figures to emphasize the widening behavior. In figure (4.12), the amplitude profile of the transmitted field as it propagates inside the waveguide is shown. Part of the transmitted field power is coupled to the guided modes and the other part is coupled to radiation modes. As the transmitted field propagates, the power coupled to the radiation modes escapes and only the power coupled to the guided modes remains in the waveguide. Figure (4.13 (a)-(c)) depicts the profiles of the transmitted field at distances of 4 μm, 8 μm and 16 μm respectively from the front-end of the waveguide. As can be seen, the profile tends to that of the calculated guided fundamental mode ($\alpha_0 F_0$) as z increases.

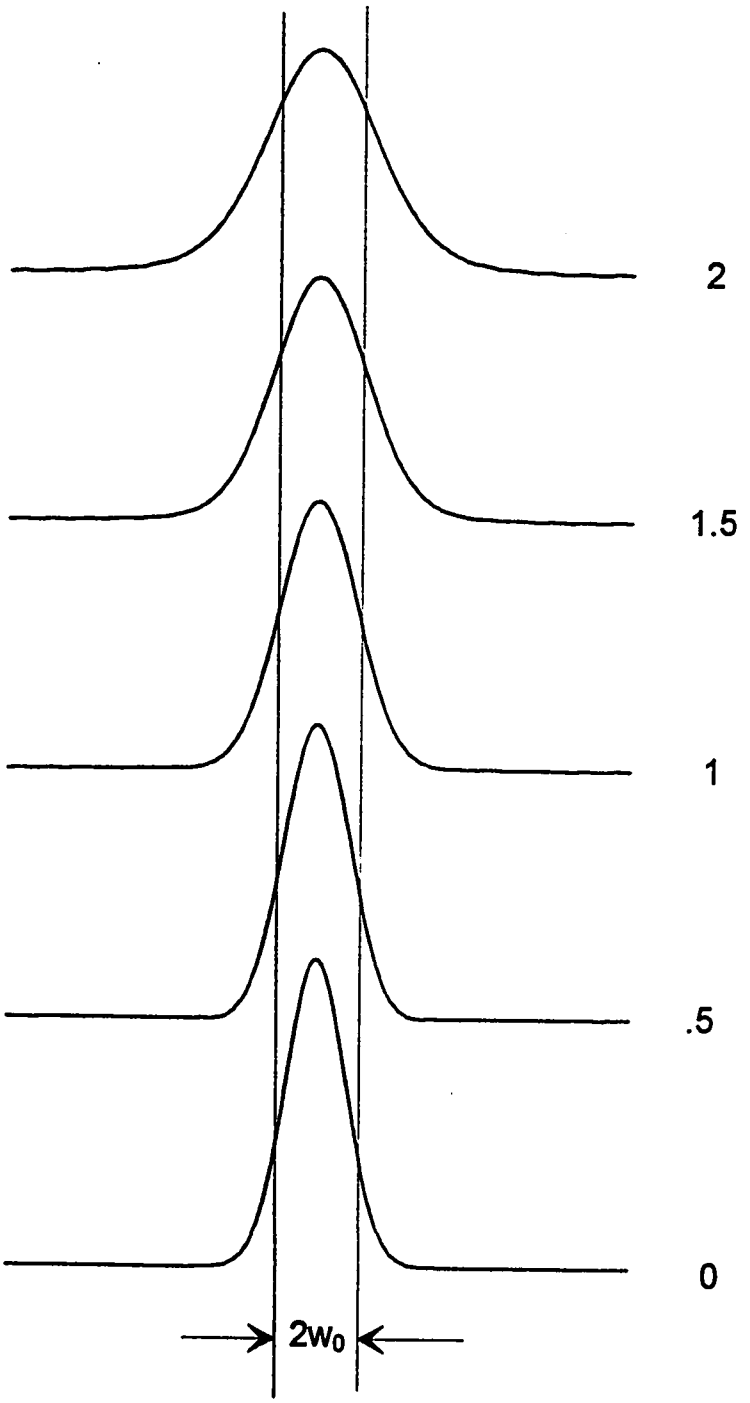

Figure (4.10) *The profile of a Gaussian beam as it travels from the focusing plane located at z=0. (Numbers indicate distances in μm).*

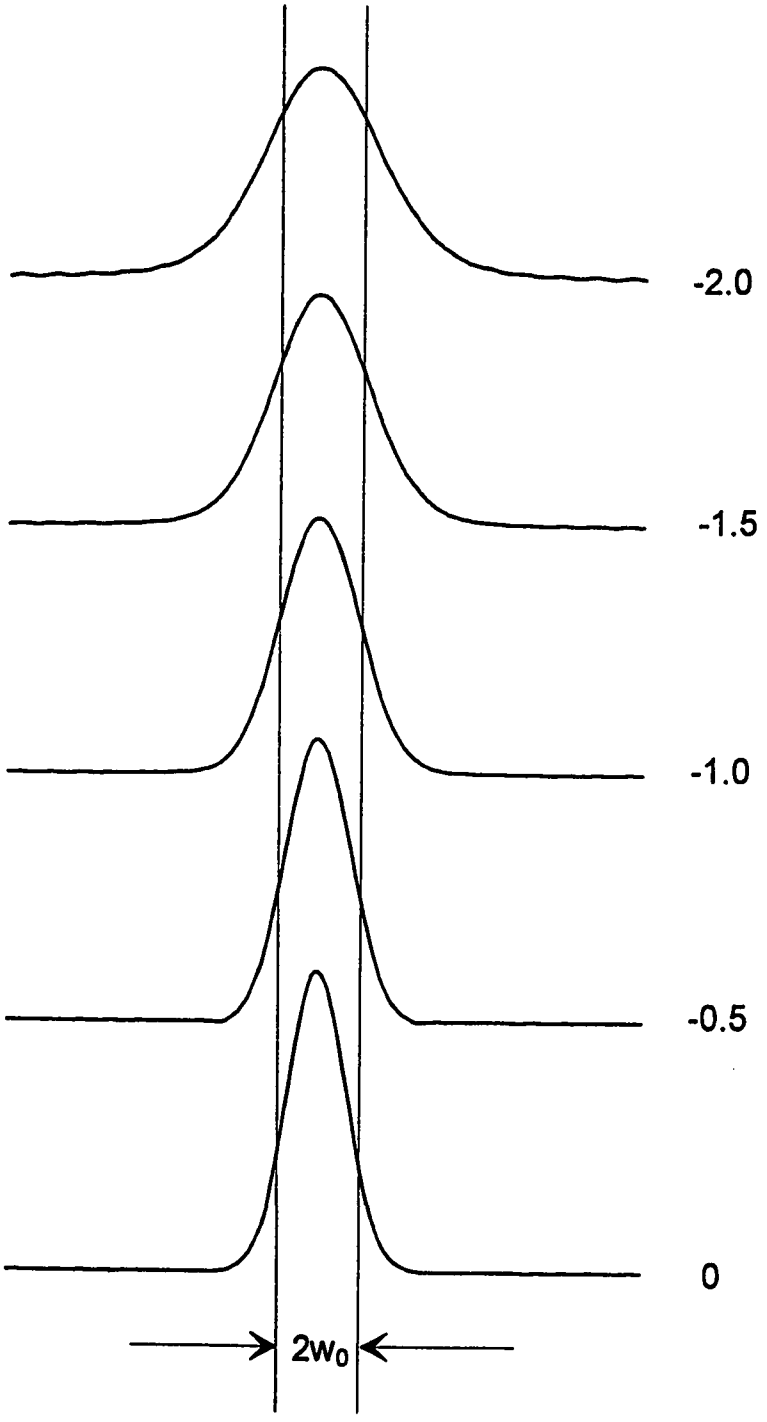

Figure (4.11) *The profile of the reflected field as it travels from the focusing plane located at z=0. (Numbers indicate distances in μm).*

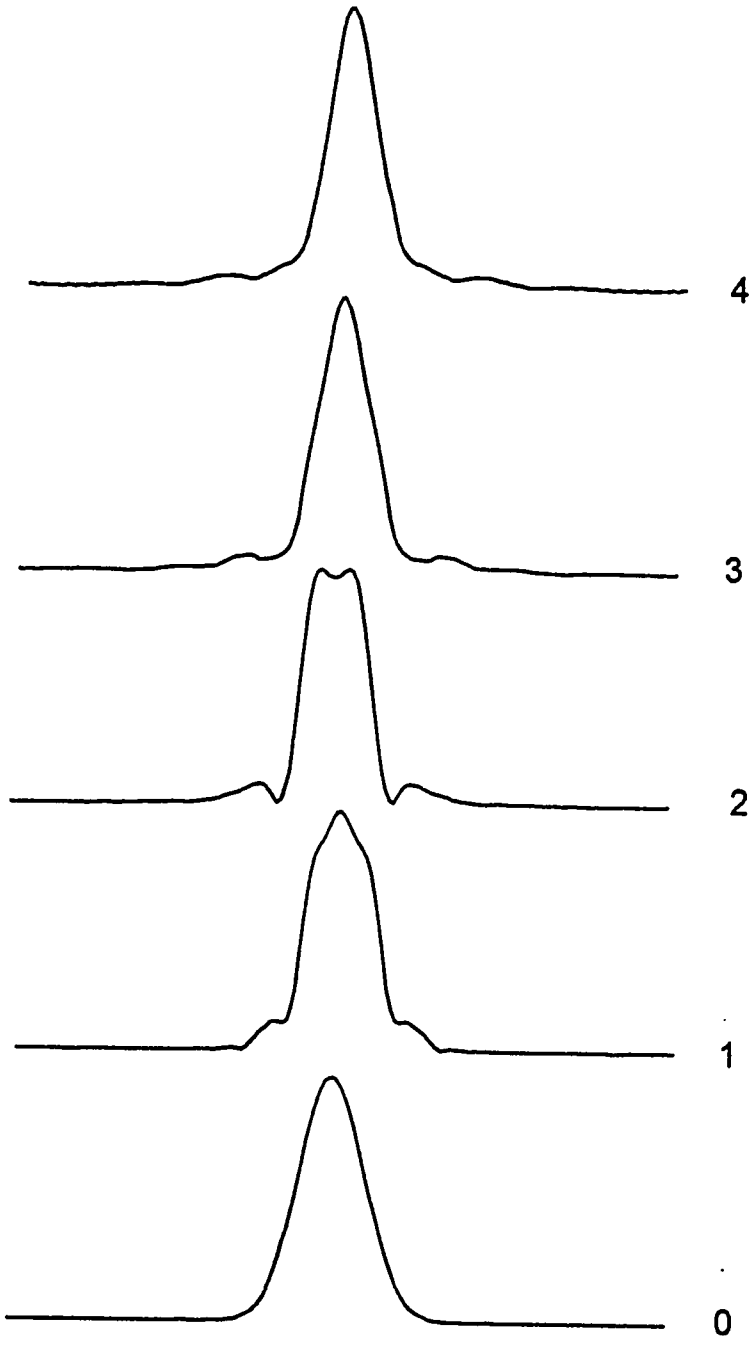

Figure (4.12) *The profile of the transmitted field as it propagates inside a waveguide loacted at z=0, (numbers indicate distances in μm).*

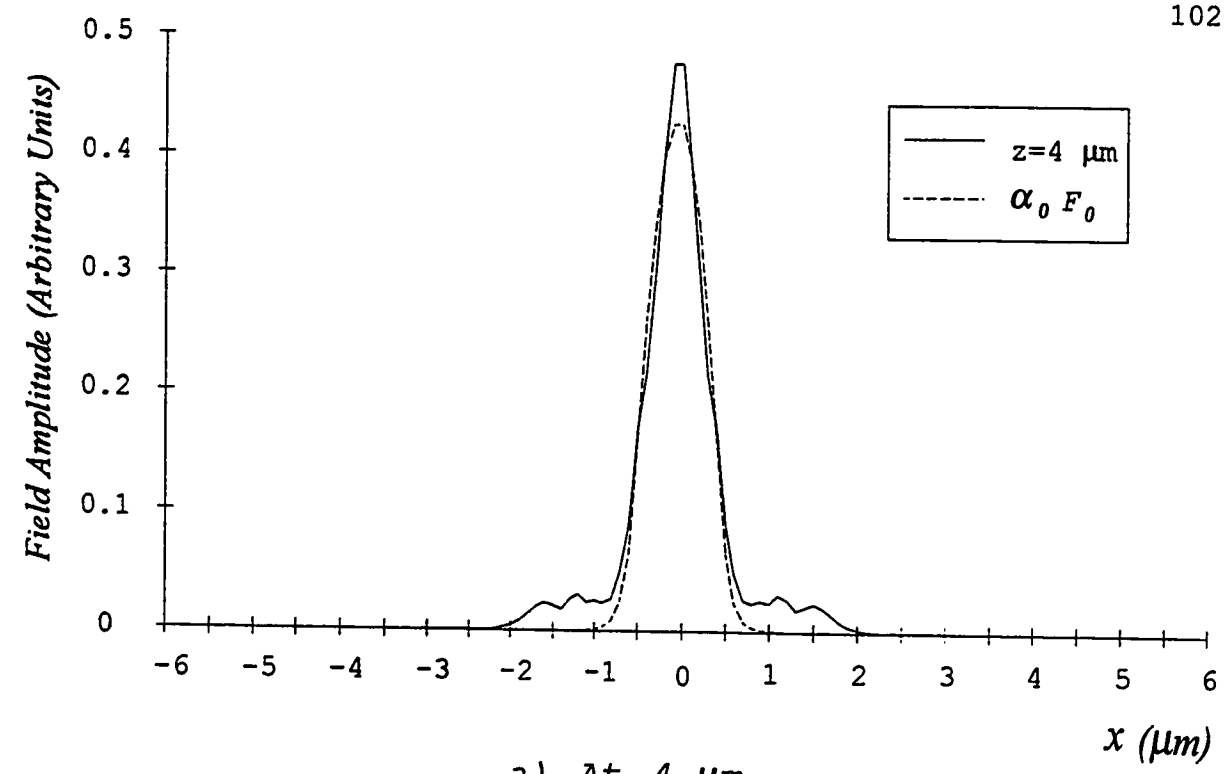

a) At 4 μm.

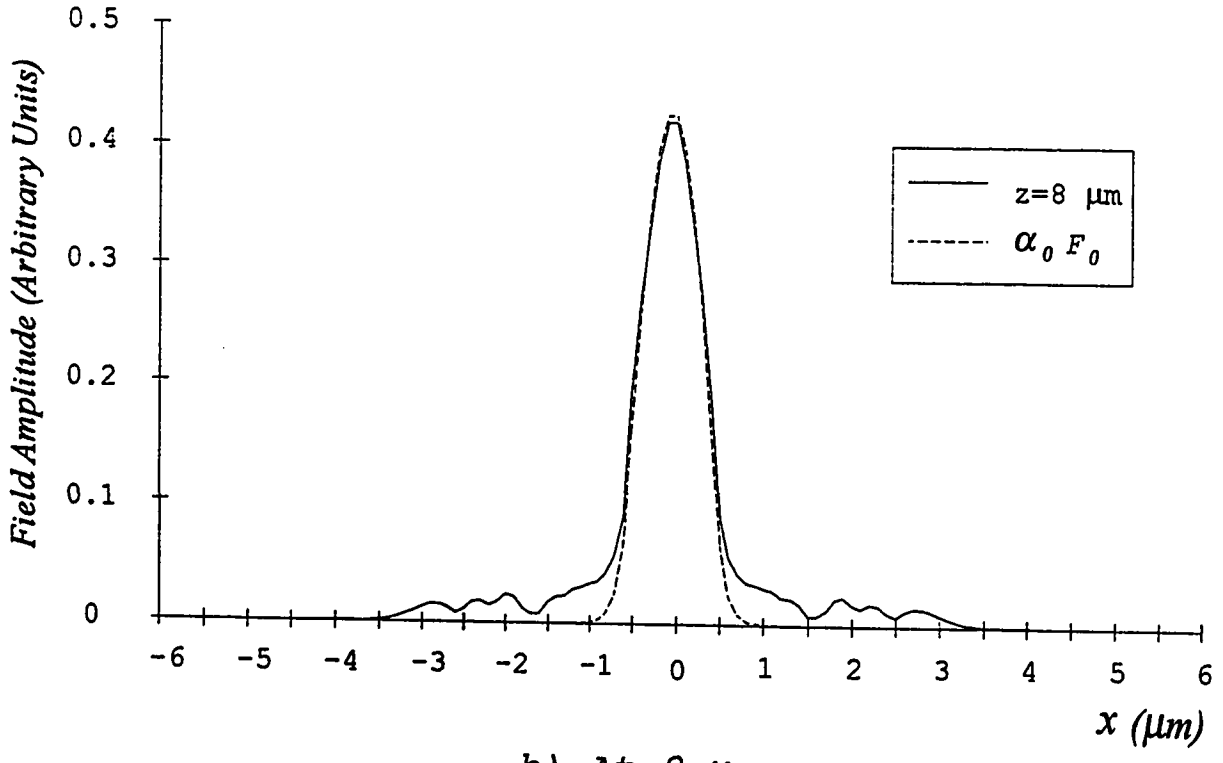

b) At 8 μm.

Figure (4.13) *Comparison between the guided fundamental mode and the transmitted field.*

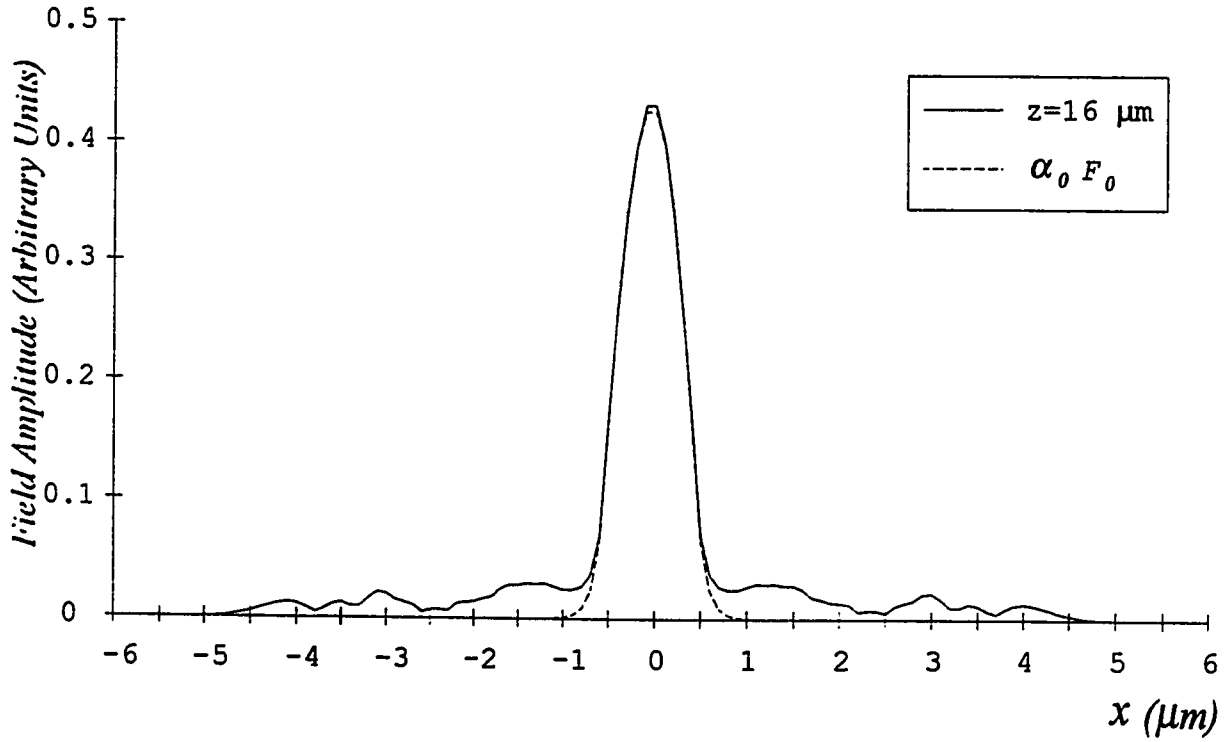

c) At 16 μm.

Figure (4.13) *Comparison between the guided fundamental mode and the transmitted field.*

For the purpose of comparison and to examine the accuracy of our method, we have plotted in figure (4.14) the coupling efficiency curves as calculated by the MoL and those shown in figures (4) and (5) of reference [32]. The results show good agreement. Moreover, the MoL showed good power balance, that the difference term ε (where $\varepsilon = \frac{P_t + P_r}{P_i} - 1$) has values that ranges between $9.8E-04$ and $1.0E-16$.

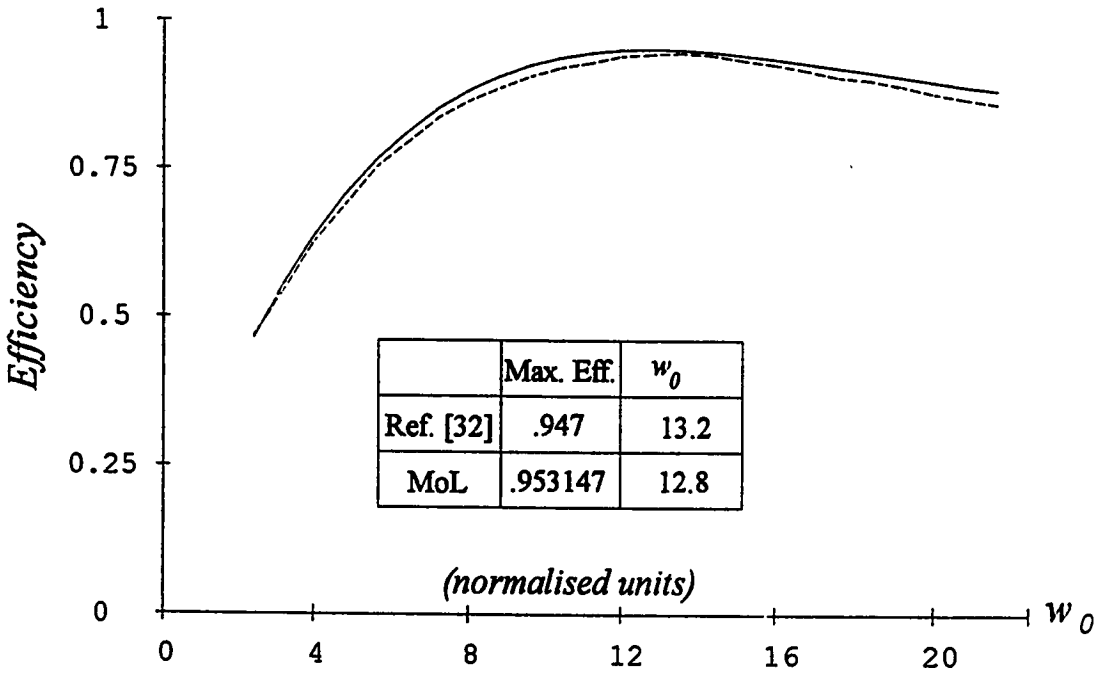

	Max. Eff.	w_0
Ref. [32]	.947	13.2
MoL	.953147	12.8

a) n_2 *=1.432;* Δ *= .01;* w*= 3.*

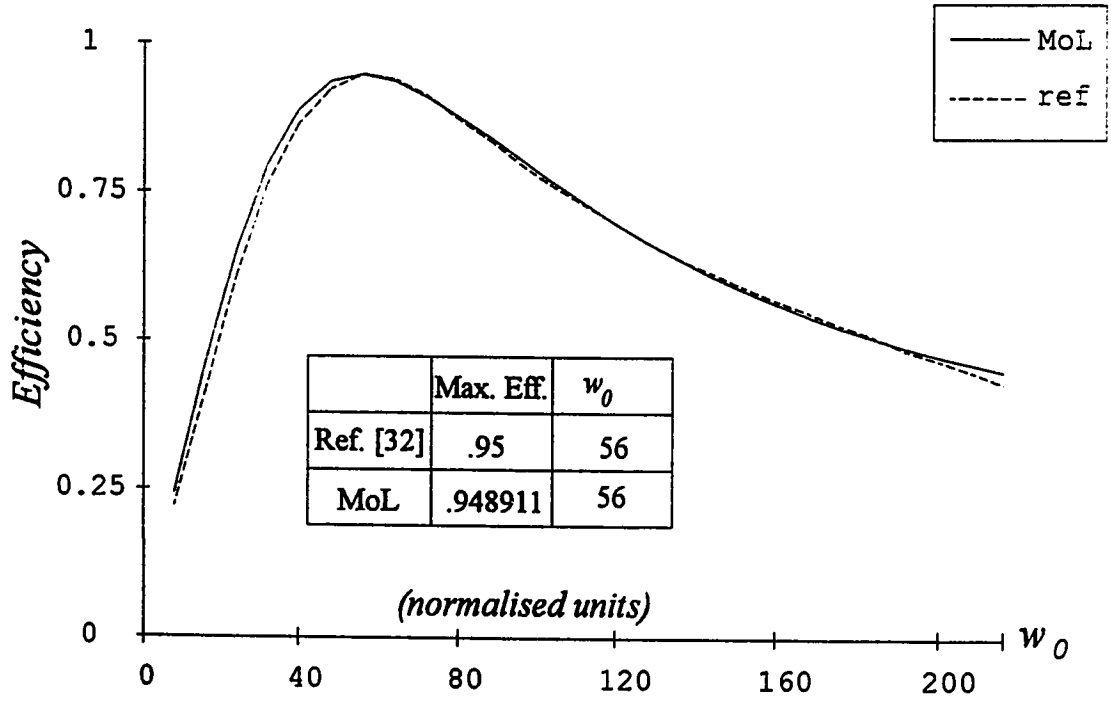

	Max. Eff.	w_0
Ref. [32]	.95	56
MoL	.948911	56

b) n_2 *=1.5;* Δ *= .01;* w*= 73.9.*

Figure (4.14) *Comparison between coupling efficiency curves calculated by the MoL and those of reference [32].*

4.3.3 Effect of Lateral Offset

In this subsection we consider the effect of the lateral offset of the Gaussian beam on the power coupling efficiency. The structure of the treated problem is as shown in figure (4.3). The waveguide parameters are $n_1 = 3.6$, $\lambda = .86\ \mu m$. To ensure that there is no interaction between the Gaussian beam and the metallic boundaries of the problem space, the length along the x-direction; lx has been extended to 10 μm (mx=100) and efficiency figures were compared with the case when lx=5 μm (mx=50). In general, both cases showed agreement in the third decimal.

Figure (4.15) demonstrates the variation of the power coupling efficiency with the transverse displacement of the Gaussian beam x_0 with respect to the waveguide axis. The results are shown for a cladding index; $n_2 = 3.4$, a waveguide core halfwidth $w = .2\ \mu m$ and four different Gaussian beam spot sizes; w_0=.3, .6, .9 and 1.2 μm. Figures (4.16) and (4.17) show similar curves for $w = .4\ \mu m$ and .6 μm. It can be concluded from these figures that the maximum efficiency is attained at $x_0 = 0$, that is when the offset is minimum. The differences between the efficiency curves for different w_0 decreases as the core width increases. It is noteworthy also

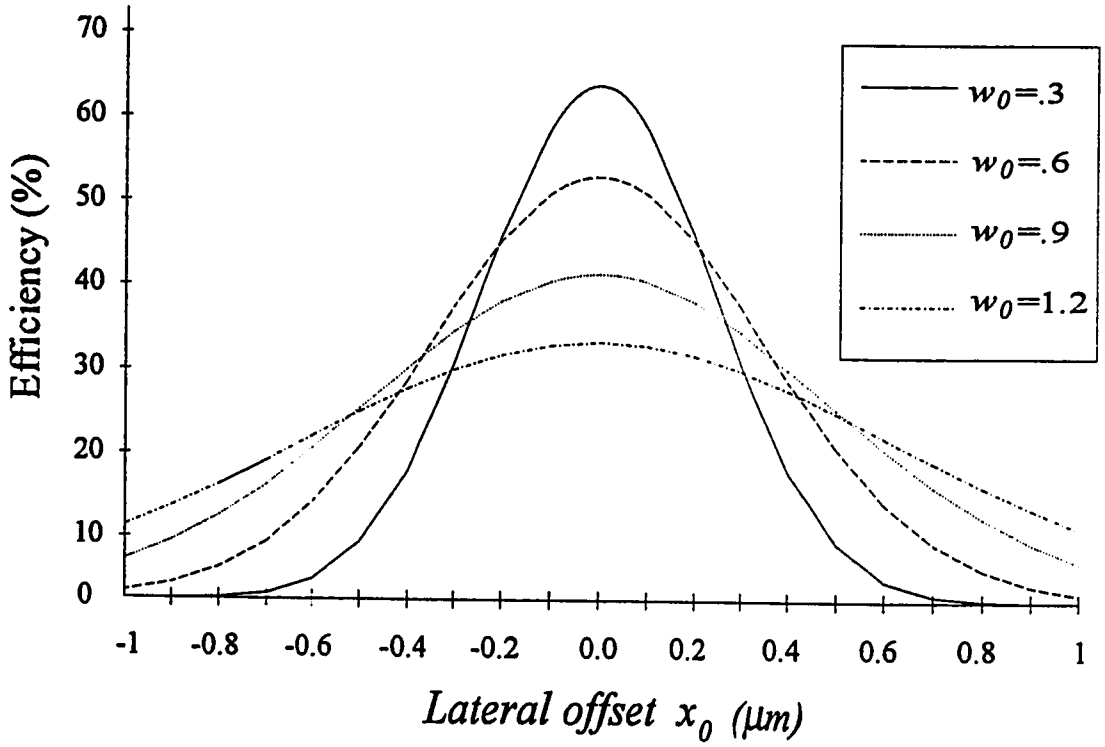

Figure (4.15) *Effect of lateral offset (w= .2 μm) on coupling efficiency.*

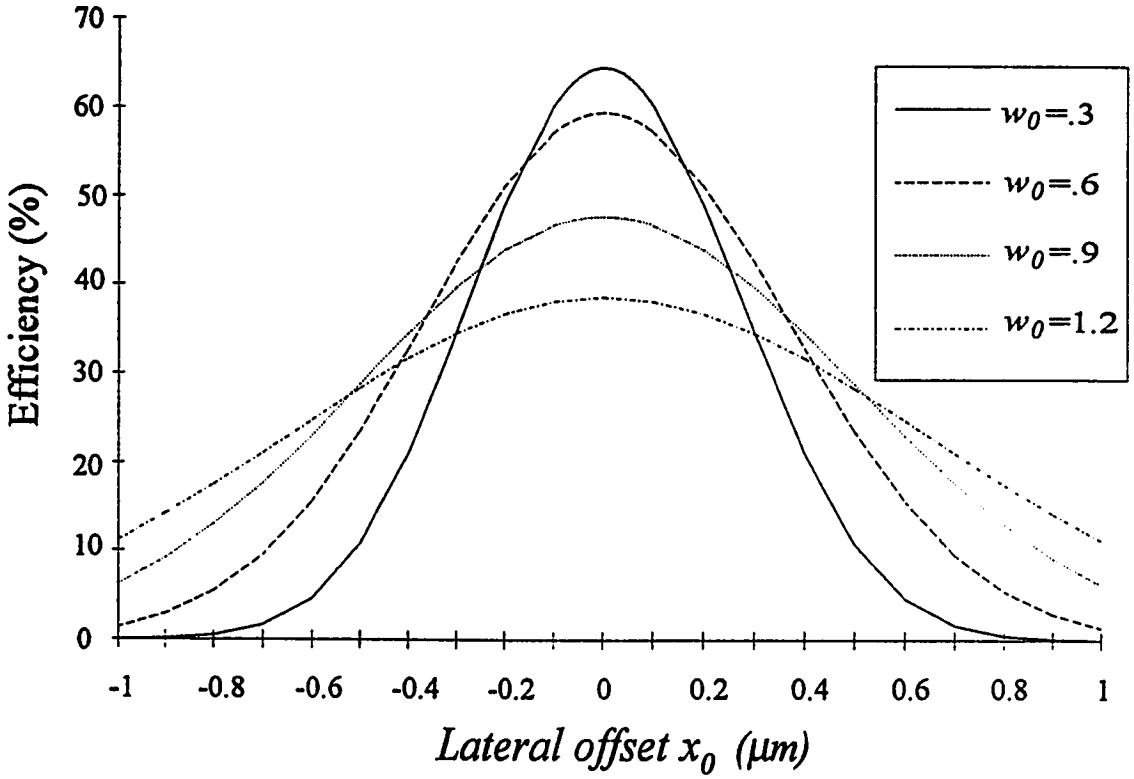

Figure (4.16) *Effect of lateral offset (w=.4 μm) on coupling efficiency.*

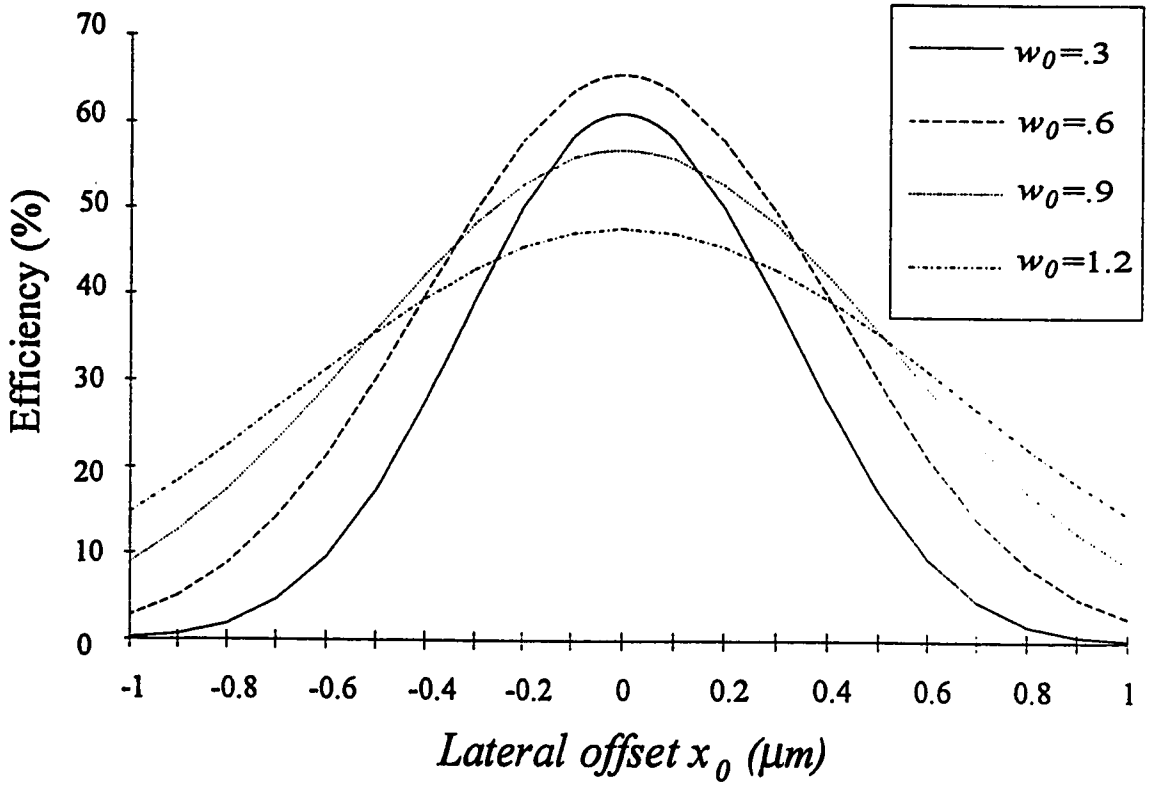

Figure (4.17) *Effect of lateral offset (w=.6 μm) on coupling efficiency.*

that as the HBW; w_0 increases, the effect of lateral offset on power efficiency becomes smoother and less dramatic. This can be seen in particular for w_0= 1.2 μm.

In order to illustrate the effect of changing the waveguide cladding index of refraction; n_2 on the coupling efficiency, we have plotted the efficiency curves versus the lateral offset for the following values of n_2: 3.3, 3.4, 3.5 and 3.55 as depicted in figure (4.18). The waveguide core halfwidth was fixed at w=.2 μm and the incident Gaussian HBW; w_0 value is .4 μm. In general, the coupling efficiency showed the same effect by having its maximum at x_0=0. As in the case of perfect alignment, coupling efficiency increases as the difference between the refractive indices of the core and cladding decreases.

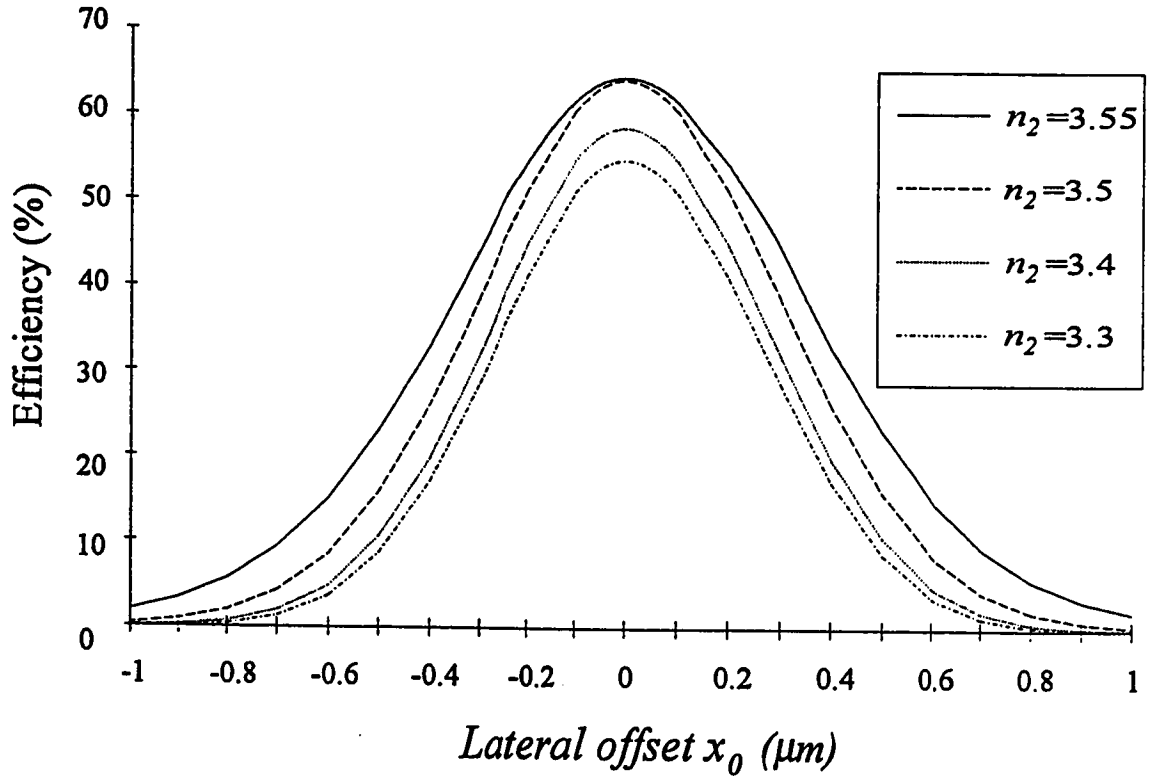

Figure (4.18) *Effect of lateral offset for different values of cladding refractive indices (w=.2 μm).*

4.3.4 Effect of Longitudinal Offset

To monitor the effect of the interaction between the incident Gaussian beam and the problem space metallic boundaries in longitudinal offset, we have checked the efficiency figures at different values of lx. If the results are close (with a difference in the order of 10^{-4}), then we use the smaller lx as this will result in less computational time with negligible loss of accuracy. In general, the choice of $lx = 5\ \mu m$ with $mx = 50$ leads to converging results.

Figures(4.19), (4.20) and (4.21) show the variations of the coupling efficiency with respect to the longitudinal offset; z_0 for waveguide half core widths $w = .2$, .4 and .6 μm respectively. In each of these figures, four curves are plotted, corresponding to Gaussian HBW w_0 of .3, .6, .9 and 1.2 μm. As can be noticed, the effect of the longitudinal offset is very dramatic for $w_0 = .3\ \mu m$ and becomes less strong as w_0 increases. This is because as w_0 increases, the rate of increase in the HBW as seen by the waveguide decreases for the larger longitudinal offset. Efficiency is maximum when there is no longitudinal shift except for the case when $w = .2\ \mu m$ and $w_0 = .3\ \mu m$.

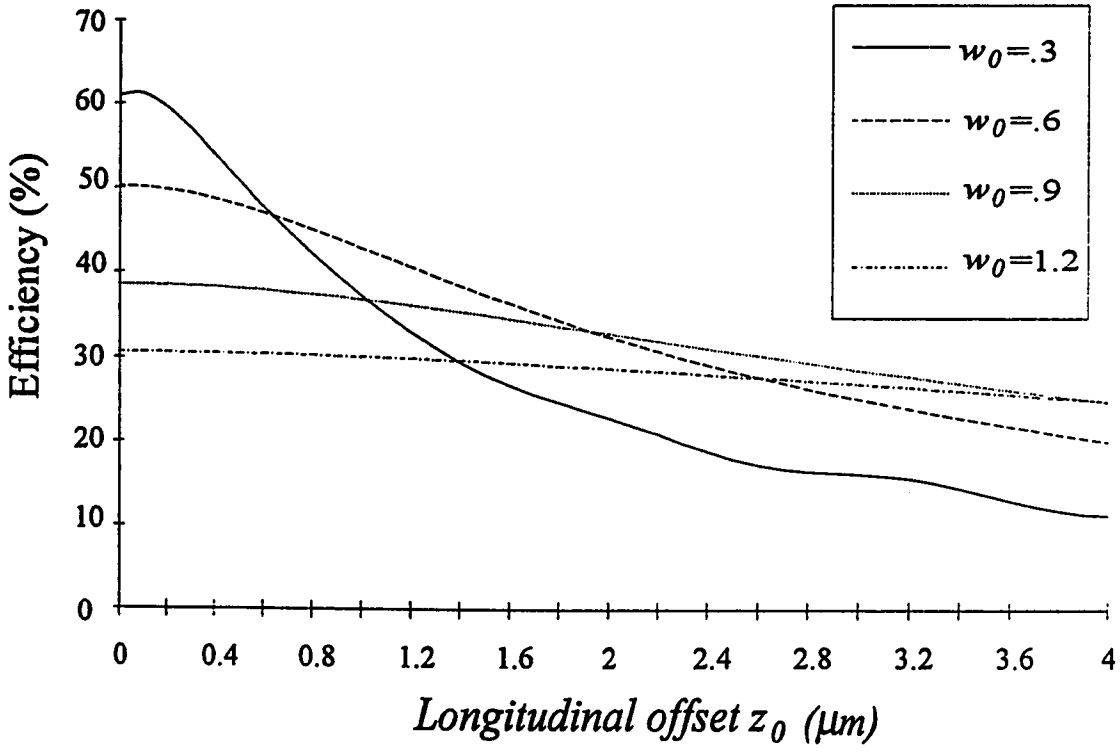

Figure (4.19) *Effect of longitudinal offset (w= .2 μm) on coupling efficiency.*

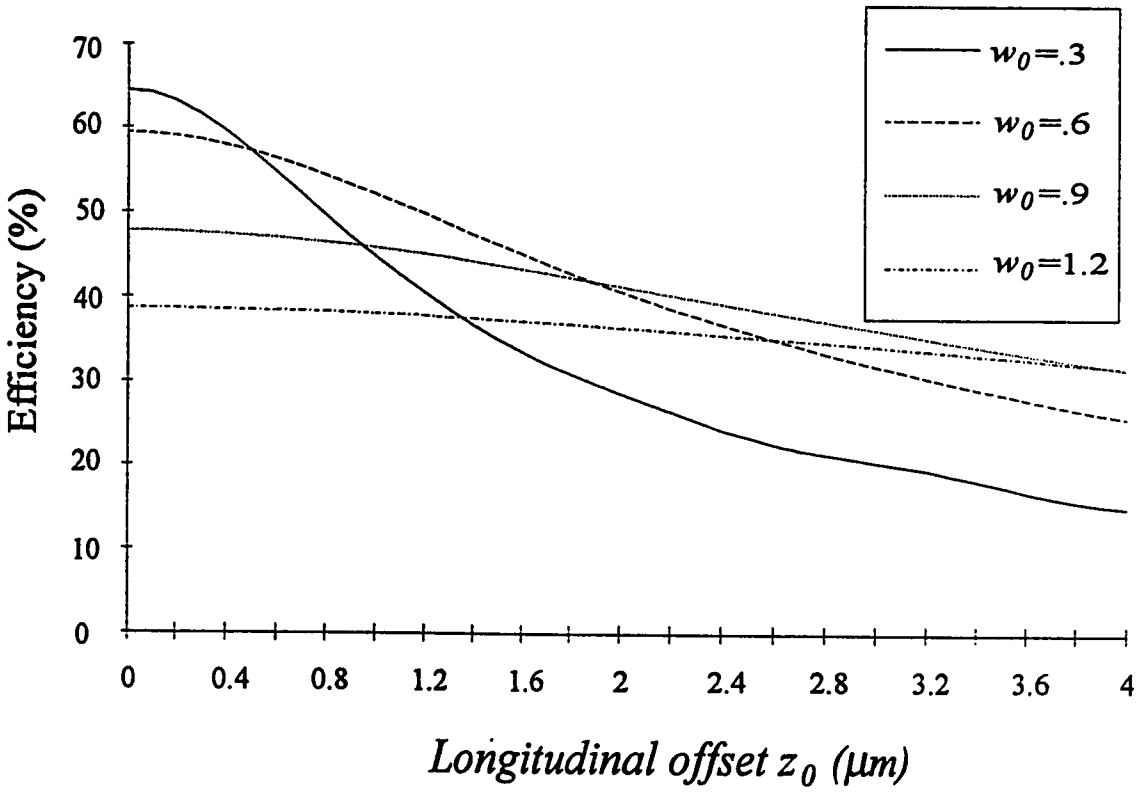

Figure (4.20) *Effect of longitudinal offset (w= .4 μm) on coupling efficiency.*

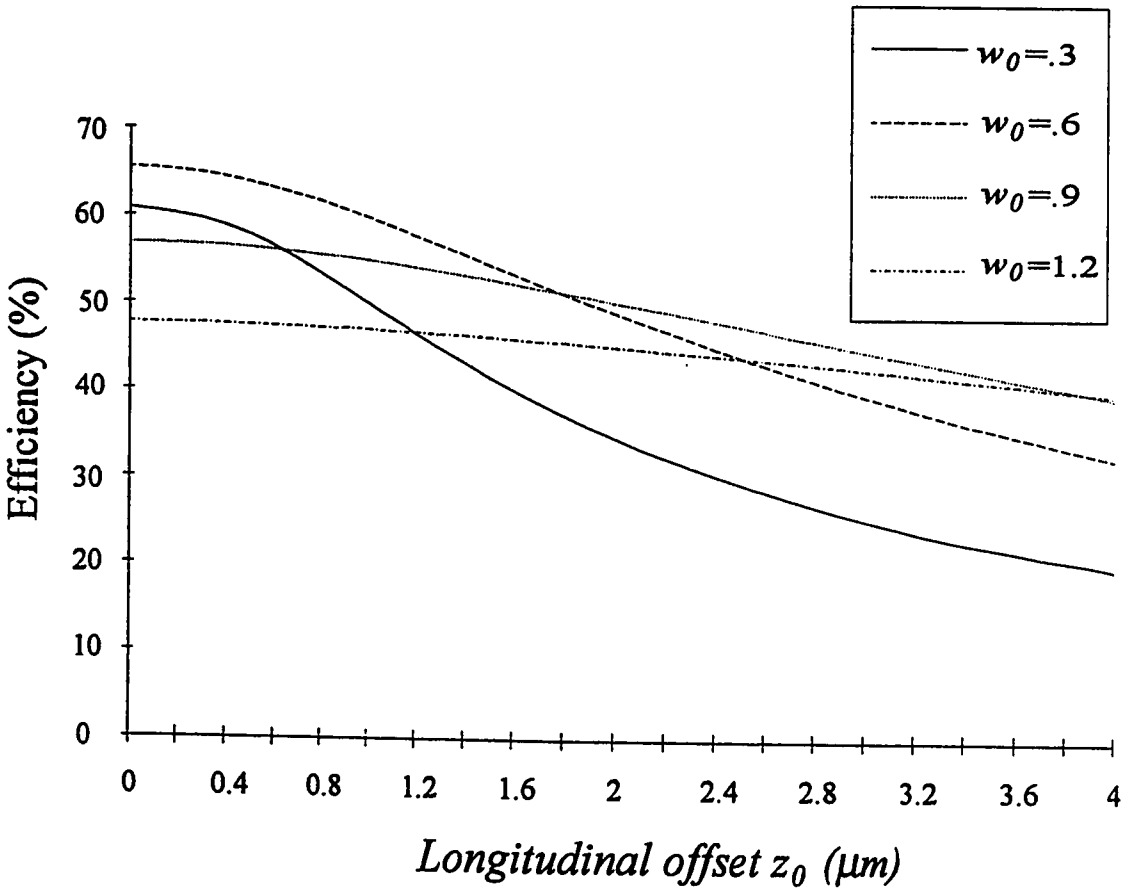

Figure (4.21) *Effect of longitudinal offset (w= .6 μm) on coupling efficiency.*

To compare the effect of changing the waveguide core width on longitudinal offset, figure (4.22) demonstrates the variations of efficiency against z_0 for three values of core halfwidths; w=.2, .4 and .6 μm for w_0= .3 μm. As shown in this figure, w= .4 μm results in the highest efficiency in the interval $0<z_0<.4$ μm. For $z_0>.4$ μm, w= .6 μm produces the highest efficiency.

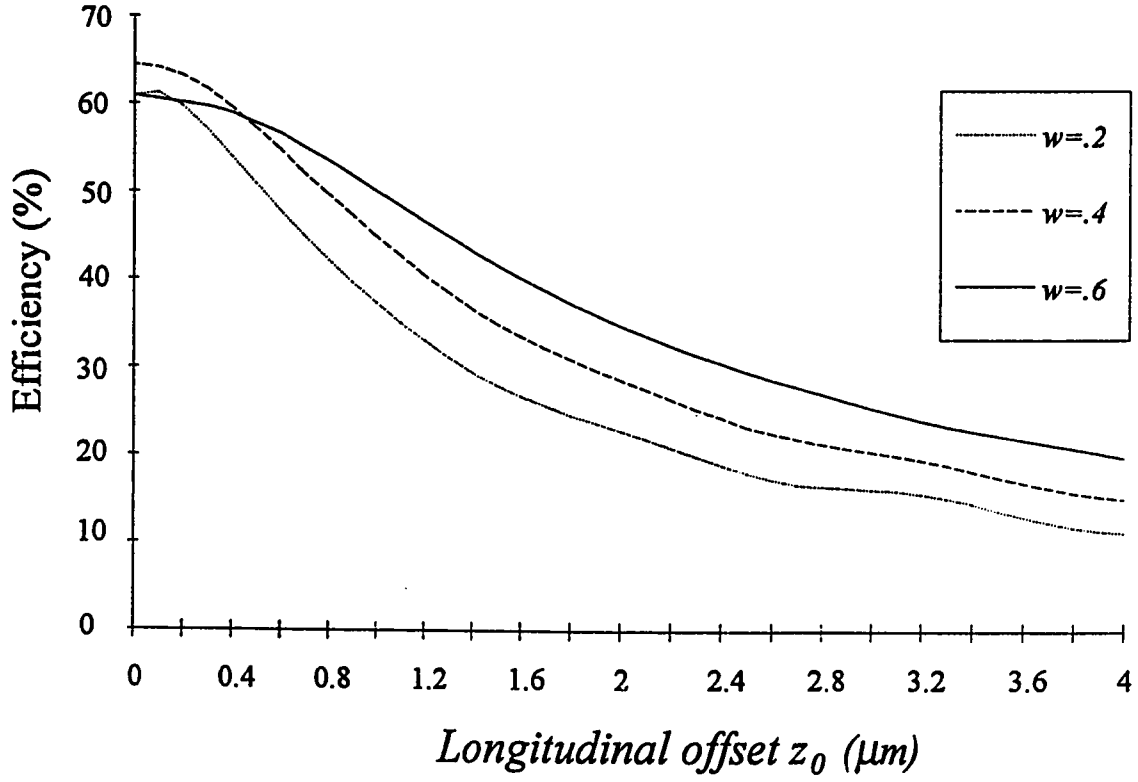

Figure (4.22) *Effect of longitudinal offset for different core widths (w_0 = .3 μm).*

4.4 Computational Constraints

The MoL provided very strong capability in the calculations of the transmitted and reflected powers under perfect alignment as well as in the presence of longitudinal or lateral offsets. The conservation of power at coupling interfaces provided a good indicator for the convergence of this method. However, there were two occasions where the method failed to give the required results. One problem encountered was the instability of the power conservation condition for values of the Gaussian beam HBW lying in the interval $0<w_0<.3\ \mu m$. Possible reasons for this problem are attributed to the three-point central difference approximation used in the MoL as discussed in the previous Subsection (4.3.2).

Another problem associated with the MoL is its inability to accurately account for the effect of negative longitudinal offset. In some applications it might be necessary to have the beam waist of the incident Gaussian beam positioned inside the slab waveguide as a part of optical integration process. In such cases, the MoL becomes unstable, producing extremely large efficiency figures. The reason for this is that the reflected field $e^{-jQ_1^{1/2}z}$ will have

growing terms. The computer cannot handle calculations with growing exponentials because it leads to instability.

4.5 Summary

All the acquired knowledge developed in the previous chapters about optical waveguides and the MoL has been applied in this chapter to study the main parameters affecting the power coupling efficiency from a laser source into a dielectric slab waveguide. Variations of efficiency versus the incident Gaussian beam HBW w_0, the waveguide core halfwidth w and the refractive index of the cladding have been analyzed. The analysis was conducted for perfect alignment as well as for lateral and longitudinal offsets. Computational constraints that limit the application of the MoL has been also considered and causes were presented.

In general, the maximum power coupling efficiency figures were obtained under perfect alignments and they did not exceed 70. This implies the necessity for a means to increase this efficiency. One way is the insertion of a transparent anti-reflection coating , which will be the subject of discussion of the next chapter.

General conclusions about the results of this chapter will be left to Chapter VI; " Conclusions and Future Work" and will not be repeated here.

CHAPTER V

THE EFFECT OF THE PRESENCE OF AN ANTI-REFLECTION LAYER

5.1 Introduction

An excellent coupling system is strongly dependent on the optical feedback caused by the reflections from the waveguide front face. This feedback can result in a remarkable distortion on the laser output characteristics such as the output power and the operational wavelength, and the power coupling efficiency, in turn, will be severely affected by these reflections.

One of the most successful means of increasing the power coupling efficiency is the insertion of an anti-reflection layer between the incident light beam and the slab waveguide. If the antireflective coating is chosen such that its thickness and refractive index are optimum, then the resulting reflection radiation from one side of the coating will be approximately 180° out-of-phase with the radiation

from the other side , thus canceling the overall reflected field.

Several rigorous methods have been proposed for the analysis of reflections at the output facet of a laser diode with anti-reflection coating. Reference [51] outlines some of these methods and proposes another approximate technique. In this chapter, we will apply the MoL to account for the presence of an anti-reflective coating at the end face of the slab waveguide under consideration. It will be seen that the MoL application is straight forward and less complex as compared to the other proposed methods.

5.2 Derivation of the Anti-Reflection Layer Optimum Parameters

The inserted anti-reflection layer (AR) is characterized by its refractive index and thickness. In order to have the best performance of this AR coating, these two parameters have to be optimized. Optimum parameters are different for the TE and TM polarization. In the following analysis, we will consider TE polarized fields only.

We start our discussion by considering a layer of thickness d and refractive index n_3 (region I) inserted between air (region 0) and a slab waveguide (region II) as shown in figure (5.1-a). To ease this analysis, the incident field will be treated as a plane wave and the incidence will be assumed to be normal. In addition, the three regions; 0, I, II will be considered as homogeneous media with refractive indices n_0, n_3 and n_e respectively. As can be seen from this figure, the fields in the three regions can be expressed as

$$\psi_0 = a_0 e^{j\beta_0 z} + b_0 e^{-j\beta_0 z} \tag{5.1}$$

$$\psi_1 = a_1 e^{j\beta_1 z} + b_1 e^{-j\beta_1 (z-d)} \tag{5.2}$$

$$\psi_2 = a_2 e^{j\beta_2 (z-d)} \tag{5.3}$$

where the indices; 0, 1, and 2 refer to regions 0, I and II respectively.

Applying the continuity of the electric field at $z=0$

$$a_0 e^{j\beta_0 z} + b_0 e^{-j\beta_0 z}\Big|_{z=0} = a_1 e^{j\beta_1 z} + b_1 e^{-j\beta_1 (z-d)}\Big|_{z=0}$$

which simplifies to

$$a_0 + b_0 = a_1 + b_1 e^{j\beta_1 d} \tag{5.4}$$

The continuity of the first derivative of ψ with respect to z at $z=0$ leads to

$$\beta_0 a_0 - \beta_0 b_0 = \beta_1 a_1 - \beta_1 b_1 e^{j\beta_1 d} \tag{5.5}$$

It shall be noticed that all the quantities in the above equations are scalars.

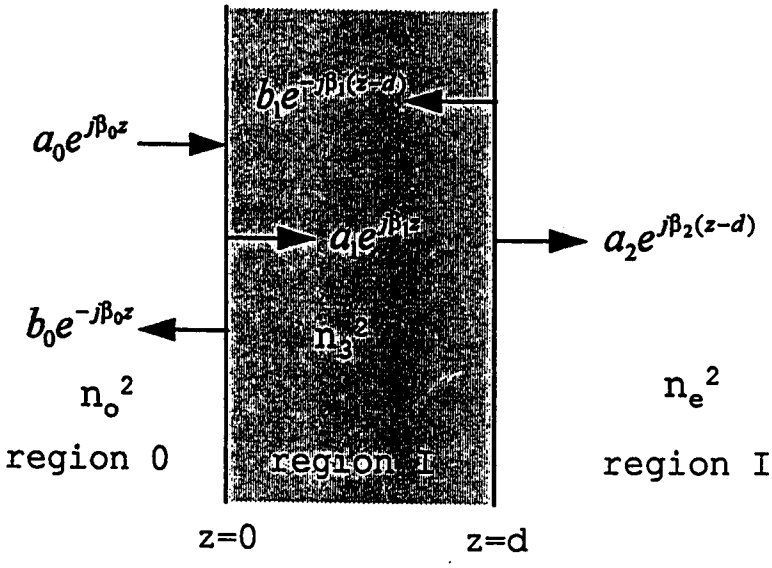

a) Normally incident plane wave upon an anti-reflection layer between two homogeneous media.

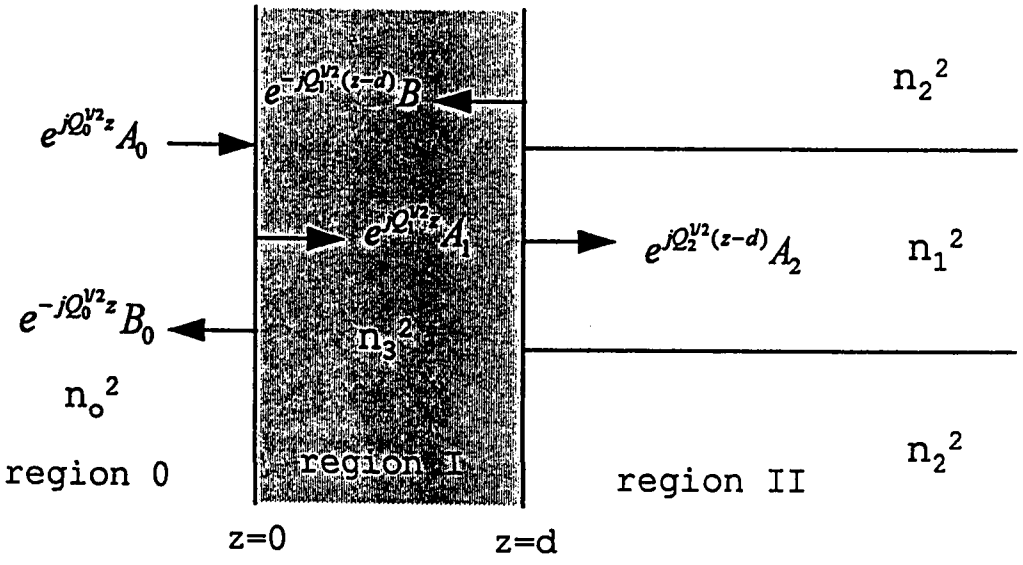

b) MoL representation

Figure (5.1) Illustration of the insertion of the anti-reflection layer

Similarly, applying the boundary conditions at the second boundary; $z=d$, results in the following:

$$a_1 e^{j\beta_1 d} + b_1 = a_2 \tag{5.6}$$

and

$$\beta_1 a_1 e^{j\beta_1 d} - \beta_1 b_1 = \beta_2 a_2$$

or

$$\frac{\beta_1}{\beta_2} a_1 e^{j\beta_1 d} - \frac{\beta_1}{\beta_2} b_1 = a_2 \tag{5.7}$$

Subtracting equation (5.7) from (5.6) yields the following relation for the reflection coefficient b_1:

$$b_1 = \left(\frac{\beta_1 - \beta_2}{\beta_1 + \beta_2}\right) e^{j\beta_1 d} a_1$$

or

$$b_1 = u.e^{j\beta_1 d}.a_1 \tag{5.8}$$

where

$$u = \frac{\beta_1 - \beta_2}{\beta_1 + \beta_2} \tag{5.9}$$

Substituting the results of equation (5.8) in both; equations (5.4) and (5.5) yields the following two relations for the coefficient a_1:

$$a_1 = \frac{(a_0 + b_0)}{\left(1 + e^{2j\beta_1 d} u\right)} \tag{5.10}$$

and

$$a_1 = \frac{\beta_0}{\beta_1} \frac{(a_0 - b_0)}{\left(1 - e^{2j\beta_1 d} u\right)} \tag{5.11}$$

Subtracting equation (5.11) from (5.10) leads to

$$\frac{(a_0+b_0)}{\left(1+e^{2j\beta_1 d}u\right)}-\frac{\beta_0}{\beta_1}\frac{(a_0-b_0)}{\left(1-e^{2j\beta_1 d}u\right)}=0 \qquad (5.12)$$

If we let $$w_1=\left(1+e^{2j\beta_1 d}u\right)$$

and $$w_2=\left(1-e^{2j\beta_1 d}u\right) \qquad (5.13)$$

then equation (5.12) reduces to

$$w_2a_0+w_2b_0-\frac{\beta_0}{\beta_1}w_1a_0+\frac{\beta_0}{\beta_1}w_1b_0=0$$

from which the reflection field coefficient b_0 can be related to the incident field coefficient a_0 by

$$b_0=\left(\frac{\beta_0w_1-\beta_1w_2}{\beta_0w_1+\beta_1w_2}\right)a_0 \qquad (5.14)$$

The AR coating is optimum when the reflected field in region 0 vanishes, i.e., when $b_0=0$. Equating the left-hand-side of equation (5.14) to zero leads to

$$\beta_0w_1-\beta_1w_2=0 \qquad (5.15)$$

Substituting the values of w_1 and w_2 back in equation (5.15) and grouping the similar terms, results in the following relation

$$\left(\beta_0\beta_1+\beta_0\beta_2-\beta_1^2-\beta_1\beta_2\right)$$
$$+\left(\beta_0\beta_1-\beta_0\beta_2+\beta_1^2-\beta_1\beta_2\right)e^{2j\beta_1 d}=0 \qquad (5.16)$$

The left-hand-side of the above equation can be equal to zero only if both of the following conditions are satisfied:

i) $e^{2j\beta_1 d} = -1$, and

ii) $(\beta_0\beta_1 + \beta_0\beta_2 - \beta_1^2 - \beta_1\beta_2) = (\beta_0\beta_1 - \beta_0\beta_2 + \beta_1^2 - \beta_1\beta_2)$.

for the first condition to be satisfied,

$$2\beta_1 d = m\pi, \qquad m = \pm 1, \pm 3, \pm 5, \ldots, \textit{odd multiples}$$

but

$$\beta_1 = \frac{2\pi}{\lambda} = \frac{2\pi n_3}{\lambda_0}$$

therefore, the optimum value of the AR layer thickness d shall be

$$d = \frac{m\lambda_0}{4n_3} \tag{5.17}$$

To satisfy the second condition,

$$(\beta_0\beta_2 - \beta_1^2) = -(\beta_0\beta_2 - \beta_1^2)$$

which implies that

$$(\beta_0\beta_2 - \beta_1^2) = 0$$

or

$$\beta_1^2 = \beta_0\beta_2$$

Writing the propagation constants in terms of their corresponding refractive indices yields the following:

$$\left(\frac{2\pi}{\lambda_0} n_3\right)^2 = \left(\frac{2\pi}{\lambda_0} n_0 \cdot \frac{2\pi}{\lambda_0} n_e\right)$$

from which the optimum refractive index of the AR layer; n_3 can be found to be

$$n_3 = \sqrt{n_0 n_e} \tag{5.18}$$

5.3 Application of the MoL to the Anti-Reflection Layer

Consider a converging Gaussian beam incident from air into a dielectric slab waveguide. A layer of anti-reflection coating is inserted (region I) between the air (region 0) and the waveguide (region II) as illustrated in figure (5.1-b). According to the principle of the MoL, the fields in the three regions can be described in the following discretized form:

$$\psi_0 = e^{jQ_0^{1/2}z}A_0 + e^{-jQ_0^{1/2}z}B_0 \qquad (5.19)$$

$$\psi_1 = e^{jQ_1^{1/2}z}A_1 + e^{-jQ_1^{1/2}(z-d)}B_1 \qquad (5.20)$$

$$\psi_2 = e^{jQ_2^{1/2}(z-d)}A_2 \qquad (5.21)$$

where A_0, B_0 and A_1 represent the discretized form of the incident, reflected and transmitted fields at $z=0$ respectively, while B_1 is the reflected field and A_2 is the transmitted field at $z=d$.

In order to find out the percentage of power coupled from the incident Gaussian beam into the fundamental mode of the waveguide, we need to solve for the vector A_2. In the above three equations, the incident field distribution A_0 is the only known field quantity. To find the relation between the other four vectors and A_0, we will apply the appropriate boundary conditions at $z=0$ and $z=d$ (i.e., the continuity of

ψ and its first derivative with respect to z at both $z=0$ and $z=d$).

Applying the boundary condition at $z=0$:

$$\psi_0(0)=\psi_1(0)$$

$$A_0+B_0=A_1+e^{j\Omega_1^{1/2}d}B_1 \tag{5.22}$$

and

$$\left.\frac{d\psi_0}{dz}\right|_{z=0}=\left.\frac{d\psi_1}{dz}\right|_{z=0}$$

results in

$$\left[jQ_0^{1/2}e^{j\Omega_0^{1/2}z}A_0-jQ_0^{1/2}e^{-j\Omega_0^{1/2}z}B_0\right]_{z=0}=\left[jQ_1^{1/2}e^{j\Omega_1^{1/2}z}A_1-jQ_1^{1/2}e^{-j\Omega_1^{1/2}(z-d)}B_1\right]_{z=0}$$

$$Q_0^{1/2}A_0-Q_0^{1/2}B_0=Q_1^{1/2}A_1-Q_1^{1/2}e^{j\Omega_1^{1/2}d}B_1$$

or

$$Q_1^{-1/2}Q_0^{1/2}A_0-Q_1^{-1/2}Q_0^{1/2}B_0=A_1-e^{j\Omega_1^{1/2}d}B_1 \tag{5.23}$$

To simplify equation (5.23), we let

$$T_1=Q_1^{-1/2}Q_0^{1/2} \tag{5.24}$$

Equation (5.23) can then be written as

$$T_1A_0-T_1B_0=A_1-e^{j\Omega_1^{1/2}d}B_1 \tag{5.25}$$

Applying the boundary condition at $z=d$:

$$\psi_1(d)=\psi_2(d)$$

leads to

$$e^{j\Omega_1^{1/2}d}A_1+B_1=A_2 \tag{5.26}$$

and

$$\left.\frac{d\psi_1}{dz}\right|_{z=d} = \left.\frac{d\psi_2}{dz}\right|_{z=d}$$

leads to

$$\left[jQ_1^{1/2}e^{jQ_1^{1/2}z}A_1 - jQ_1^{1/2}e^{-jQ_0^{1/2}(z-d)}B_1\right]_{z=d} = \left[jQ_2^{1/2}e^{jQ_2^{1/2}(z-d)}A_2\right]_{z=d}$$

simplifies to

$$Q_2^{-1/2}Q_1^{1/2}e^{jQ_1^{1/2}d}A_1 - Q_2^{-1/2}Q_1^{1/2}B_1 = A_2$$

or
$$T_2e^{jQ_1^{1/2}d}A_1 - T_2B_1 = A_2 \qquad (5.27)$$

where
$$T_2 = Q_2^{-1/2}Q_1^{1/2} \qquad (5.28)$$

Equation (5.27) relates A_2 to A_1 and B_1. Our aim is to find a direct relation between A_2 and A_0. In order to achieve this, further manipulations are required.

Subtracting equation (5.27) from (5.26) leads to

$$(I - T_2)e^{jQ_1^{1/2}d}A_1 + (I + T_2)B_1 = 0$$

results in

$$B_1 = \left[(I + T_2)^{-1}.(T_2 - I).e^{jQ_1^{1/2}d}\right].A_1 \qquad (5.29)$$

where I is the identity matrix.

By letting

$$V = \left[(I + T_2)^{-1}.(T_2 - I).e^{jQ_1^{1/2}d}\right] \qquad (5.30)$$

Equation (5.29) reduces to the following form

$$B_1 = V.A_1 \tag{5.31}$$

Substituting equation (5.31) in (5.22) leads to

$$A_0 + B_0 = A_1 + e^{jQ_1^{1/2}d}.VA_1$$
$$= \left(I + e^{jQ_1^{1/2}d}.V\right).A_1$$

from which

$$A_1 = S_1.(A_0 + B_0) \tag{5.32}$$

where

$$S_1 = \left(I + e^{jQ_1^{1/2}d}.V\right)^{-1} \tag{5.33}$$

Similarly, by substituting equation (5.31) in (5.25)

$$T_1(A_0 - B_0) = A_1 - e^{jQ_1^{1/2}d}VA_1$$
$$= \left(I - e^{jQ_1^{1/2}d}V\right).A_1$$

resulting in

$$A_1 = S_2.(A_0 - B_0) \tag{5.34}$$

where

$$S_2 = \left(I - e^{jQ_1^{1/2}d}V\right)^{-1}.T_1 \tag{5.35}$$

A_1 can be eliminated by subtracting equation (5.34) from (5.32)

$$(S_1 - S_2)A_0 + (S_1 + S_2)B_0 = 0$$

or

$$B_0 = (S_1 + S_2)^{-1}.(S_2 - S_1).A_0 \tag{5.36}$$

Combining equations (5.22) and (5.25) and substituting the results of (5.36) yields the following relation

$$A_1 = \left[(I + T_1) + (I - T_1)(S_1 + S_2)^{-1}(S_2 - S_1)\right]\frac{A_0}{2} \qquad (5.37)$$

Substituting equations (5.31) and (5.37) in (5.26) leads to the following expression relating the transmitted field in region II; A_2 to the incident field of region 0; A_0

$$A_2 = \frac{1}{2}\left(e^{jk_{2i}v_{2i}d} + V\right)\left[(I + T_1) + (I - T_1)(S_1 + S_2)^{-1}(S_2 - S_1)\right]A_0 \qquad (5.38)$$

Now, we have found the value of A_2 in terms of A_0, we can calculate the fundamental mode excitation coefficient α_0. From equation (2.50), α_0 is given by

$$\alpha_0 = \frac{\int_{-\infty}^{\infty} \psi(x,d) f_0(x) dx}{\int_{-\infty}^{\infty} f_0^2(x) dx}$$

$$\approx \frac{A_2' F_0 \Delta x}{F_0' F_0 \Delta x}$$

$$= \frac{A_2' F_0}{F_0' F_0} \qquad (5.39)$$

where F_0 is the discretized form of the fundamental mode distribution. Consequently, the average incident and guided power can be expressed as

$$P_i = \mathrm{Re}\left\{\frac{1}{2\omega\mu}\left(Q_0^{1/2}A_0\right)^* A_0\right\}.\Delta x \qquad (5.40)$$

$$P_g = \mathrm{Re}\left\{\frac{1}{2\omega\mu}\left(Q_2^{1/2}\alpha_0 F_0\right)^*\left(\alpha_0 F_0\right)\right\}.\Delta x \qquad (5.41)$$

The power coupling efficiency is therefore given by

$$\eta = \frac{P_g}{P_i} = \frac{\mathrm{Re}\left\{\left(Q_2^{1/2}\alpha_0 F_0\right)^*\left(\alpha_0 F_0\right)\right\}}{\mathrm{Re}\left\{\left(Q_0^{1/2}A_0\right)^* A_0\right\}} \qquad (5.42)$$

5.4 Effect of Introducing the Anti-Reflection Layer

In this section we apply the MoL to analyze the effect of inserting an anti-reflection coating characterized by optimum parameters as derived above and given by equations (5.17) and (5.18). Since these parameters are approximate, we will investigate values around them in order to approach the maximum efficiency and the lowest possible reflectivity. As the optimum parameters leading to the highest efficiency are expected to differ from those resulting in lowest reflectivity, we will investigate the effect of the AR on both the efficiency and reflectivity individually. The program developed for this purpose is "MoL10" and it is listed in Appendix-B.

5.4.1 Effect on the Efficiency

Consider the illustration of figure (5.1-b), in which a transparent layer of antireflective coating is inserted between the incident beam and the waveguide. The AR layer has been optimized according to the results of Section (5.2) to have a refractive index $n_3=\sqrt{n_e}$ and a thickness $d=\frac{\lambda_0}{4n_3}$, where n_e is taken to be the effective index of the fundamental TE mode of the slab waveguide.

For the same reasons outlined in the previous chapter, calculations for the interval $0<w_0<.3\ \mu m$, yield values for the $R+T$ term $(R+T=\frac{1}{P_i}(P_t+P_r))$ that exceed unity as shown in figure (5.2) and are , therefore, excluded. Figures (5.3), (5.4) and (5.5) present the effect of the AR coating for three different core halfwidths; w= .2, .4, and .6 μm, for varying w_0 and a cladding index; n_2= 3.4. The dashed curves represent the efficiency without the AR layer while the solid ones show the efficiency with the AR layer inserted. It can be seen that the efficiency has in general, increased more than 30% and efficiency figures greater than

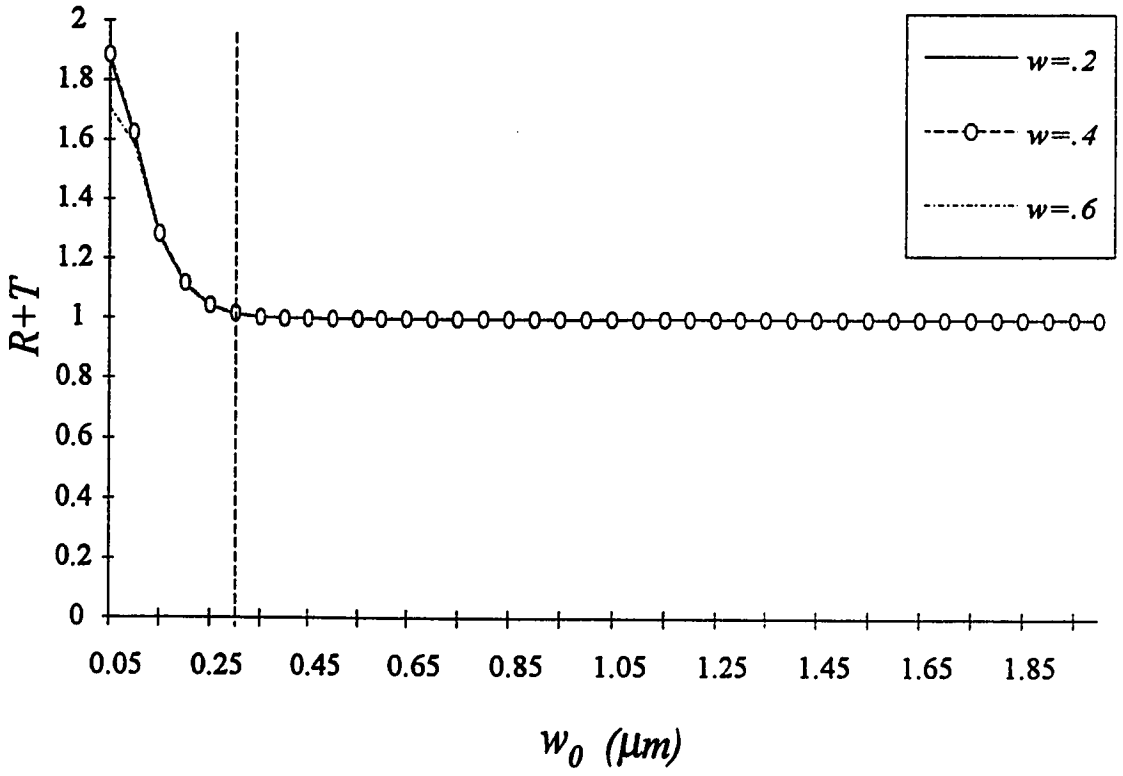

Figure (5.2) *Illustration of the (R+T) term behaviour versus* w_0.

$$R+T=\frac{1}{P_i}(P_t + P_r)$$

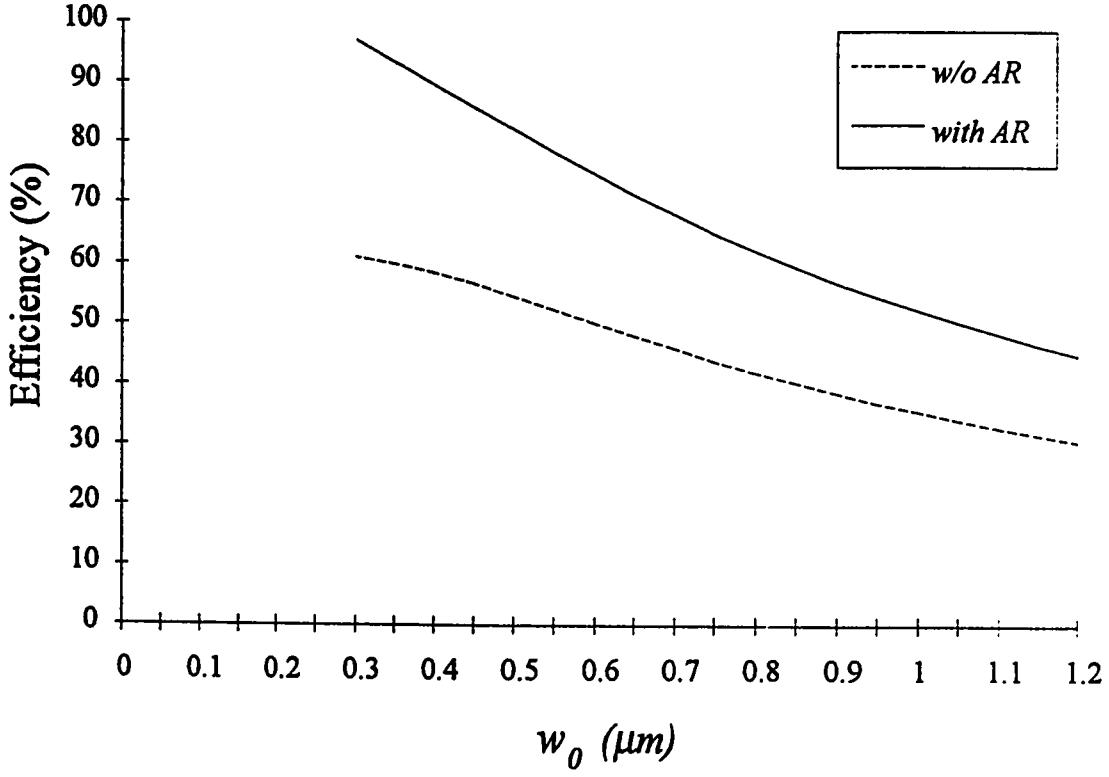

Figure (5.3) *Effect of the AR layer on efficiency (w= .2 μm).*

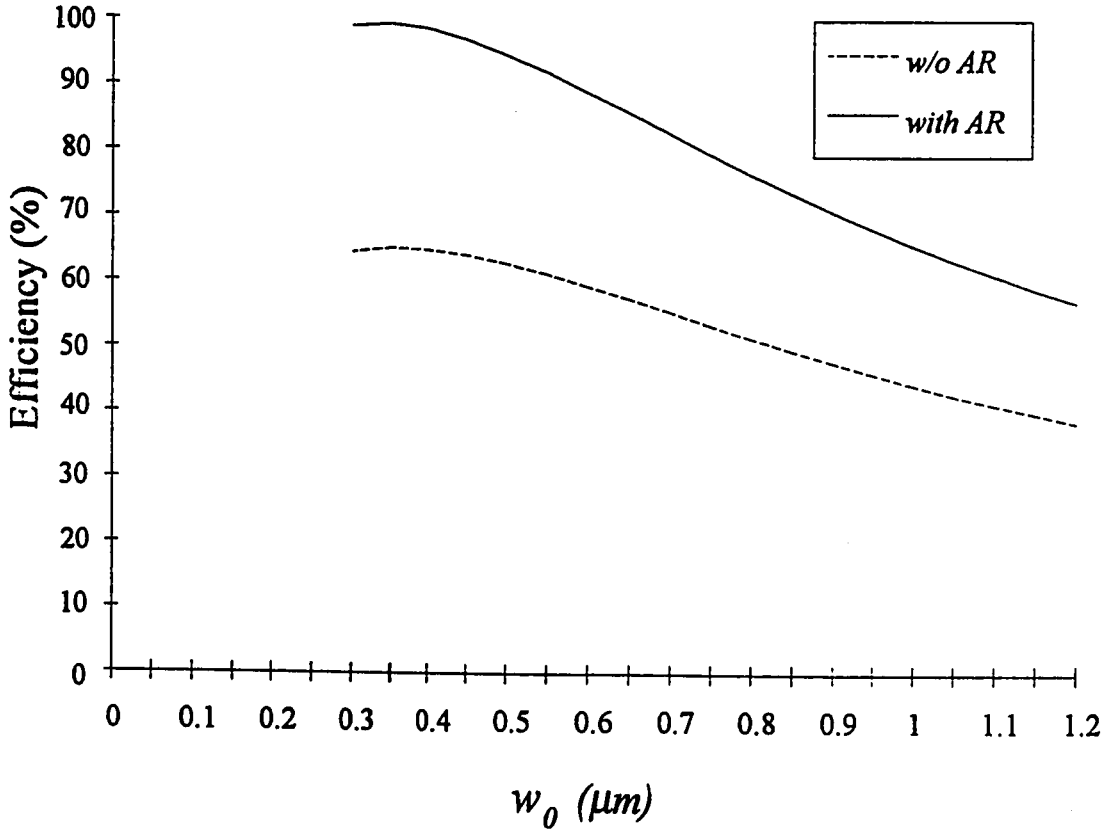

Figure (5.4) *Effect of the AR layer on efficiency (w= .4 μm).*

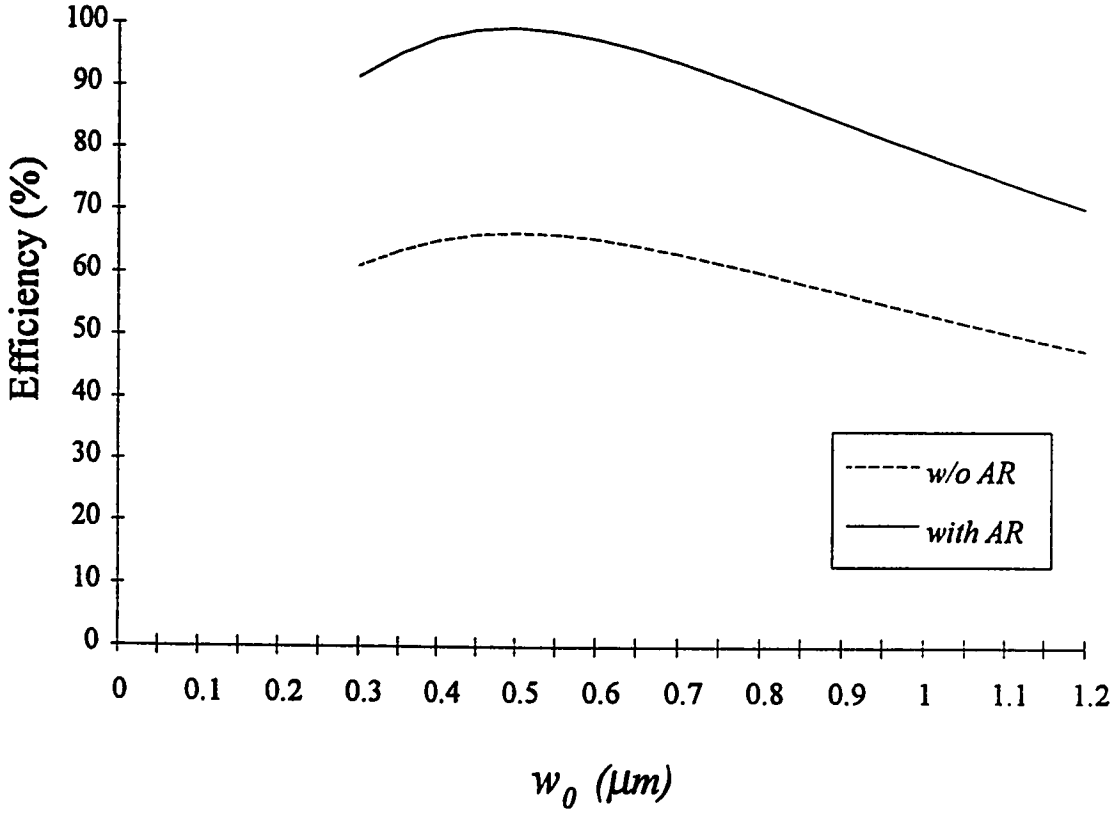

Figure (5.5) *Effect of the AR layer on efficiency (w= .6 μm).*

99% were obtained. The curves, however, maintained their maximum values at the same w_0 in both cases.

Figure (5.6) provides a comparison of the variations of the efficiency with and without the AR layer for two different values of cladding index; n_2= 3.3 and 3.55 and a core halfwidth; w=.2 μm. Similar graphs have been developed for w=.4 μm and .6 μm as shown on figures (5.7) and (5.8) respectively. We note from these graphs that as n_2 increases, sensitivity of changing w_0 on efficiency decreases. Referring to figure (5.7) for example, to maintain efficiency ; $\eta \geq$ 90%, for a cladding index; n_2= 3.55, the HBW of the incident Gaussian beam can have any value in the interval $.3 \leq w_0 \leq .9$ μm, while for the case of n_2= 3.3, w_0 is limited to the interval $.3 \leq w_0 \leq .55$ μm. Figure (5.9) illustrates the conformity of the transmitted field calculated at z=16 μm and the profile of the guided fundamental mode $(\alpha_0 F_0)$.

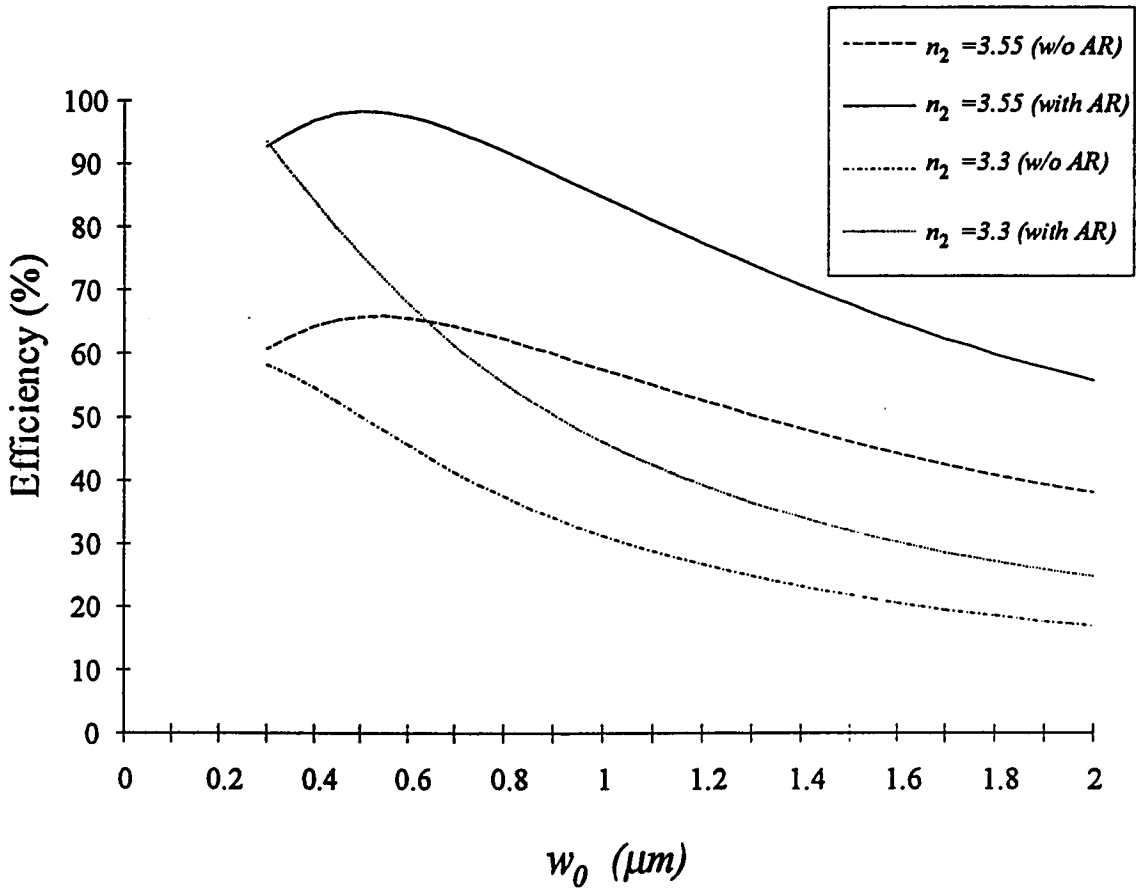

Figure (5.6) *Effect of the AR layer on efficiency for different* n_2 *(w= .2 μm).*

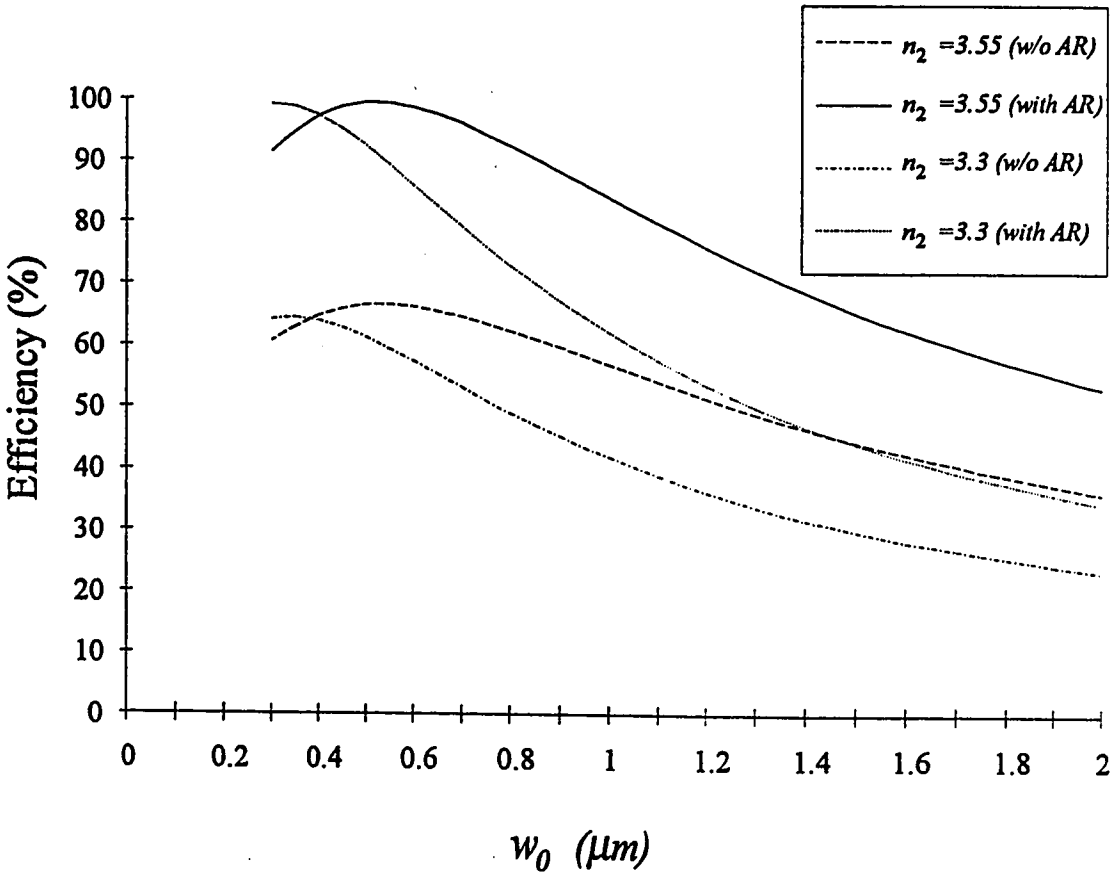

Figure (5.7) *Effect of the AR layer on efficiency for different n_2 ($w = .4$ μm).*

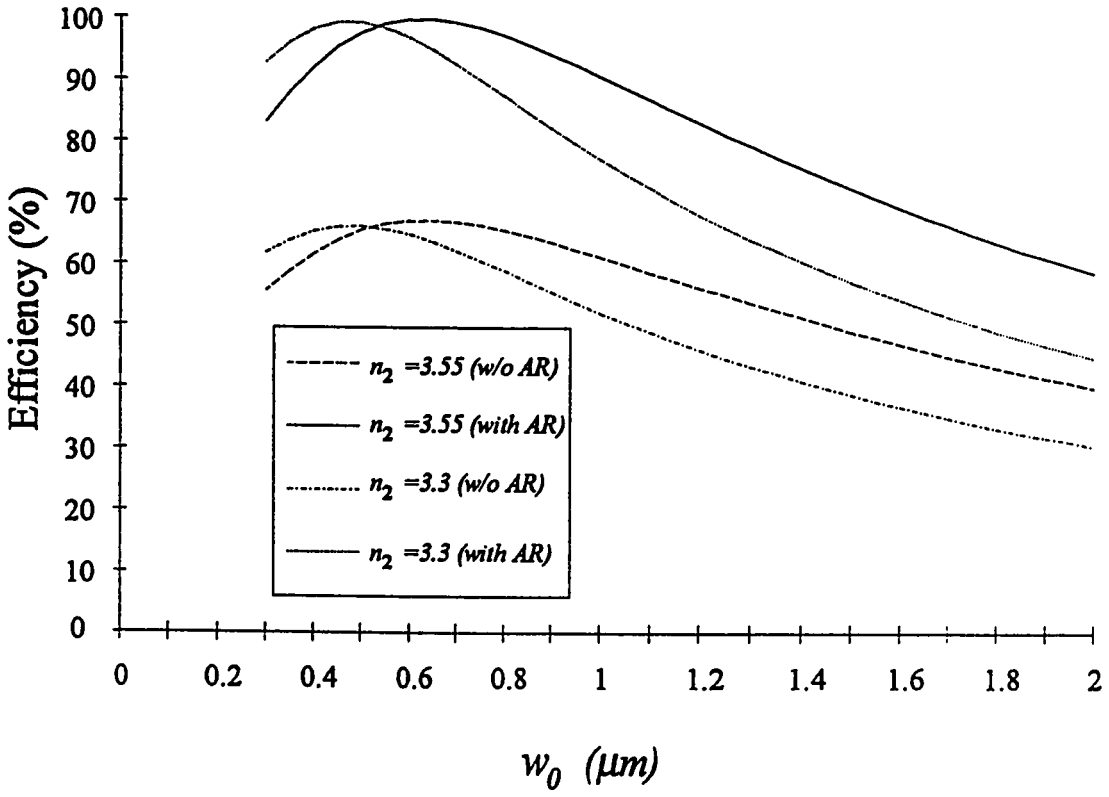

Figure (5.8) *Effect of the AR layer on efficiency for different* n_2 *(w= .6 μm).*

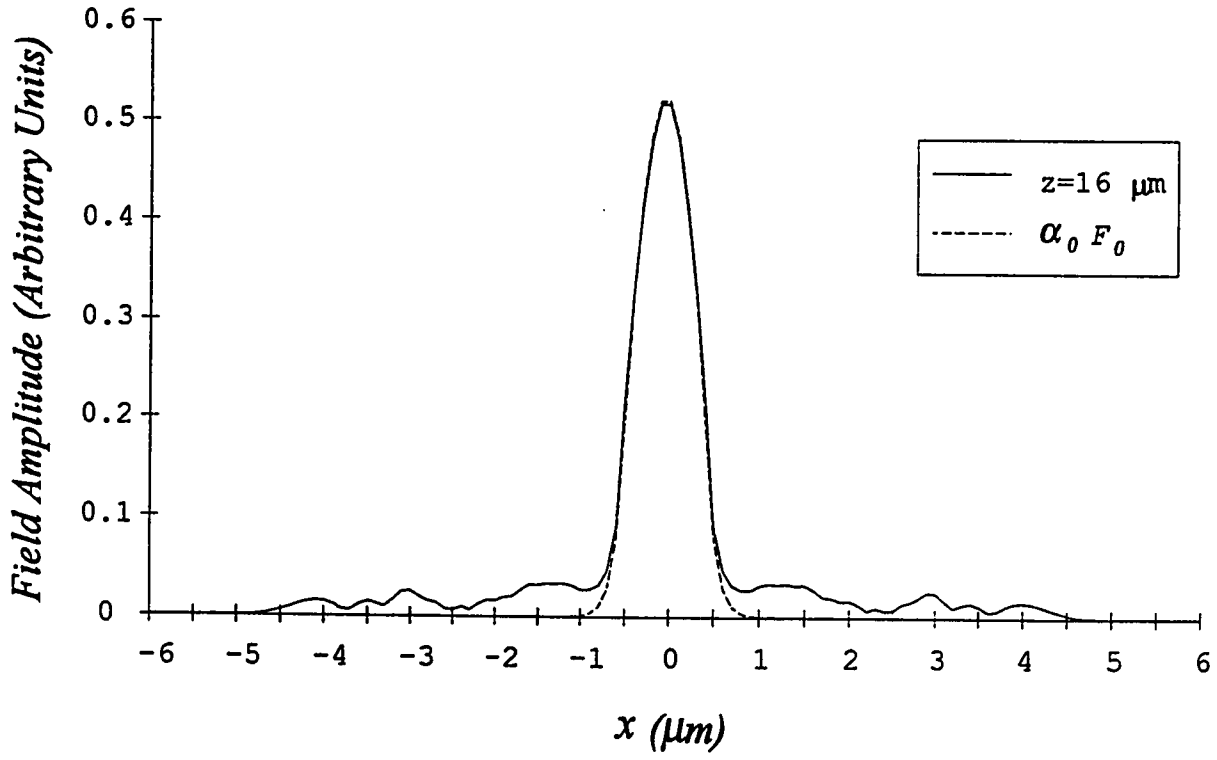

Figure (5.9) *Comparion between the guided fundamental mode and the transmitted field at z= 16 μm.*

5.4.2 Effect on the Reflectivity

In many applications such as in precision measurement devices, it is very important to minimize the amount of reflected power as this reflection will interfere with the incident light, resulting in disturbance to the accuracy upto which the device is to operate. In such instances, the designer preference for yielding less reflectivity exceeds his desire to have a higher figure of power coupling efficiency.

For the same configuration as that of the previous subsection, we will consider here the effect of the insertion of the AR layer on reflectivity (R). Figures (5.10), (5.11) and (5.12) present this effect for a waveguide with a cladding refractive index; n_2= 3.4 and core halfwidths; w= .2, .4 and .6 μm respectively. It can be seen also that for spot sizes lying in the interval $.55<w_0<1.2\ \mu m$, R attains values on the order of 10^{-4} which is acceptable for most practical applications [52]. Figure (5.13) illustrates this effect for a cladding index; $n_2 = 3.55$ and a core halfwidth; w=.2 μm. Whereas the minimum value of reflectivity obtained without the AR exceeds .3, figures of

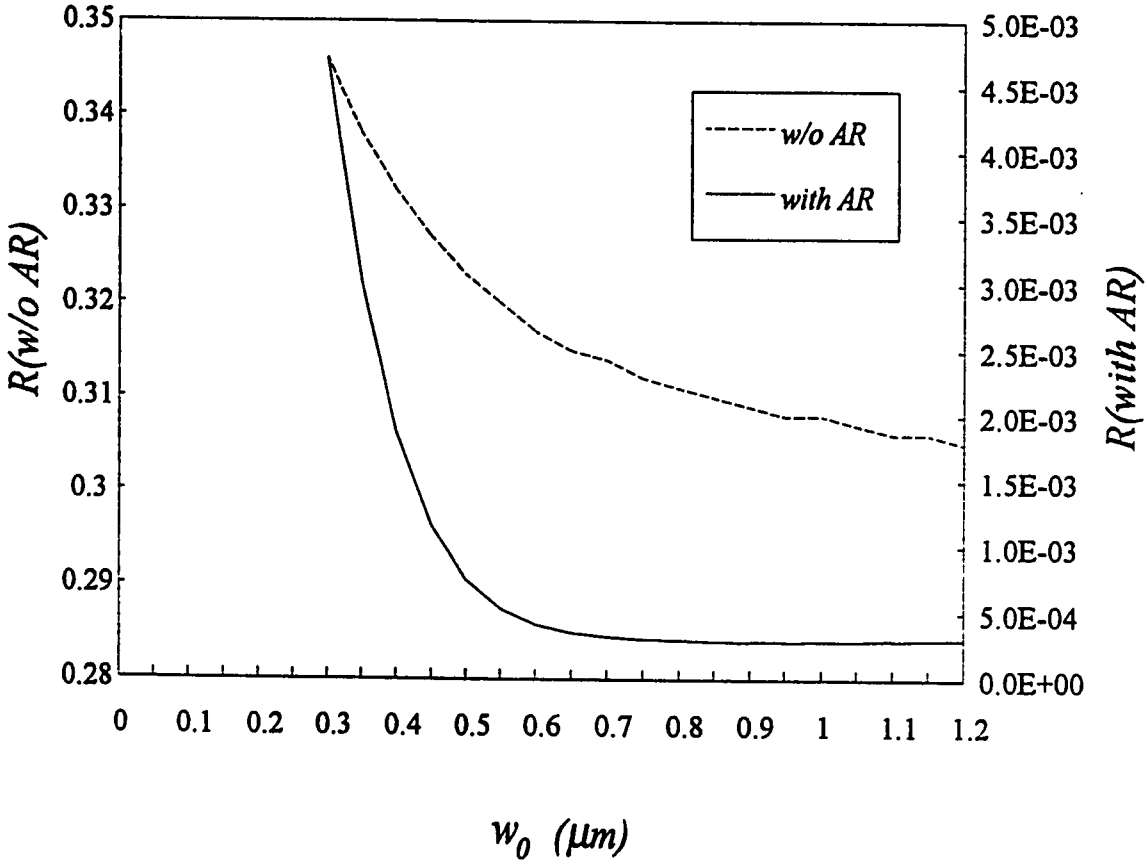

Figure (5.10) *Effect of the AR layer on reflectivity. (w= .2 μm).*

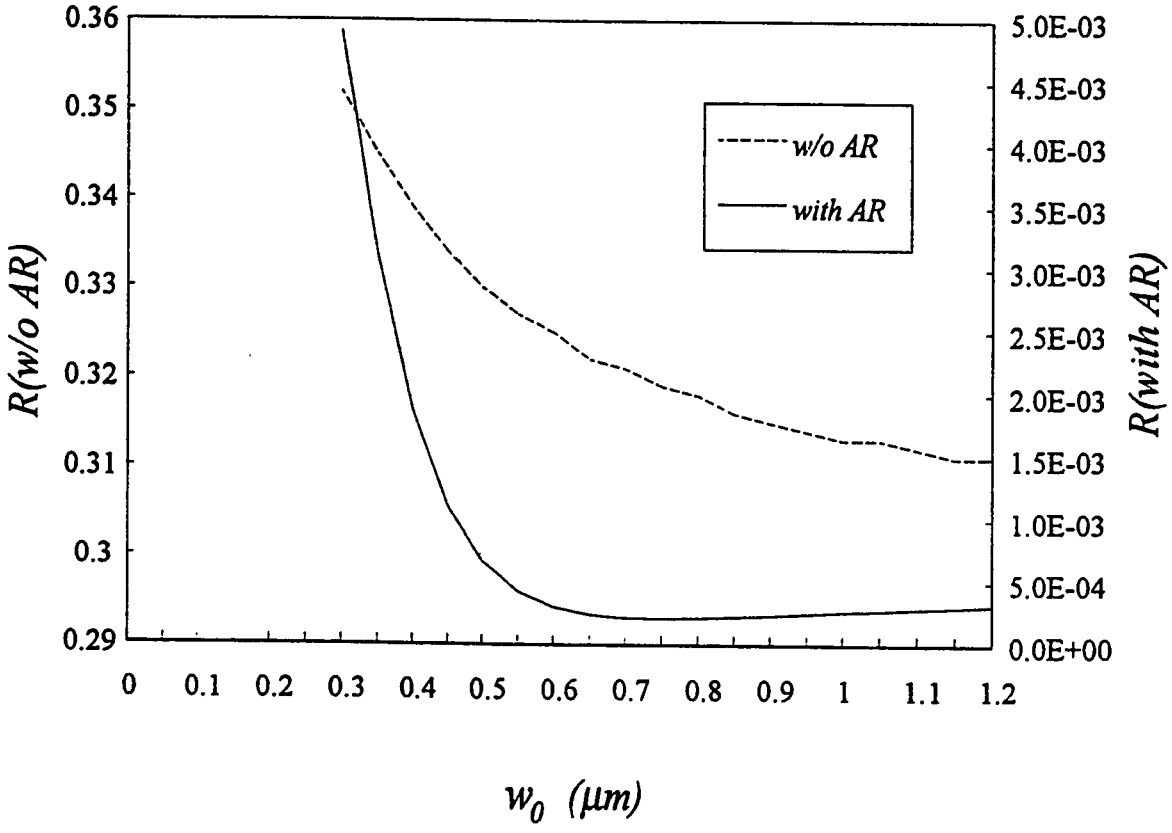

Figure (5.11) *Effect of the AR layer on reflectivity. (w= .4 μm).*

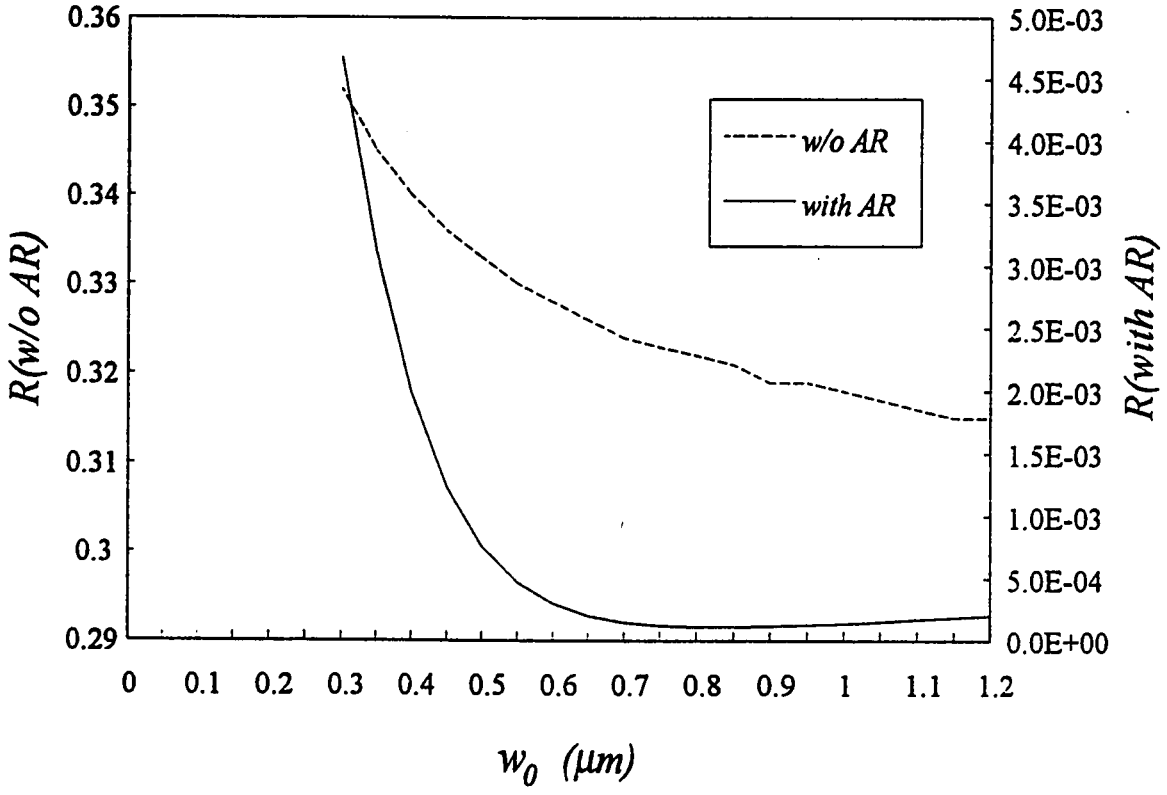

Figure (5.12) *Effect of the AR layer on reflectivity. (w= .6 μm).*

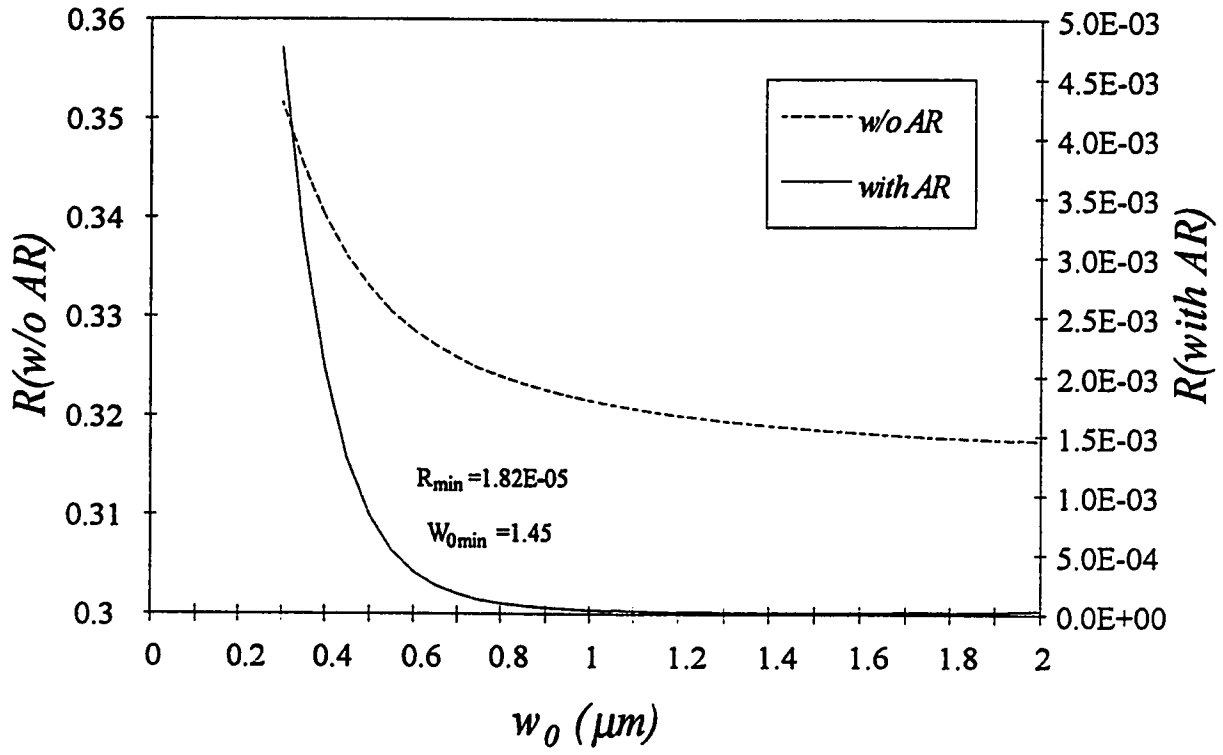

Figure (5.13) Effect of the AR Layer on Reflectivity (n_2 =3.55, w=.6 μm).

reflectivity in the order of 10^{-5} were possible after the insertion of the AR coating.

To illustrate the amount of tolerance a designer can have to achieve both objectives; higher efficiency and lower reflectivity, we have plotted both η and R on the same figure for w= .4 and .6 μm as shown in figures (5.14) and (5.15). For w= .4 μm, maximum efficiency is obtained at w_0=.35 μm, while the lowest reflectivity occurs at .75 μm. For w= .6 μm, they occur at .5 μm and .85 μm respectively. Figure (5.16) depicts the profile of the reflected field as it travels from the AR layer in the negative z-direction. The divergence from a Gaussian profile is attributed to the fact that this field is composed of the sum of all the reflected fields resulting from the insertion of the AR layer. It shall be noticed that the oscillating variations at the tails of these profiles are smaller than half a wavelength, therefore, they are caused by numerical errors and cannot be considered as being physical. Moreover, the amplitudes of these variations are in the order of 10^{-4} which can be ignored without loss of accuracy.

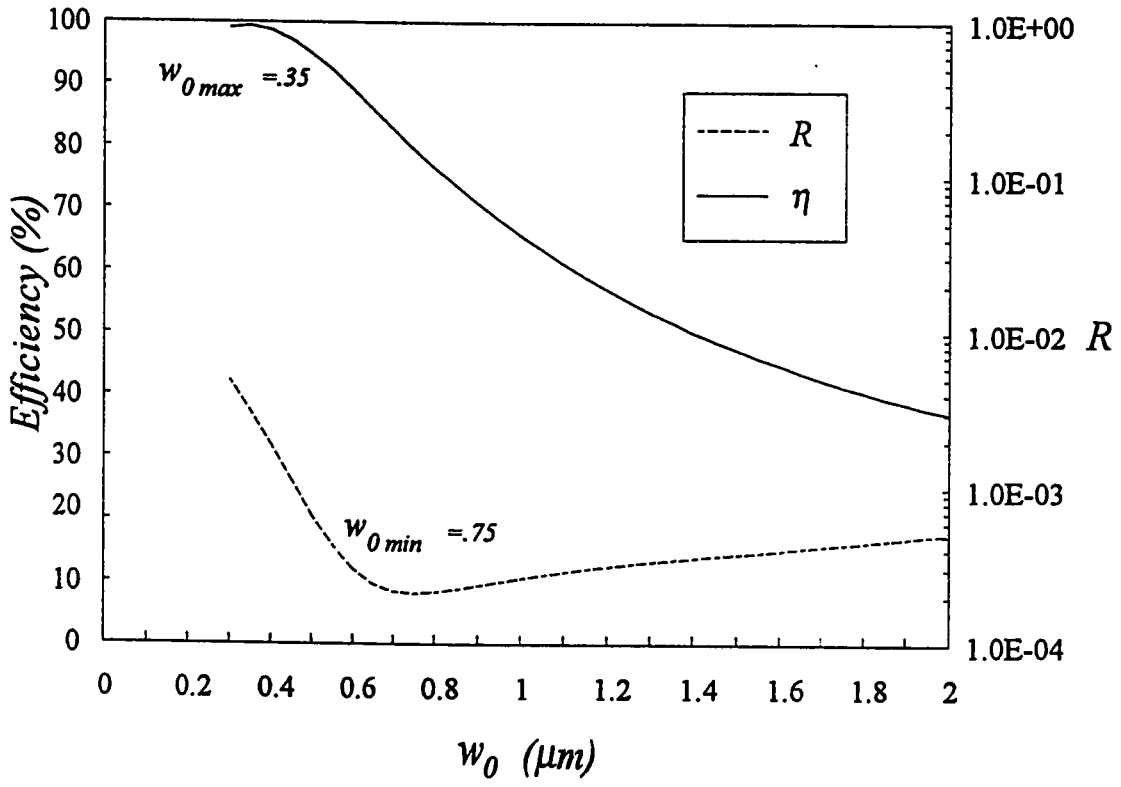

Figure (5.14) *Efficiency and reflectivity versus* w_0 *.* *(w= .4 μm)*

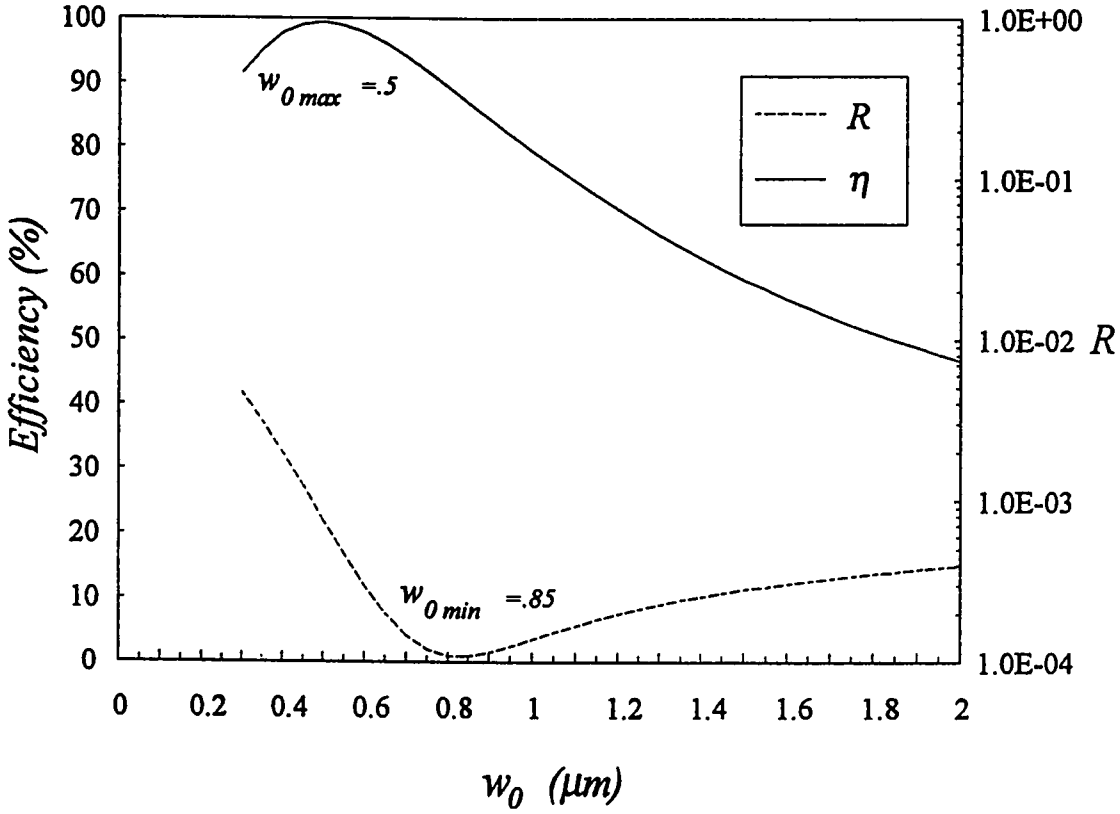

Figure (5.15) *Efficiency and reflectivity versus* w_0 *.* *(w= .6 μm)*

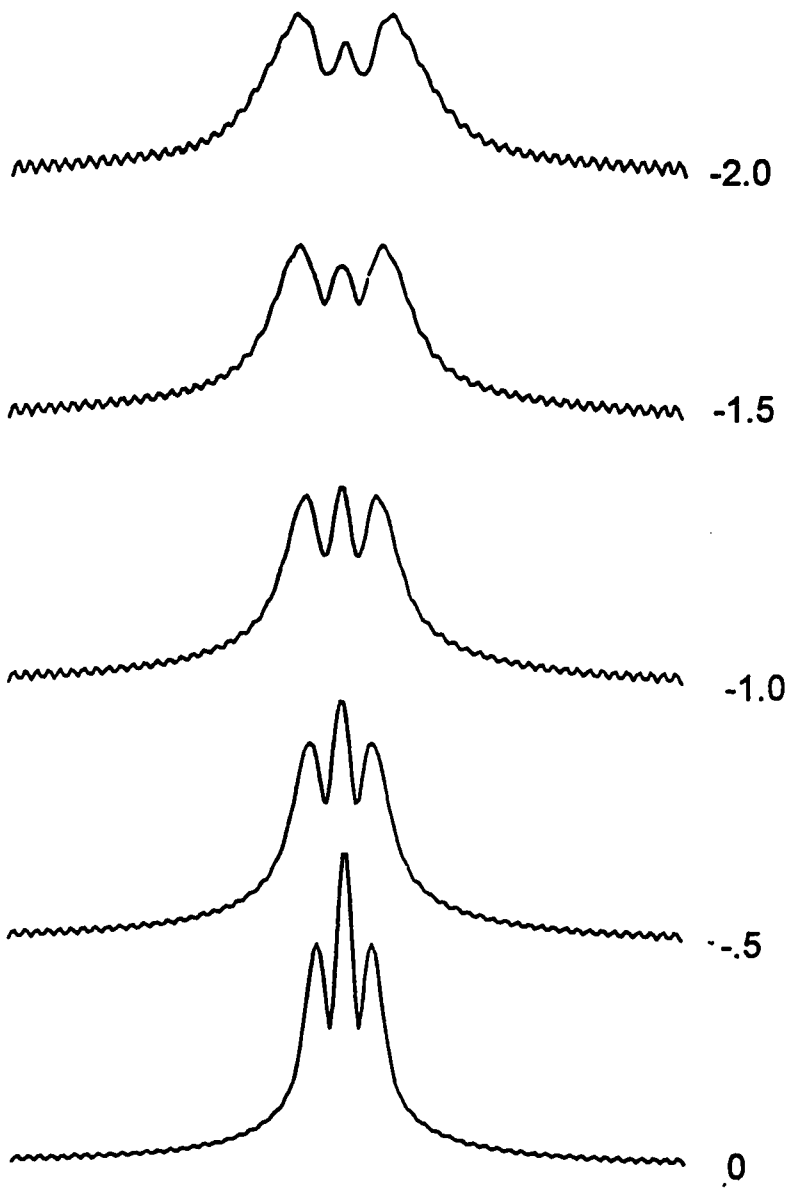

Figure (5.16) *The profile of the reflected field as it travels from the focusing plane located at z=0 , (numbers indicate distances are in μm).*

5.4.3 Effect of Varying the AR Layer Thickness and Refractive Index

As stated in Section (5.2), the derivation of the AR layer optimum parameters was based on treating the incident beam as a plane wave normally incident into homogeneous media. In reality, however, the incident beam is a Gaussian which can be considered as being composed of several plane waves incident at different angles. In addition, whereas region 0 and 1 of the treated structure are uniform, region 2 (the slab waveguide) is nonuniform and is composed of three layers.

The above approximation implies that better efficiency and reflectivity values may be found by finely tuning the derived AR parameters; d and n_3. To investigate that, we varied the thickness; d from .1 of its optimized value; $\frac{\lambda_0}{4n_3}$, to six times that value, where $n_3 = \sqrt{n_e}$. The results are shown in figure (5.17). As can be noticed from this figure, the periodicity of the maximum η and lowest R are functions of odd multiples of the ratio $\frac{d1}{d}$, where $d1$ is the variable thickness. We notice also that as the thickness increases, the maximum efficiency decreases. This is because as $d1$

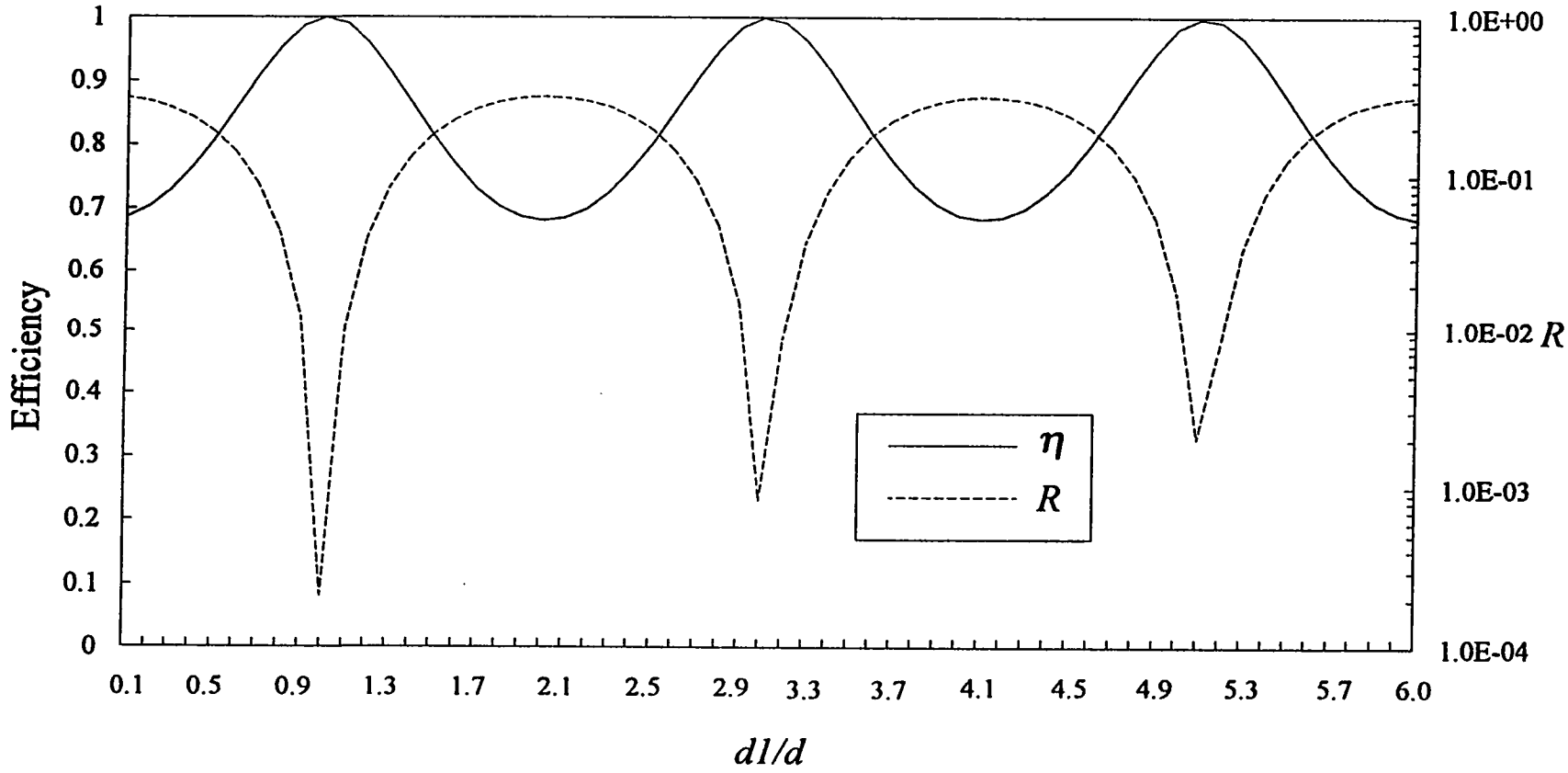

Figure (5.17) *Effect of varying the AR layer thickness*
(w= .4 μm, n_2 = 3.4, w_0 =.75 μm)

increases, the Gaussian beam expands, and the actual resulting HBW; w_0 as seen by the waveguide will be greater than the theoretical one. As a result, the overlap between the beam and the fundamental mode reduces and hence the power coupling efficiency decreases. Contrary to that, as the thickness increases, the minimum reflectivity increases.

Figure (5.18) shows that for a core halfwidth; w= .4 μm, n_2= 3.4, $n_3 = \sqrt{n_e}$ and HBW; w_0= .75 μm, the minimum reflectivity is; R=1.8285E-04, and it is obtained when the AR layer thickness; d is equal to 1.005 $\left(\frac{\lambda_0}{4n_3}\right)$. For w= .4 μm, n_2= 3.4, w_0= .3375 μm and $d = \frac{\lambda_0}{4n_3}$, it was found that the maximum efficiency is obtained when $n_3 = .985\sqrt{n_e}$, and its value is η_{max} = .9938185 as shown on figure (5.19). A summary of the effect of varying d and n_3 for the different waveguide parameters and beam HBW is presented in table (5.1).

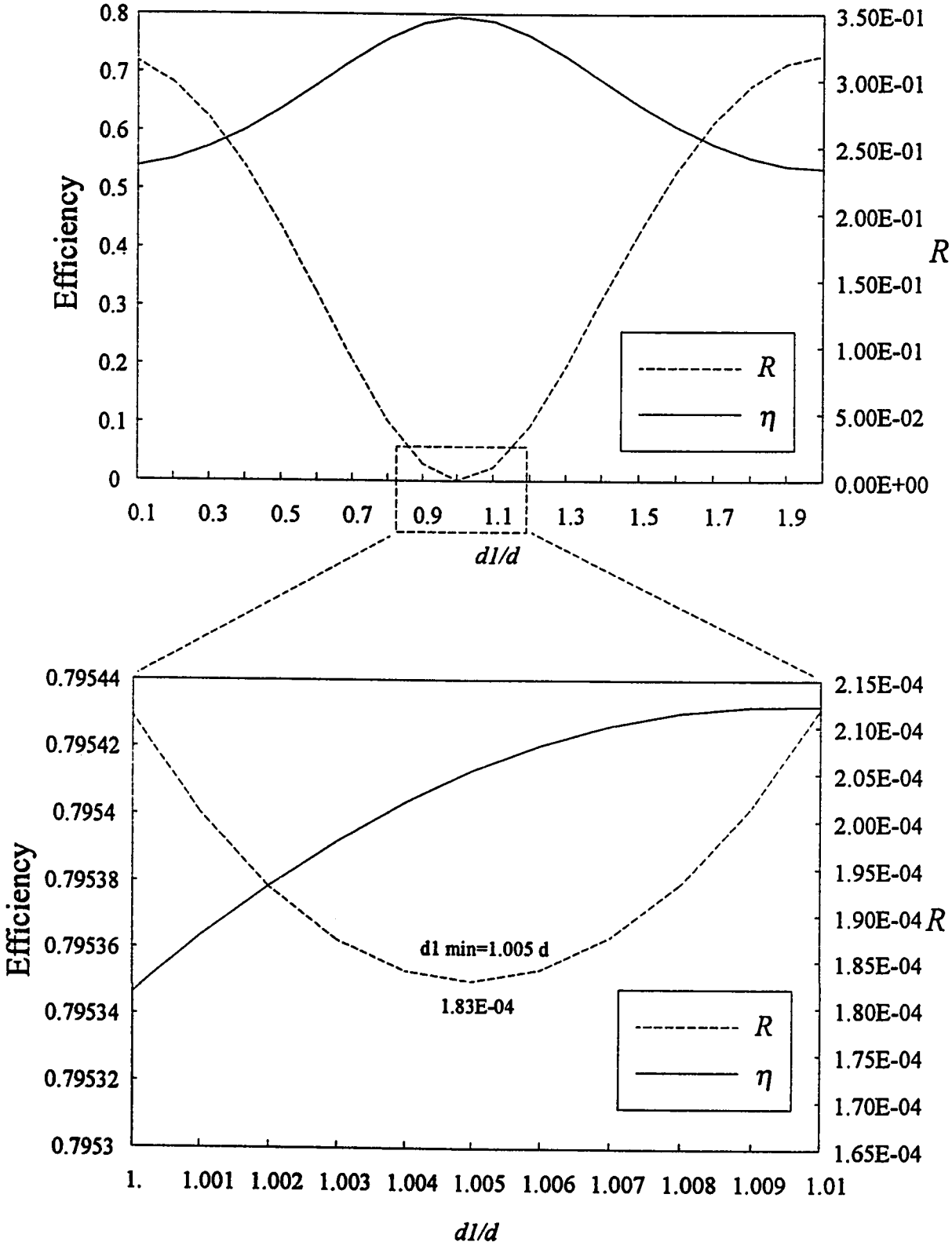

Figure(5.18) *Effect of varying the AR layer thickness on both efficiency and reflectivity.*

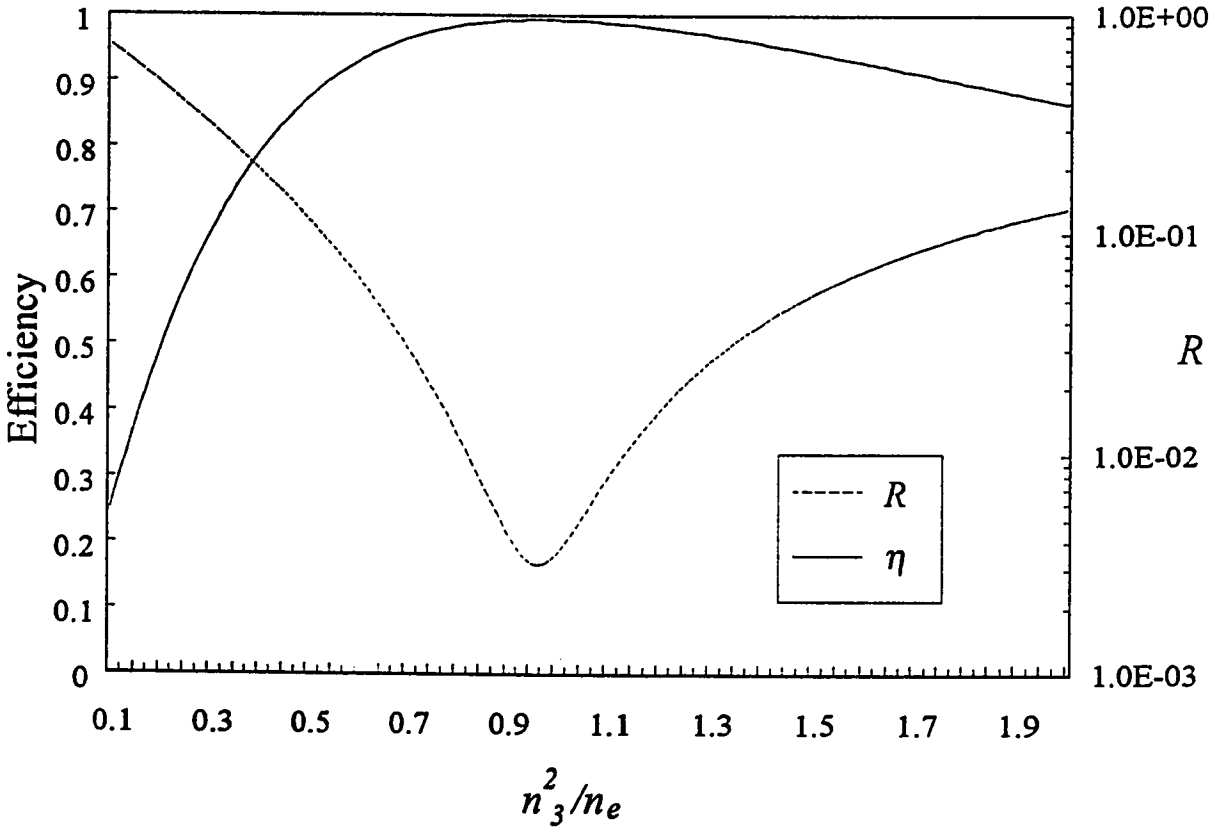

Figure (5.19) *Effect of varying the AR layer index of refraction.* ($w = .4\ \mu m$, $n_2 = 3.4$, $w_0 = .3375\ \mu m$)

w	n_2	w_0	n_3^2/n_e	d1/d	η	R
0.2	3.3	0.3	1	1	0.93514302	4.5254E-03
0.2	3.3	0.65	1	1	0.64499237	6.3306E-04
0.4	3.3	0.3	1	1	0.993	4.7000E-03
0.4	3.3	0.65	1	1	0.827	2.5400E-04
0.6	3.3	0.45	1	1	0.99230626	1.1887E-03
0.6	3.3	0.75	1	1	0.90019829	1.6480E-04
0.2	3.4	0.3	0.98	1	0.97073592	4.3334E-03
0.2	3.4	0.9	1	1.005	0.5692542	2.7731E-04
0.4	3.4	0.3375	0.97	1	0.9938185	3.1715E-04
0.4	3.4	0.75	1	1.005	0.79541286	1.8285E-04
0.6	3.4	0.5	0.99	1	0.99450409	6.9190E-04
0.6	3.4	0.9	1	1.003	0.84339897	1.0123E-04
0.2	3.5	0.3	1	1	0.9941634	4.9838E-03
0.2	3.5	1.35	1	1	0.53589261	6.2412E-05
0.4	3.5	0.4	1	1	0.995	2.0300E-03
0.4	3.5	1.1	1	1	0.692	7.4800E-05
0.6	3.5	0.55	1	1	0.99663373	5.0994E-04
0.6	3.5	1.05	1	1	0.82147299	4.0801E-05
0.2	3.55	0.5	1	1	0.98286692	7.9935E-04
0.2	3.55	1.45	1	1	0.69156729	1.9251E-05
0.4	3.55	0.5	1	1	0.996	8.0600E-04
0.4	3.55	1.4	1	1	0.689	2.3500E-05
0.6	3.55	0.65	1	1	0.9977752	2.4188E-04
0.6	3.55	1.45	1	1	0.74037937	1.8157E-05

Table (5.1) *Effect of the insertion of the AR layer summary sheet.*

5.5 Summary

In this chapter, the effect of the presence of an anti-reflection coating at the end facet of a dielectric slab waveguide has been analyzed using the MoL. The effect of this coating on both; the efficiency as well as on the reflectivity is found to be dramatic. Maximum efficiency figures increased from 70% to 99% and minimum reflectivity also dropped from .28 to 10^{-5} as a result of this insertion.

CHAPTER VI

CONCLUSIONS AND FUTURE WORK

6.1 Conclusions

The Method of Lines (MoL) has been applied in this thesis for the analysis of coupling a Gaussian beam into a dielectric slab waveguide. Referring to the results of the work, the following can be concluded:

a) The MoL demonstrated full capability in the computation of the reflected power under perfect alignment as well as in the presence of longitudinal or lateral offsets. The method is seen to be suited to the analysis of planar waveguides having longitudinal inhomogeneties, step discontinuities or periodic structures. The semi-analytical approach that characterizes the method results in higher accuracy and reduces the computational requirements.

b) The MoL has been applied in Chapter IV to the analysis of a planar structure having one longitudinal discontinuity. It has been then extended in Chapter V to the analysis of problems with two longitudinal discontinuities. It has been demonstrated that the method is suitable for the treatment of planar structures having longitudinally varying characteristics in an easy and straight forward manner.

c) It is very crucial to choose the proper number of mesh discretization points (M). On one hand, increasing M results in a higher accuracy while on the other, computational time and storage requirements increase very dramatically as M becomes large. In this work, convergence of the results was achieved with M=50.

d) The conservation of power at the coupling boundary provided a good means for testing the accuracy of the MoL results. In order to have power conservation, both reflectivity (R) and transmittivity (T) should add up to unity within some acceptable tolerance.

e) By varying the beam HBW, it was found that among the three tested core halfwidths; w= .2, .4 and .6 μm, w= .6 μm resulted in higher efficiency in general.

f) As the difference between the refractive indices of both the core and cladding decreases, the efficiency increases. In addition, the difference between the efficiency curves for different cladding index; n_2 decreases as the core width w increases. The reason for this is attributed to the fact that the modal field has a larger spatial extent when the difference between n_1 and n_2 decreases.

g) Perfect Gaussian beam alignment, i.e., $(x_0=0, z_0=0)$ resulted in maximum coupling efficiency. In addition, it was found that as the HBW; w_0 increases, the effect of lateral and longitudinal offsets on power efficiency becomes smoother and less dramatic.

h) The optimum AR layer thickness and refractive index that resulted in the maximum coupling efficiency and minimum reflectivity, were close to the ones derived by the plane wave approximation.

i) The introduction of an anti-reflection (AR) layer at the end facet of the dielectric slab waveguide has been shown to result in increasing the maximum power coupling efficiency considerably. Whereas the maximum efficiency without the AR layer did not exceed 70%, efficiency

figures greater than 99% have been achieved by the insertion of the AR coating.

j) The reflectivity also dropped more than 10,000 times and figures in the order of 10^{-5} were obtained as a result of this insertion. However, the AR layer has been shown to be less effective for narrow incident beams. It is of interest to note that the MoL is found to be reliable in calculating reflectivities of this small order of magnitude. It is concluded that the method can be used in the calculation of very low reflectivity films as in optical amplifier structures.

k) The incident Gaussian beam widens as it travels away from the focusing plane. The same behavior was noticed for the reflected field which maintained a Gaussian profile after reflection from the boundary. In addition, As the transmitted field propagates for a certain number of wavelengths inside the slab waveguide, its profile conforms to that of the guided fundamental mode $(\alpha_0 F_0)$.

l) Two problems in the present application of the MoL have been encountered. One was that the power conservation condition for values of the incident Gaussian beam HBW less than .3 μm is not satisfied. This is caused by the

error in the three-point central difference approximation used in the MoL. The other problem was the inability to account for the effect of negative longitudinal offsets. The reason for this is that in the present problem, the source is located outside the waveguide. This results in that the reflected field $e^{-jQ_1^{1/2}z}$ will have growing terms, leading to unstable results.

6.2 Recommended Future Work

A number of areas of research exists in this field. These include the following:

a) The MoL algorithm developed for the purpose of this thesis can be extended for the treatment of planar structures having multi-longitudinal discontinuities. An example of such structures is the analysis of the reflectivity of the end facet of a dielectric slab waveguide with multiple coatings [51]. The algorithm also can be utilized for the treatment of asymmetric and graded index slab waveguides.

b) In this thesis work, the effect of both Gaussian beam lateral and longitudinal offsets has been investigated. The MoL is suitable for the analysis of angular offset as well. The effect of angular alignment has been treated in the literature [29] because of its importance in coupling analysis.

c) The three point implementation of the MoL has been found to breakdown in the analysis of half-beam widths w_0<.3 μm and also of negative longitudinal offsets. This problem remains to be solved either by a modification to the MoL or by using alternative techniques.

Appendix- A

****

STF-1 PROGRAM

****

********** "STF1" PROGRAM **********

This program computes the eigenvalues and eigenfunctions and the propagation constant of a multilayer slab waveguide. All the necessary parameters characterizing the waveguide have to be supplied. The routine requires an initial guess for a value near the zero to be found. The program was developed by Dr. H. A. Jamid for an ealier work and has been used in this thesis mainly to find the values of the effective indices of the treated dielectric slab waveguide. These values were then fed to the Method of Lines programs for further computations.

------#### *THE PROGRAM STARTS HERE* ####------

```
      IMPLICIT REAL*8 (A-H,O-Z)
      EXTERNAL FN
      LOGICAL FNREAL
      COMPLEX*16  ZEROS(20),VALUE(20)
      COMMON /ABC/TAP,FLAG
      OPEN(6,FILE='STF1.RS')
      FNREAL=.FALSE.
C  ENTER INITIAL GUESSES IF DESIRED.
      WRITE(*,866)
866   FORMAT(1X,'ENTER GUESS')
```

```
      READ(*,*)ZEROS(1)
      WRITE(*,333)
333   FORMAT(1X,'ENTER A NONZERO FOR TE AND ZERO FOR TM')
      READ(*,*)FLAG
C     ZEROS(1)=DCMPLX(1.50558D0,.0001D0)
      ZEROS(2)=DCMPLX(1.1188D0,000.D0)
      ZEROS(3)=DCMPLX(1.0335D0,.000D0)
      ZEROS(4)=DCMPLX(1.2222D0,000.D0)
      ZEROS(5)=DCMPLX(1.049D0,000.D0)
C ENTER NUMBER OF ZEROS TO BE SEARCHED FOR.
      N=1
C ENTER THE NUMBER OF ZEROS PREVIOUSLY KNOWN.
      NPREV=0
C ENTER THE MAX. NUMBER OF FUNCTION EVALUATION FOR EACH ZERO
      MAXIT=8
C ENTER THE MAXIMUM ERROR CONTROL PARAMETERS
      EP1=10.0**(-10)
      EP2=10.0**(-15)
      CALL MULLER (FN,FNREAL,ZEROS,N,NPREV,MAXIT,EP1,EP2)
      TAP=1.D0
      DO 312 I=1,N
      CALL FN(ZEROS(I),VALUE(I))
      WRITE(*,*)ZEROS(I),VALUE(I)
      WRITE(6,*)ZEROS(I),VALUE(I)
312   CONTINUE
```

```
      STOP
      END
```

******* *Subroutine "MULLER"* *******

Subroutine MULLER determines up to N zeros of the function specified by another subroutine "FN", using quadratic interpolation , i.e., Muller's method.

****

LIST OF DEFINITIONS:

FN=NAME OF A SUBROUTINE ,OF THE FORM FN(Z,FZ)

FNREAL= A LOGICAL VARIABLE.IF.TRUE.,ALL APPROXIMATIONS ARE TAKEN TO BE REAL,ALLOWING THIS ROUTINE TO BE USED EVEN IF F(Z) IS ONLY DEFINED FOR REAL Z.

ZEROS(1),...,ZEROS(NPREV) CONTAINS PREVIOUSLY FOUND ZEROS (IF NPREV .GT. 0)

ZEROS(NPREV+1),...,ZEROS(N) CONTAINS FIRST GUESS FOR THE ZEROS TO BE FOUND.

MAXIT= MAXIMUM NUMBER OF FUNCTION EVALUATIONS ALLOWED PER ZERO.

N= TOTAL NUMBER OF ZEROS TO BE FOUND.

NPREV= NUMBER OF ZEROS TO BE FOUND.

****

```
      SUBROUTINE MULLER (FN,FNREAL,ZEROS,N,NPREV,MAXIT,EP1,EP2)
      IMPLICIT REAL*8(A-H,O-Z)
      EXTERNAL FN
```

```
      LOGICAL FNREAL
      INTEGER MAXIT,N,NPREV,KOUNT
      COMPLEX*16 ZEROS(N),C,DEN,DIVDF1,DIVDF2,DVDF1P,FZR
      COMPLEX*16 FZRDFL,FZRPRV,H,ZERO,SQR
      EPS1 =DMAX1(EP1, 1.D-30)
      EPS2 =DMAX1(EP2, 1.D-40)
      DO 100 I=NPREV+1,N
      KOUNT=0
1     ZERO=ZEROS(I)
C  COMPUTE FIRST THREE ESTIMATES FOR ZERO AS
C   ZEROS(I)+.5D-6,ZEROS(I)-.5D-6,ZEROS(I).
      H=.5D-6
      CALL DFLATE(FN, ZERO+.5D-6,I,KOUNT,FZR,DVDF1P,ZEROS,*1)
      CALL DFLATE(FN,ZERO-.5D-6,I,KOUNT,FZR,FZRPRV,ZEROS,*1)
      HPREV=-1.0D-6
      DVDF1P=(FZRPRV-DVDF1P)/HPREV
      CALL DFLATE(FN,ZERO,I,KOUNT,FZR,FZRDFL,ZEROS,*1)
40    DIVDF1=(FZRDFL-FZRPRV)/H
      DIVDF2=(DIVDF1-DVDF1P)/(H+HPREV)
      HPREV=H
      DVDF1P=DIVDF1
      C=DIVDF1+H*DIVDF2
      SQR=C*C-4.*FZRDFL*DIVDF2
      IF (FNREAL .AND. REAL(SQR) .LT.0.) SQR=0.
      SQR=CDSQRT(SQR)
```

```
      IF (REAL(C)*REAL(SQR)+DIMAG(SQR) .LT. 0.) THEN
         DEN=C-SQR
      ELSE
         DEN=C+SQR
      END IF
      IF (CDABS(DEN) .LE. 0.0D0) DEN=1.0D0
      H=-2.*FZRDFL/DEN
      FZRPRV=FZRDFL
      ZERO=ZERO+H
      IF (KOUNT .GT. MAXIT)  GO TO 99
70    CALL DFLATE(FN,ZERO,I,KOUNT,FZR,FZRDFL,ZEROS,*1)
C  CHECK FOR CONVERGENCE.
      IF (CDABS(H) .LT. EPS1*CDABS(ZERO)) GO TO 99
      IF (DMAX1(CDABS(FZR),CDABS(FZRDFL)).LT.EPS2) GO TO 99
C  CHECK FOR CONVERGENCE.
      IF (CDABS(FZRDFL) .GE. 10.*CDABS(FZRPRV)) THEN
         H=H/2.
         ZERO=ZERO-H
                                   GO TO 70
      ELSE
                                   GO TO 40
      END IF
99    ZEROS(I)=ZERO
100   CONTINUE
      RETURN
```

```
      END
```

******* *Subroutine "DFLATE"* *******

```
      SUBROUTINE DFLATE (FN,ZERO,I,KOUNT,FZERO,FZRDFL,ZEROS,* )
C  TO BE CALLED BY MULLER.
      IMPLICIT REAL*8 (A-H,O-Z)
      EXTERNAL FN
      INTEGER I,KOUNT,J
      COMPLEX*16  FZERO,FZRDFL,ZERO,ZEROS(I), DEN
      KOUNT=KOUNT+1
      CALL FN (ZERO,FZERO)
      FZRDFL=FZERO
      IF (I .LT. 2) RETURN
      DO 10 J=2,I
      DEN=ZERO-ZEROS(J-1)
      IF(CDABS(DEN).EQ.0.0D0) THEN
        ZEROS(I)=ZERO*1.001
                  RETURN1
      ELSE
        FZRDFL=FZRDFL/DEN
      END IF
10    CONTINUE
                  RETURN
      END
```

******* *Subroutine "FN"* *******

This subroutine is designed to solve problems of slab waveguides having nonlinear cladding (substrate) material.where the substrate occupies the region x<0.The waveguide consists of NN layers (not counting the substrate or the supre strate) with each layer having homogeneous refractive index distribution.

****

LIST OF DEFINITIONS

NN= NUMBER OF LAYERS NOT COUNTING THE SUBSTRATE OR THE SUPERSTRATAE.

NSUP= SUPERSTRATE INDEX.

NSUB= SUBSTRATE INDEX.

LAMBDA= FREE SPACE WAVELENGTH.

K=FREE SPACE WAVE NUMBER.

NEFF=PROPAGATION CONSTANT/K

P(I)= ARRAY THAT CONTAINS THE POSITIONS OF THE ENDS OF THE LAYERS.

THE FIRST LAYER ENDS AT P(1),IT IS BELOW THE SUPERSTRATE. THE SUPERSTRATE STARTS AT X=0 TO MINUS INFINITY. THE FINAL LAYER ENDS AT P(NN).IT IS THE IMMEDIATE NEIGHBOR OF THE SUBSTRATE. THE SUBSTRATE STARTS AT P(NN) TO INFINITY. THE SUBSTRATE IS LOCATED AT P(NN).

N(I)= AN ARRAY CONTAINING THE REFRACTIVE INDICES OF THE VARIOUS layers.

```
N(1)= THE INDEX OF THE LAYER ADJACENT TO THE SUPERSTRATE.
N(NN)= THE INDEX OF THE FINAL LAYER WHICH IS ADJACENT TO THE
       SUBSTRATE.
                    ********************
      SUBROUTINE FN(NEFF,FZ)
      IMPLICIT REAL*8(A-H,O-Z)
      COMPLEX*16 NSQ(510),NSUP,NSUPSQ,NSUB,NSUBSQ,NPEAK,GA,THETA
      COMPLEX*16 A(510),B(510),D,Q(510),RHO,NEFF,NESQ,F,T2,DC,FZ
      REAL*8 P(510),K,LAMBDA
      REAL*4 X
      COMMON /AA/Q,D,A,B,GA,P,NN,THETA,K
      COMMON /ABC/TAP,FLAG
      DATA CH/0.0D0/
      NN=1
      PI=2.D0*DASIN(1.D0)
      LAMBDA=0.860D0
      K=2.D0*PI/LAMBDA
      NESQ=NEFF**2
      NPEAK=DCMPLX(3.60D0,0.0D0)
      NSUP=DCMPLX(3.550D0,0.0D0)
      NSUPSQ=NSUP**2
      NSUB=DCMPLX(3.550D0,0.0D0)
      NSUBSQ=NSUB**2
C ENTER LAYR WIDTH
      P(1)=1.20D0
```

```
      NSQ(1)=DCMPLX(3.60D0,0.D0)**2
C       DO 501 I=1,NN
C       P(I)=FLOAT(I)*P(1)
C501    CONTINUE
C
C ENTER REFRACTIVE INDEX DISTRIBUTION
C
C       IF(CH.EQ.1.0D0)GO TO 587
C       DA=4.0D0
C       DO 502 I=1,NN
C       XA=(P(I)-P(1))/DA
C EXPONENTIAL.
C     NSQ(I)=NSUBSQ+(NPEAK**2-NSUBSQ)*DEXP(-XA)
C PARABOLIC.
C     NSQ(I)=NPEAK**2-(NPEAK**2-NSUBSQ)*XA**2
C GAUSSIAN.
C     NSQ(I)=NSUBSQ+(NPEAK**2-NSUBSQ)*DEXP(-XA**2)
C COMPLIMENTARY ERROR FUNCTION.
C       W=1.0D0/(1.0D0+.47047D0*XA)
C       A1=0.3480242D0
C       A2=-.0958798D0
C       A3=0.7478556D0
C       NSQ(I)=NSUBSQ+(NPEAK**2NSUBSQ)*(A1*W+A2*W*W+A3*W**3)*
     $DEXP(-XA**2)
```

```
C LINEAR.
C       NSQ(I)=NPEAK**2-(NPEAK**2-NSUBSQ)*XA
C ALPHA PROFILE.
C       NSQ(I)=NPEAK**2-(NPEAK**2-NSUBSQ)*(XA**0.90D0)
C502    CONTINUE
C       CH=1.0D0
587     DO 577 I=1,NN
        Q(I)=K*CDSQRT(NSQ(I)-NESQ)
577     CONTINUE
        THETA=K*CDSQRT(NESQ-NSUPSQ)
        GA=K*CDSQRT(NESQ-NSUBSQ)
        RHO=1.0D0
        IF(FLAG.EQ.0.0D0)RHO=NSUPSQ/NSQ(1)
        A(1)=-CDSIN(Q(1)*P(1))+THETA*CDCOS(Q(1)*P(1))/RHO/Q(1)
        B(1)=CDCOS(Q(1)*P(1))+THETA*CDSIN(Q(1)*P(1))/RHO/Q(1)
        DO 12 I=1,NN-1
        IF(FLAG.EQ.0.0D0)RHO=NSQ(I)/NSQ(I+1)
        A(I+1)=-B(I)*CDSIN(Q(I+1)*(P(I+1)-P(I)))+A(I)*Q(I)*CDCOS(Q(I+
     $*(P(I+1)-P(I)))/RHO/Q(I+1)
        B(I+1)=B(I)*CDCOS(Q(I+1)*(P(I+1)-P(I)))+A(I)*Q(I)*CDSIN(Q(I+1
     $*(P(I+1)-P(I)))/RHO/Q(I+1)
12      CONTINUE
        D=B(NN)
        IF(FLAG.EQ.0.0D0)RHO=NSQ(NN)/NSUBSQ
        DC=-A(NN)*Q(NN)/GA/RHO
```

```
      FZ=DC-D
      WRITE(*,*)FZ,NEFF
      IF(TAP.NE.0)GO TO 21
      RETURN

**************************
C OBTAIN FIELD AMPLITUDE F.
**************************
21    DO 15 I=1,401
      X=-1.D0+FLOAT(I-1)*.01D0
      CALL FIELD(F,X)
      WRITE(6,*)X,REAL(F)
15    CONTINUE
      WRITE(*,901)
901   FORMAT(1X,'SEE RESULTS IN FILE STF1.RS')
      RETURN
      END
      SUBROUTINE FIELD(F,X)
      IMPLICIT REAL*8(A-H,O-Z)
      COMPLEX*16 F,D,GA,Q(510),A(510),B(510),THETA
      REAL*8 P(510),K
      REAL*4 X
      COMMON /AA/Q,D,A,B,GA,P,NN,THETA,K
      IF(X.GT.0.D0)GO TO 31
      F=CDEXP(THETA*X)
```

```
      GO TO 101
31    DO 41 I=1,NN
      IF(X.LE.P(I))GO TO 51
41    CONTINUE
      GO TO 61
51    F=A(I)*CDSIN(Q(I)*(X-P(I)))+B(I)*CDCOS(Q(I)*(X-P(I)))
      GO TO 101
61    F=D*CDEXP(-GA*(X-P(NN)))
101   RETURN
      END
```

Appendix-B

****

THE MoL PROGRAMS

****

****

THE METHOD OF LINES PROGRAMS

****

Enclosed in this appendix are the two main MoL programs developed for the purpose of this thesis. The programs run under MATLAB software which has been chosen for its powerful capabilities in dealing with matrix manipulations resulting from the application of the MoL on the analysis of the coupling problem.

The first program; "MoL5", analyzes the different parameters affecting the power coupling efficiency of a Gaussian beam into a symmetric slab waveguide. The output results of this program are presented in Chapter IV. The second program; "MoL10", calculates the effect of inserting an anti-reflection layer between the incident field and the waveguide and the results are discussed in Chapter V.

Throughout the course of the preparation of this thesis data, these two programs have been modified in certain aspects and variables were interchanged to provide the required results.

********** *List of Definitions* **********

lx= The total problem width in the transvers direction micrometer(μm).

d = Waveguide core halfwidth(μm).

mx= Number of mesh points in the x-direction.

dx= Space between two adajacent lines (μm).

mx1= Number of points in the core.

mx2= Number of points in one side of the cladding.

n0= Air refractive index.

n1= Core refractive index.

n2= Cladding refractive index.

ne= The effective index.

w0= The incident beam spot size (μm).

Z0= Longitudinal offset (μm).

x0= Lateral offset (μm).

A0= The distribution of the incident field.

fx1= The modal distribution in the substrate.

fxc= The modal distribution in the core.

fxu= The modal distribution in the superstrate.

F0= The overall modal distribution at z=0.

A1= The transmitted field at z=0.

AZ1= The transmitted field at z.

alfa0= Fundamental mode excitation coefficient.

e= Power coupling efficiency.

```
d1= Thickness of the anti-reflection layer.
n3= Refractive index of the anti-reflection layer.
```

********** MoL5 Program **********

```
lx=5;
d=1.2/2;
mx=50;
dx=lx/(mx-1);
mx1=2*integer(d/dx);
mx2=(mx-mx1)/2;
dx=2*d/mx1;
lx=(mx-1)*dx;
lambda=0.86;
k0=2*pi/lambda;
n0sq=1^2;
n1sq=3.6^2;
n2sq=3.55^2;
%  ne is found using a zero-finding program
ne=3.5908159132;
w0=.25;
for s=1:35
w0=w0+.05
z0=0;
x0=0;
j=1:mx;
```

```
x=(j-1)*dx-lx/2;
A0=exp(-x.^2/w0^2);
N0=n0sq*eye(mx);
% Finding the tri-diagonal matrix
C=diag(ones(mx-1,1),1)+diag(ones(mx-1,1),-1)-2*eye(mx);
%       [Q] = 1/dx^2 * [C] + k0^2 * [N]
Q0=k0*k0*N0+C/(dx*dx);
QQ0=Q0^(-.5);
%
% A1 = 2*inv((I+Q0^-.5 * Q1^.5)) * A0
%
N1=[n2sq*ones(1,mx2) n1sq*ones(1,mx1) n2sq*ones(1,mx2)];
N1=diag(N1);
Q1=k0*k0*N1+C/(dx*dx);
QQ1=Q1^.5;
%
l=k0*sqrt(n1sq-ne*ne);
gamma=k0*sqrt(ne*ne-n2sq);
%
% Discretization of the fundamental mode distribution:
x=1:mx2;
x=(x-1)*dx-lx/2;
fx1=(cos(l*d))*exp(gamma*(x+d));
x=mx2+1:mx2+mx1;
x=(x-1)*dx-lx/2;
```

```
fxc=cos(l*x);
x=mx2+mx1+1:mx;
x=(x-1)*dx-lx/2;
fxu=(cos(l*d))*exp(-gamma*(x-d));
F0=[fxl fxc fxu].';
%
A1=2*(inv(eye(mx)+QQ0*QQ1))*A0.';% trans. field at z=0.
B0=A1-A0.';
%[u1,v1]=eig(Q1);
%vv1=sqrt(v1);
%AZ1=(u1*diag(exp(diag(i*vv1*z)))*inv(u1))*A1
%AZ1=abs(AZ1);
QQ0=Q0^.5;
%
% Calculations of power coupling efficiency:
%
alfa0=A1.'*F0/(F0.'*F0);
Pg=real(alfa0*F0.'*conj(QQ1*alfa0*F0));
%Pg1=k0*ne*(alfa0*F0)'*(alfa0*F0)
Pt=real(A1.'*conj(QQ1*A1));
Pi=real(A0*conj(QQ0*A0.'));
Pr=real(B0.'*conj(QQ0*B0));
T=Pt/Pi
R=Pr/Pi
RT=R+T
```

```
e=abs(Pg/Pi)
%e1=abs(Pg1/Pi)
%
% Output data presentation
A(s,1)=w0;
A(s,2)=T;
A(s,3)=R;
A(s,4)=R+T;
A(s,5)=Pi;
A(s,6)=Pg;
A(s,7)=e;
end
A
save en12.d A /ascii
```

********** MoL10 Program **********

```
lx=5;
d=.8/2;
mx=50;
dx=lx/(mx-1);
mx1=2*integer(d/dx);
mx2=(mx-mx1)/2;
dx=2*d/mx1;
lx=(mx-1)*dx;
lambda=0.86;
k0=2*pi/lambda;
n0sq=1^2;
n1sq=3.6^2;
n2sq=3.4^2;
% ne is obtained using a zero-finding program
ne=3.5760109241;
n3sq=ne;
w0=.75;
%
for s=1:11
dl=(lambda/4)/sqrt(ne);
n3sq=1*ne;
n3=sqrt(n3sq);
%dl=(lambda/4)/n3;
```

```
dl=(.999+.001*s)*dl;
%fact=n3sq/ne
fact=.999+.001*s
j=1:mx;
x=(j-1)*dx-lx/2;
% Discretization of the incident field
A0=exp(-x.^2/w0^2);
A0=A0.';
%A0=cos(k0*x);
%       [Q] = 1/dx^2 * [C] + k0^2 * [N]
I=eye(mx);
N0=n0sq*I;
% Formulation of the tri-diagonal matrix
C=diag(ones(mx-1,1),1)+diag(ones(mx-1,1),-1)-2*I;
Q0=k0*k0*N0+C/(dx*dx);
%
N1=n3sq*I;
Q1=k0*k0*N1+C/(dx*dx);
%
N2=[n2sq*ones(1,mx2) n1sq*ones(1,mx1) n2sq*ones(1,mx2)];
N2=diag(N2);
Q2=k0*k0*N2+C/(dx*dx);
%
l=k0*sqrt(n1sq-ne*ne);
gamma=k0*sqrt(ne*ne-n2sq);
```

```
%
% Discretization of the fundamental mode distribution:
x=1:mx2;
x=(x-1)*dx-lx/2;
fxl=(cos(l*d))*exp(gamma*(x+d));
x=mx2+1:mx2+mx1;
x=(x-1)*dx-lx/2;
fxc=cos(l*x);
x=mx2+mx1+1:mx;
x=(x-1)*dx-lx/2;
fxu=(cos(l*d))*exp(-gamma*(x-d));
F0=[fxl fxc fxu].';
%
QQ0=Q0^.5;
QQ1=Q1^(-.5);
t=QQ1*QQ0;
QQ1=Q1^.5;
QQ2=Q2^(-.5);
t1=QQ2*QQ1;
% Finding the eignvalues and eigenvectors of Q:
[u1,v1]=eig(Q1);
vv1=sqrt(v1);
% Calculations of Q exponentials:
el=(u1*diag(exp(diag(i*vv1*dl)))*inv(u1));
v=(inv(I+t1))*(t1-I)*el;
```

```
s1=inv(I+el*v);
s2=inv(I-el*v)*t;
A2=.5*(el+v)*((I+t)+(I-t)*inv(s1+s2)*(s2-s1))*A0;
B0=inv(s1+s2)*(s2-s1)*A0;
% Calculations of the power coupling efficiency:
alfa0=A2.'*F0/(F0.'*F0);
%alfsq=(abs(alfa0))^2;
QQ2=Q2^.5;
Pg=real(alfa0*F0.'*conj(QQ2*alfa0*F0));
%Pg1=k0*ne*(alfa0*F0)'*(alfa0*F0)
Pi=real(A0.'*conj(QQ0*A0));
e=abs(Pg/Pi)
Pt=real(A2.'*conj(QQ2*A2));
Pr=real(B0.'*conj(QQ0*B0));
T=Pt/Pi;
R=Pr/Pi
RT=R+T
%el=abs(Pg1/Pi)
%
% Output data presentation
A(s,1)=fact;
A(s,2)=dl;
%A(s,2)=n3;
A(s,3)=T;
A(s,4)=R;
```

```
A(s,5)=R+T;
A(s,6)=e;
end
A
save ar10b.d A /ascii
```

REFERENCES

[1] M. Saruwatari and K. Nawata, "Semiconductor Laser to Single-Mode Fiber Coupler," Appl. Optcs, vol. 18, no. 11, pp 1847-1856, 1979.

[2] D. Su, A. Boecshat and J. Jones, "Beam Delivery by large-Core fibers: Effect of Launching Conditions on Near-Field Output Profile," Applied Optics, vol. 31, no. 27, pp. 5816-5821, 1992.

[3] M. Ross (ed.), Laser Applications, Academic Press, New York, 1974.

[4] M. D. Feit and J. A. Fleck, "Light Propagation in Graded-Index Optical Fibers," Applied Optics, vol. 17, pp. 3990-3998, 1978.

[5] S. Chu, and S. Chaudhuri, "A Finite-Difference Time-Domain Method for the Design and Analysis of Guided-Wave Optical Structures," J. Light. Tech., vol. 7, no. 12, pp 2033-2037, 1989.

[6] R. Pregla and W. Pascher, "The Method of Lines," in *Numerical Techniques for Microwave and Millimeter Wave Passive Structures*, T. Itoh, ed., wiley, New York, pp 381-446, 1989.

[7] R. Pregla, "About the Nature of the Method of Lines," Arch. Elektron Ueber., vol. 41, no. 6, pp. 368-370, 1987.

[8] D. Marcuse, "Reflection of a Gaussian Beam from a Nonlinear Interface," Applied Optics, vol. 19, no. 18, pp. 3130-3139, 1980.

[9] R. Pregla, "Analysis of Planar Microwave Structures on Magnetized Ferrite Substrate," Arch. Elektron Ueber., vol. 40, pp. 270-274, 1986.

[10] S. Worm and R. Pregla, "Hybrid Mode Analysis of Arbitrarily Shaped Planar Microwave Structures by the Method of Lines," IEEE Trans. Microwave Theory Tech., vol. MTT-32, pp. 191-196, 1984.

[11] J. Gerdes, B. Lunitz, D. Benish, and R. Pregla, "Analysis of Slab Waveguide Discontinuities Including Radiation and Absorption Effects," Elec. let., vol. 28, no. 11, pp 1013-1015, 1992.

[12] D. Sarid, "High Efficiency Input-Output Prism Waveguide Coupler: an Analysis," Appl. Opt. 18; pp 2921-2926, 1979.

[13] T. Tamir and S. Peng, "Analysis and Design of Grating Couplers," Appl. Phys. vol.14, pp 235-254, 1977.

[14] R. Hunsperger, A. Yariv, and A. Lee,"Parallel End-Butt Coupling for Optical Integrated Circuits," Appl. Optcs, vol. 16, no. 4, pp 1026-1032, 1977.

[15] S.Martellucci and A. N. Chester, Integrated Optics, plenum Press, New York, 1983.

[16] D. Marcuse,"Excitation of the Dominant Mode of a Round Fiber by Gaussian Beam," Bell Syst. tech. j., vol.49, no.8,pp.1695-1703, Oct. 1970.

[17] H. P. Hsu and A. F. Milton, "Single Mode Coupling Between Fibers and Indiffused Waveguides," IEEE J. Quantum Electron. vol. QE-13, no. 4, pp 224-233, 1977.

[18] C. S. Tsai (ed.), Guided-Wave Acousto-Optics, Springer-Verlag, Berlin, 1990.

[19] J. A. Kong, Electromagnetic Wave Theory, John Wiley, New York, 1986.

[20] D. Marcuse, Light Transmission Optics, Van Nostrand Co., New York, 1982.

[21] H. Ribot, P. Sansonetti, and A. Carenco, " Improved Design for the Monolithic Integration of a Laser and Optical Waveguide Coupled by an Evanescent Field," IEEE J. Quantum Electron., vol. 26, no. 11, pp 1930-1941, 1990.

[22] W. K. Burns and G. B. Hocker, "Endfire Coupling between Optical Fibers and Diffused Channel Waveguides," Applied Optics, vol. 16, no. 8, pp 2048-2050, 1977.

[23] J. C. Palais, Fiber Optic Communications, Prentice-Hall, New Jersey, 1984.

[24] F. Tosco (ed.), Fiber Optic Communications Handbook, TAB Books, Blue Ridge, 1990.

[25] M. L. Dakss, L. Kuhn, P. F. Heidrich, and B. A. Scott, "Grating Coupler for efficient Excitation of Optical Guided Waves in Thin Films," Appl. Phy. Lett., 16:523-525,1970.

[26] H. Kogelnik and R. P. Sosnowsky, "Holographic Thin Film Couplers," Bell Sys. Tech. J. 49, pp 1602-1608, 1970.

[27] L. Li and M. C. Gupta, "Effects of Beam Focusing on the Efficiency of Planar Wavegiude Grating Couplers," Appl. Opt., vol. 29, no. 36, pp 5320-5325, 1990.

[28] D. Marcuse and E. Marcatili, "Excitation of Waveguides for Integrated Optics with Laser Beams," Bell Sys. Tech. J., 50, pp 43-57, 1971.

[29] C. Mueller, C. Sullivan, W. Chang, D. Hall, J. Zino, and R. Rice, " An Analysis of the Coupling of an Injection Laser Diode to a Planar LiNbO3 Waveguide," IEEE J. Quantum Elect., vol. QE-16, no. 3, pp 363-371, 1980.

[30] D. Hall, J. Zino, H. Koenig, R. Rice, J. Powers, G. Burkhart, and P. Bear, " Edge coupling of a GaAlAs DH Laser Diode to a Planar Ti:$LiNbO_3$ Waveguide," Applied Optics, vol. 19, no. 11, pp. 1847-1852, 1980.

[31] R. Herrmann and J. Hertel, " Mode Launching on a Multimode Slab-Waveguide by a Plane Wave," Appl. Phys. 9, pp. 307-313, 1976.

[32] C. Vassallo, " On a Rigorous Calculation of the Efficiency for Coupling Light Power into Optical Waveguides," IEEE J. Quant. Elect., vol. QE-13, no. 4, pp. 165-173, 1977.

[33] K. Mizuuchi, K. Yamamoto, and T. Taniuchi, " High Efficiency Coupling of Laser Diodes in Tapered Proton-exchanged Waveguides," Elect. Lett., vol. 26, no. 24, pp. 1992-1994, 1990.

[34] M. J. Adams, An Introduction to Optical Waveguiude, John Wiley, New York, 1981.

[35] J. M. Senior, Optical Fiber Communications, Prentice Hall, New York, 1985.

[36] P. K. Cheo (ed.), Handbook of Solid-State Lasers, Marcel Dekker, Inc., New York, 1989.

[37] D. G. Hall, Innovations Section of the IEEE Spectrum Magazine, pp. 8, April, 1993.

[38] H. D. Wu and F. S. Barnes (ed.), Microlenses; Coupling Light to Optical Fibers, IEEE Press, New York, 1991.

[39] L. G. Cohen and M. V. Schneider, "Microlenses for Coupling Junction Lasers to Optical Fibers," Appl. Opt. vol. 13, no. 1, pp. 89-94, 1974.

[40] S. Mukai, H. Yajima, M. Watanabe, H. Itoh, Y. Takabe, and Y. Tsunekawa, "A Semiconductor Laser with a Converging Output Beam," Appl. Phys. Lett, vol. 46, no. 9, pp. 805-806, 1985.

[41] S. Mukai, H. Yajima, Y. Tsunekawa, and Y. Takabe, "Monolithic Integration of a Lens Inside a Diode-Laser Cavity for Beam Convergence," Appl. Phys. Lett., vol. 47, no. 3, pp. 188-190, 1985.

[42] S. Mukai, M. Watanabe, H. Itoh, and H. Yajima, "Integration of a diode Laser and an Electronic Lens for Controlling the Beam Focus Position," Appl. Phys. Lett. vol. 54, no. 4, pp. 315-316, 1989.

[43] K. Kato et al., "22 GHz Photodiode Monolithically Integrated with Optical Waveguide on Semi-Insulating InP Using Novel Butt-Joint Structure," Elec. Lett., vol. 28, no. 12, pp. 1140-1142, 1992.

[44] U. Rogge and R. Pregla, "Method of Lines for the Analysis of Strip-Loaded Optical Waveguide," J. Opt. Soc. Am. B, vol. 8, no. 2, pp 459-463, 1991.

[45] F. Schmuckle and R. Pregla, "The Method of Lines for the Analysis of Planar Waveguides with Finite Metallization Thickness," IEEE Trans. Mic. Tech., vol. 39, no. 1, pp 107-111, 1991.

[46] H. Diestel, "Analysis of Planar Multiconductor Transmission-Line Systems with the Method of Lines," Arch. Elektron Ueber., vol. 41, pp. 169-175, 1987.

[47] H. Diestel and S. Worm, "Analysis of Hybrid Field Problems by the Method of Lies with Nonequidistant Discretization," IEEE Trans. Microwave Theory Tech., vol. MTT-32, no. 6, pp. 633-638, 1984.

[48] U. Schulz, "On the Edge Condition with the Method of Lines in Planar Waveguides," Arch. Elektron Ueber., vol. 34, no. 4, pp. 176-178, 1980.

[49] T. H. Zachos, "Gaussian Beams from GaAs Junction Lasers," Appl. Phys. Lett. , vol. 12, no. 9, pp. 318-320, 1968.

[50] A. Yariv, Quantum Electronics, 3rd ed., John Wiley & Sons, New York, 1989.

[51] C. Vassallo, "Theory and Practical Calculation of Antireflection Coatings on Semiconductor Laser Diode Optical Amplifiers," IEE Proc., vol. 137, pt. J, no. 4, pp. 193-202, 1990.

[52] G. Eisenstein, "Theoretical Design of Single-Layer Antireflection Coatings on Laser Facets," AT&T Bell Lab. Tech. J., vol. 63, no. 2, pp. 357-364, 1984.